University of Alberta

Thermal Diffusivity Measurement of Thin Thermal-sprayed Coatings

by

Linlin Duan

A thesis submitted to the Faculty of Graduate Studies and Research
in partial fulfillment of the requirements for the degree of

Master of Science

Department of Mechanical Engineering

Abstract

This thesis presents a method to determine the thermal diffusivities of both single-layered and two-layered coated samples. The flame spraying, air plasma spraying, and cold spraying techniques were used to fabricate the two-layered samples. Mathematical models were developed for single-layered and two-layered conduction heat transfer problems. Experiments were designed and tests were conducted to ensure that the mathematical models could give good prediction with the correct input of thermal diffusivity value. Experiments were conducted on samples, including single-layered samples of copper, aluminum, PMMA, and Pyrex and two-layered samples of TiO_2 coating on copper substrate or low carbon steel substrate, YSZ coating on low carbon steel substrate, and nano-structured TiO_2 on Pyrex substrate.

The thermal diffusivity results of all the materials showed good repeatability and for low-thermal diffusivity materials, the test results agreed with the referenced value.

Table of Contents

List of Tables

List of Figures

Chapter 1: Introduction

1.1 Thermal diffusivity measurement method

Thermal diffusivity is a parameter used to describe the transient thermal response of a material to a temperature change. This thermal property of materials is of great importance, and it is the most used parameters during transient heat transfer analysis. Researchers compile invaluable thermal physical property data of materials for engineering and science handbooks or databases. However, only a few kinds of materials have well-built thermal diffusivity database, such as pure metal, pure gas, and material with exact compounds. In industry, materials are manufactured in different places, or fabricated according to different recipes; the thermal diffusivity is always not available when required. A method to measure the thermal diffusivity value of random materials in-situ is required.

1.2 Coatings and spraying techniques

Coating is a covering layer fabricated on a surface to protect an object, which is also called substrate, from corrosion, wear or high-temperature degradation. Coating is also used to improve the electrical or thermal performance of the substrate. Coatings could be applied by several different techniques, including chemical vapor deposition, physical vapor deposition, chemical techniques, electrochemical techniques, and thermal spraying techniques. Thermal spraying techniques fabricate coatings by spraying melted or heated materials onto the substrate. Thermal spraying technique has wide application field, including protecting corrosion and fouling [1, 2],

repairing damaged surfaces [3-5], protecting the substrate from temperature and oxidation [6-8] and altering [9-11] the thermal properties and electrical properties for specific applications.

1.2.1 Flame spraying

Flame spray technique is widely used in the industry [12-15]. This spraying method has high deposition rate, provides thick coatings and gives a large choice of coatings.
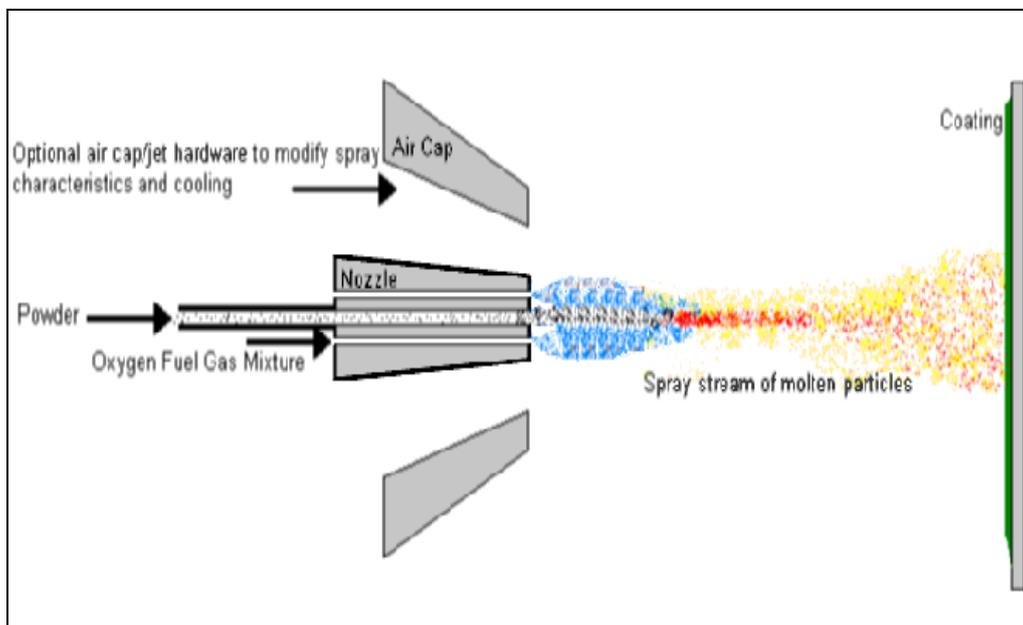
Figure 1- 1 Schematic diagram of flame spraying [16]

Figure 1-1 shows the schematic diagram of flame spraying. Coatings are fabricated by spraying molten powder of a material onto the substrate. The typical size ranges from micrometers to above 100 micrometers. This gun uses oxygen-acetylene as its combustion gas. The flame temperature could reach above 3000˚C [17], which is higher than the melting point of most materials. The powders come through the high temperature flame, being heated and melted. These melted or partially melted particles are propelled by the high

velocity gas and landed on the substrate. When impacting on the substrate, the particles spread and bond to the substrate in form of lamellar shapes. When the spraying process is repeated, the new lamellar coating materials overlay the formerly sprayed coatings to fabricate coatings of desired thickness, which normally range from 20 μm to several millimeters. Air jet is optional, which could be used to modify the spraying characteristics and to cool down the torch for protection.

1.2.2 Cold spraying

Unlike flame spraying, instead of application of high temperature to melt the particles, the cold spraying process focuses more on increasing the particle spraying velocity [18-20]. Fig. 1-2 shows the schematic diagram of cold spraying.
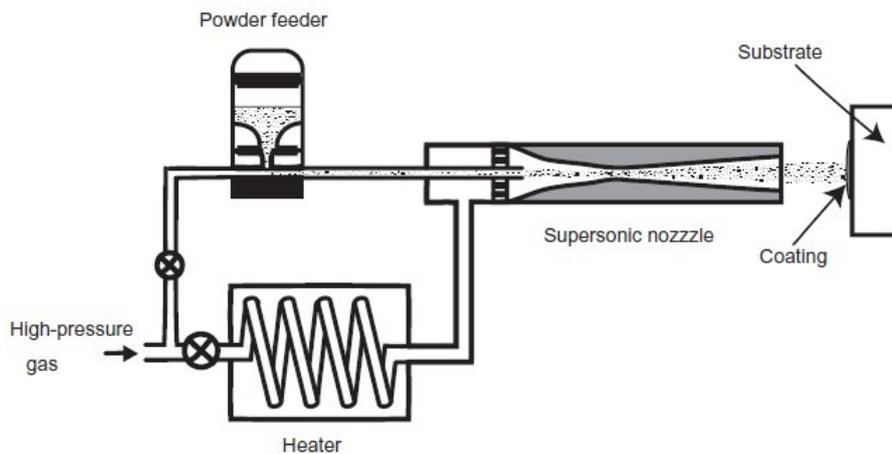
Figure 1- 2 Schematic diagram of cold spraying [21]

As shown in Fig. 1-2, high pressure compressed gas is used to propel the fine powder particles to velocities of 500 m/s to 1500 m/s. Compressed gas is heated to a certain temperature, which would be set on the console of the spray unit, then fed into a specially designed gun. The gun has a de laval type convergent-divergent nozzle to accelerate the particles. The powder particles which are stored in the powder feeder are fed into the high speed gas jet by

compressed gas. With the high-speed gas jet, the powder particles are accelerated to a certain velocity and heated to a certain temperature. When impacting on the substrate, the particle would deform plastically and bond to form a coating. In the entire process, the particles remain in solid state and at relatively low temperature. Therefore, little oxidation of the sprayed material or the substrate occurs. Ideally, properties of the coatings are kept as the properties of the original bulk materials. Cold spraying technique has wider choice of substrate due to the relatively low temperature of gas jet. However, considering the high velocity of the gas jet, the substrate should not be soft or friable.

The disadvantage of cold spray is that it has limited choices of coating powders, since it works for ductile materials such as, aluminum, alloys and so on. Hard and brittle materials cannot be sprayed directly onto a substrate, but have to be applied as composites with the ductile materials.

1.2.3 Plasma spraying

Plasma spraying is a versatile spraying method [22-25]. The plasma is an electrically conductive gas that contains charged particles. The plasma spray torch is able to produce high-temperature plasma, which is around 16000 ˚C [26], and works well with materials with high melting point, such as ceramic coatings. It also has high spraying velocity and is able to fabricate dense coatings with high bond strength.

As shown in Fig. 1-3, the anode (made of tungsten) and the cathode (made of copper) generate a strong electric arc. Plasma gas (normally nitrogen, hydrogen, helium or argon) flows through the torch. At first a high voltage is generated between the cathode and the anode, which causes the local dielectric gas to ionize. The electrons, which are generated during ionization, keep colliding with incoming neutral gas and an avalanche-like process

enhances the ionization. The primary and secondary gas then become electrically charged plasma and act as conductive path for the anode and cathode. The resistance from the plasma causes heat generation and extreme temperature. In this process, the plasma gas flows around the cathode, through the anode, and comes out of the constricting nozzle as neutral flame. Instead of shorting out, the arc extends down the nozzle. Cooling water flows around the nozzle to keep the anode and cathode cooled. Spraying powders and carrier gas are injected into the plasma flame through a port mounted close to the anode.

The rest of the spraying process is similar to the flame spraying method. The powder particles are melted and sprayed onto the substrate to form lamellar shape and overlay each other.
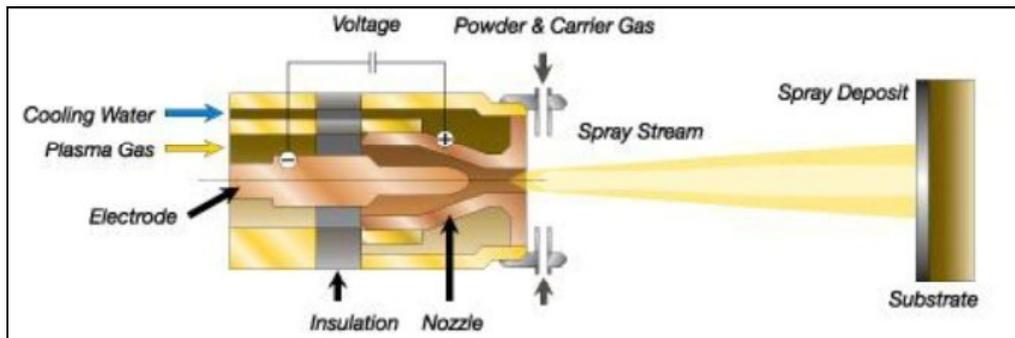
Figure 1- 3 Schematic diagram of air plasma spraying [27]

1.3 Previous studies on thermal diffusivity measurement

Several experimental techniques have been developed to measure the thermal diffusivity of thermal-sprayed coatings, based on different theories. Salazar and Sanchez *et al*. [28] developed a thermal diffusivity measurement method for low diffusivity materials based on the mirage effect. Adams and Kirkbright [29] and Adams, *et al.* [30] used the optoacoustic effect to determine the thermal diffusivity of polymer films on a copper substrate. This method was further modified and developed by other researchers and referred

as thermal wave interferometry technique, photo thermal techniques [30-32] and so on. The sample absorbs rapid pulses of light. The resulting energy is then radiated as heat, which causes detectable sound waves (thermal wave). The pressure of the air in contact with the sample changes accordingly. This optoacoustic signal depends on the thermal diffusivity and thus gives measurement the other way round. However, it requires optical properties of the material, and poor availability of desirable optical properties of the material is a disadvantage of this method.

The most widely used theory for thermal diffusivity measurement is the advanced heat transfer theory. When an energy input is performed on a test sample, the temperature of the sample would change accordingly. With the temperature dependency of thermal diffusivity, several thermal diffusivity measurement methods were developed.

Thermal diffusivity is also determined indirectly by thermal conductivity measurement. Eqn. (1-1) shows the relation between thermal diffusivity and thermal conductivity, where α is thermal diffusivity, k is thermal conductivity, ρ is the density and c_p is the heat capacity at constant pressure.

$$\alpha = \frac{k}{\rho c_p} \tag{1-1}$$

With knowledge of the density and heat capacity of the material, thermal diffusivity value could be determined accordingly. The problem of this method is that the density and heat capacity of the material are not always available to the researchers.

Figure 1-4 classifies the commonly used measurement techniques for thermal diffusivity and thermal conductivity into steady state methods and transient state methods. These techniques distinguish from each other by using different heat sources, temperature measurement methods and different geometric configurations.
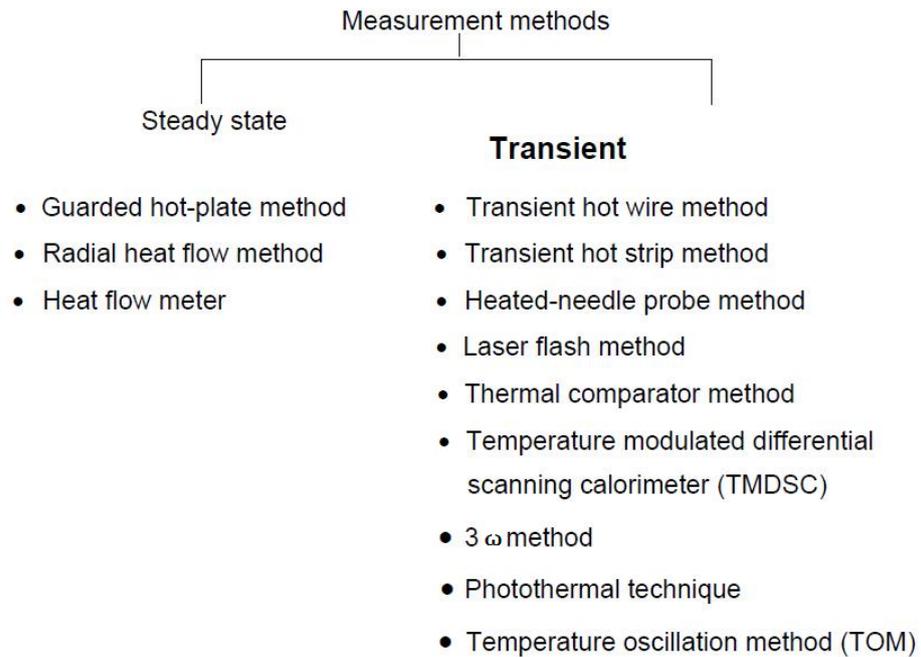
Figure 1- 4 Commonly used measurement methods for thermal diffusivity and thermal conductivity based on heat transfer theory [33]
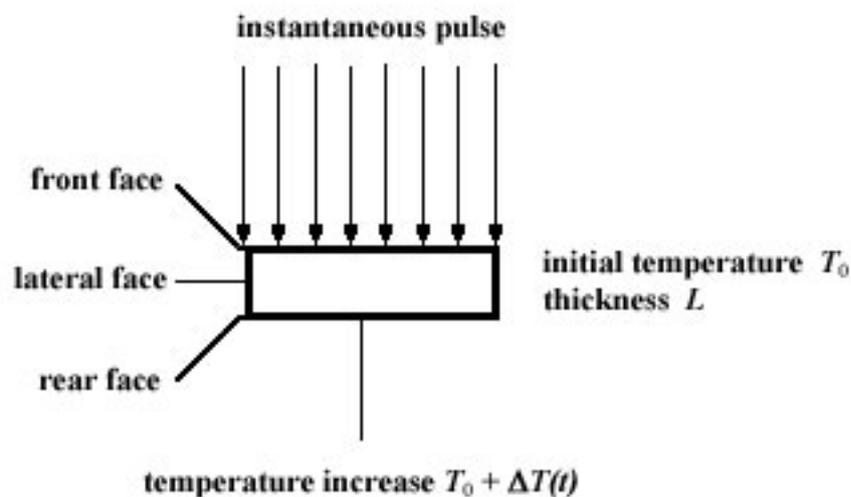
Figure 1- 5 Schematic diagram of the flash method [33]

Figure1-5 shows the schematic of the flash method. A small disk-shape sample, which is initially kept at constant and uniform temperature, is exposed to an instantaneous pulse at the front face. The instantaneous pulse usually comes from a xenon flash lamp [34] or a laser [35], although electron beams have also been used [36]. The temperature increase at its rear face is monitored. The thermal diffusivity is then determined by the temperature-versus-time data. This method was studied and improved by researchers and provided

dependable test results [37-39].

Hot wire technique [40] and hot disk technique [41] are also widely used for thermal diffusivity measurement. Researchers developed several other techniques [42, 43] based on this method for different situations and purposes. The hot wire/disk technique is developed for simultaneous determination of the thermal conductivity and thermal diffusivity of various materials. This method embeds a hot wire within the test material, or puts a hot disk between two identical slab samples. The hot wire/disk serves as both heat source and thermometer. The hot wire/disk is assumed to send out constant and uniform heat flux. A resulting temperature change at a certain position of the material is measured during a certain time period and the temperature data are used to determine the thermal diffusivity of the material.

Although these techniques have advanced the science of thermal diffusivity measurement, several problems are still present. These methods were applied to measure the thermal diffusivity thermal-sprayed coatings. Flash method and thermal wave interferometry method work best if the coating material is opaque. Semi-transparent materials, such as zirconia-based ceramics used to make thermal barrier coatings for turbine blades of aircraft engines, must be coated with carbon, gold, or platinum to improve radiation absorption. However, it has been shown that at high temperatures, evaporation of these layers occurs and reactions with the sample are possible [44]. Therefore, errors would occur to the thermal diffusivity result for the semi-transparent samples. The hot wire method is mostly used for the thermal diffusivity of liquid. Hot plate requires two identical free-standing samples to determine its thermal diffusivity.

Most of the measurements deal with single-layered material, which means that free-standing coatings are needed. Detachment and polishing of the coating is time-consuming and may cause significant damage, especially when dealing with thin coatings. Experiments proved difficult due to curling of the detached coatings [45].

Another problem includes lacking knowledge of other properties that are required in the test. For example, the method of using thermal conductivity value to determine thermal diffusivity requires the thermal capacity and density of the material, which are not available often. The method of the optoacoustic technique would require the optical properties sometimes [33], which are also unknown for random materials.

Another drawback of the current existing thermal diffusivity measurement method is that they have a high demand for the experimental equipment, which is often expensive and complicated to operate. Figs. 1-6 to 1-8 show the schematic graph of typical apparatus setup used in photo thermal technique, flash method and thermal wave interferometry method, respectively. All these methods need complex and high-resolution equipment, such as wave form recorder, noise amplifier, and oscilloscope, to name a few.
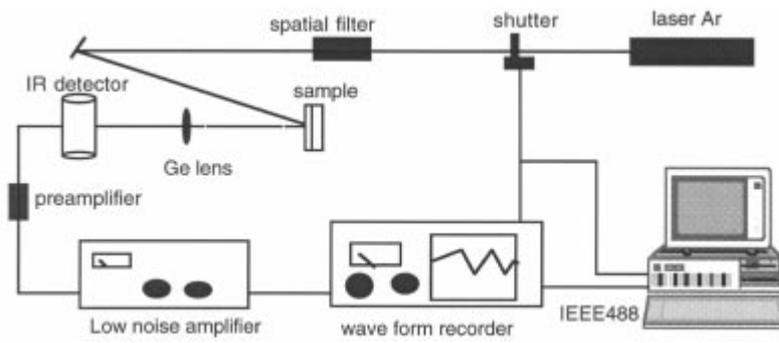
Figure 1- 6   Schematic graph of apparatus setup for photo thermal technique

[46]
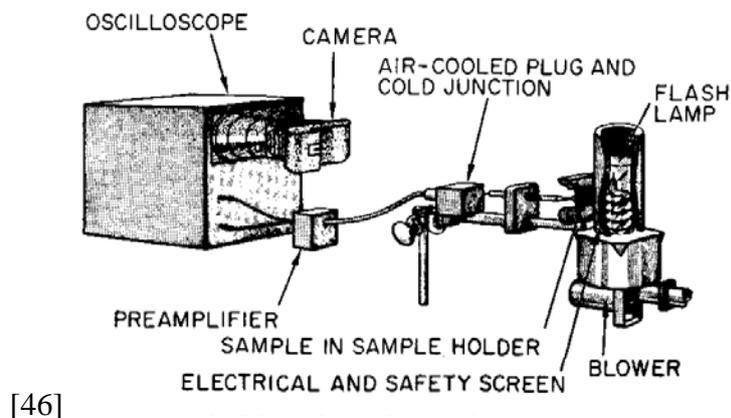
Figure 1- 7   Schematic graph of apparatus setup for flash method [47]
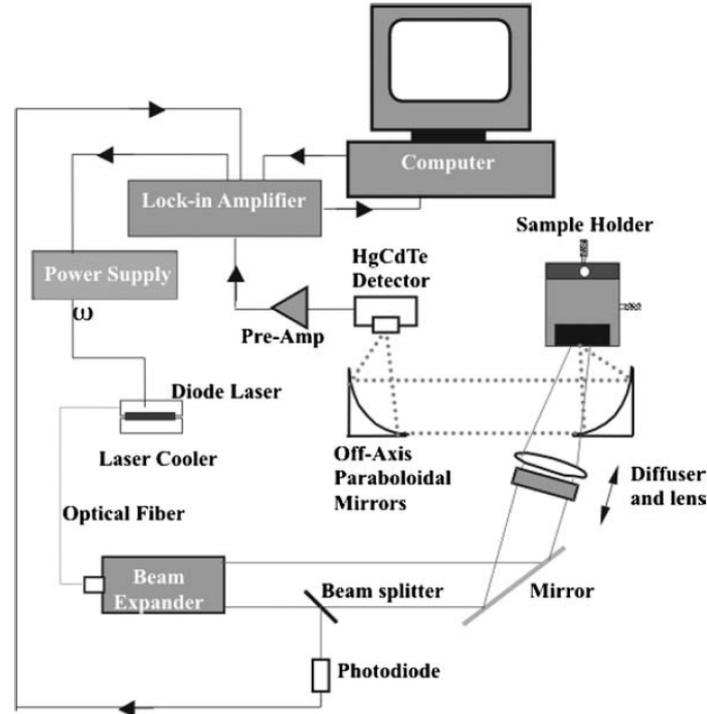
Figure 1- 8 Schematic graph of apparatus setup for thermal wave interferometry method [31]

When the high accuracy of the thermal diffusivity value [30 - 32, 35], higher than 99%, is not necessary, a rough range of thermal diffusivity value could also serve well in the industry. A novel and simple method is needed which could measure thermal diffusivity of both free-standing samples and that of coating without detachment from the substrate. This new measurement method should not require delicate and expensive equipment systems and complicated operation. This method attempts to measure the thermal diffusivity of a wide variety of thermal-sprayed coatings, including semi-transparent and strongly attached coatings, with easy accessed experimental equipment.

1.4 The objectives

The objectives of this thesis include the following:

i) Design and build an experimental method to measure the thermal diffusivity with only temperature logger and hot plate

ii) Estimate thermal diffusivity of single-layered samples

iii) Estimate the thermal diffusivity of thermal-sprayed coating without needing to remove the substrate

iv) Study the application spectrum and repeatability of this thermal diffusivity measurement method

v) Perform the heat loss analysis of the samples and analyze the test graphs for YSZ, copper, and PMMA samples.

1.5 Thesis Organization

This thesis has the following structure:

In Chapter 2, a mathematical model was built to simulate the experiment conditions. Partial differential equations were built on both single-layered sample and two-layered sample. Considering the availability of experimental equipment, boundary conditions were assumed in the model. Duhamel's method and Green's function method were used in this chapter to obtain solutions for these problems.

Chapter 3 describes the experimental equipment setup, and the preparation process of the single-layered samples and two-layered samples. The parameters used in the spraying techniques were listed in tables.

Chapter 4 explains the tuning method developed by this thesis. The data process procedure was explained. The thermal diffusivity method was described step by step. The important step of the algorithm in the MATLAB code was explained in details.

Chapter 5 presents the thermal diffusivity results of the single-layered samples and of the coating fabricated on two-layered samples. The different feature and thermal diffusivity results trend were observed, studied and

explained by the heat loss analysis.

Chapter 6 concludes this thesis. It shows the application spectrum of this tuning method developed in this thesis and makes recommendations for better results in further research.

Chapter 2: Mathematical Model and analytical solutions

This mathematical model was developed to predict the temperature profile for the designed experiment. When heat conduction problem was developed, the availability of experiment equipment and technique was considered. Some assumptions were introduced to simplify the model mostly, while ensuring good simulation of the specially designed experiment. Considering the machining technique and easy access of slab samples, Cartesian coordinates were used to develop the model.

When the mathematical heat conduction models were developed, some necessary assumptions were applied to simplify the problem. Analytical solutions were calculated. Heat transfer occurs when a temperature gradient exists in a body. Thermal diffusivity represents the speed at which heat diffuses in a body. Large thermal diffusivity values could cause faster heat transfer process through a material. To make observation of the thermal diffusivity of a certain material, we need to know how fast heat transfers through the body. Hence, we need to create a temperature gradient within the material to study thermal diffusivity. An effective way to create a temperature gradient is to add a heat source at one of the boundaries. Therefore, models for both single-layered and two-layered conduction problems were developed as partial differential equations (PDE) with temperature boundary condition.

When developing the mathematical model, since it is developed based on experiments, the availability of the experiment equipment was considered. In this chapter, not only the mathematical problems were studied, the experiment factors, which were simulated by mathematical problems, were considered in

each step, to make the model and experiment (which will be described in Chapter 3) more compatible.

2.1 Single-layered model

2.1.1 Single-layered model with one temperature boundary condition
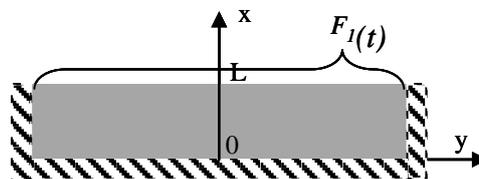
Figure 2- 1 Single-layered model

A single-layered model was the model developed on single-layered sample, and it was studied first. Fig. 2-1 shows a schematic of the heat transfer model. All the assumptions were made to simplify the problem and match the availability of the experiment equipment. The model was developed in a Cartesian coordinate system, since most of the samples are slabs. The thickness of the object is much smaller than the width and length of the sample. Therefore, the problem was assumed as one-dimensional. One surface of the slab ($x = 0$) is in contact with a heat source and all the other boundaries of the object are assumed to be insulated. No heat generation was assumed within the object to keep problem simple. One of the boundary conditions (at $x = 0$) used the adiabatic boundary condition. The other boundary condition (at $x = L$) was assumed to be time-dependent temperature boundary condition, which could be easily adjusted in the experiment.

The model sample is of thickness L. The temperature in the body is uniform as T_i before heating the sample. Thermal properties, such as thermal

diffusivity, are constant. According to the assumptions above and the boundary conditions, a PDE was developed as follows:

Governing equation:

$$\frac{\partial^2 T}{\partial x^2} = \frac{1}{\alpha}\frac{\partial T}{\partial t} \qquad 0 \le x \le L, \quad t \ge 0 \tag{2-1}$$

Boundary condition:

$$T(L,t) = F_1(t) \qquad t > 0 \tag{2-2}$$

$$\frac{\partial T(0,t)}{\partial x} = 0 \qquad t > 0 \tag{2-3}$$

Initial temperature condition

$$T(x,0) = T_i \qquad 0 \le x \le L \tag{2-4}$$

Where:

$T(x,t)$ is the temperature in the body, depending on position x and time t

α is the constant thermal diffusivity

L is the thickness of the sample

T_i is the uniform initial temperature

$F_1(t)$ *is* the temperature boundary condition at $x = L$

The governing equation is homogeneous, and one of the boundary condition Eqn. (2-3) is homogeneous. The temperature boundary condition Eqn. (2-2) is time dependent. Therefore, Duhamel's superposition integral method [48] was used to solve this time dependent boundary condition. Introducing $\theta = T - T_i$, the initial condition could be homogeneous. The whole equation changes into

the following form:

Governing equation:

$$\frac{\partial^2 \theta}{\partial x_2} = \frac{1}{\alpha} \frac{\partial \theta}{\partial t} \qquad 0 \le x \le L, \quad t \ge 0 \tag{2-5}$$

Boundary condition:

$$\theta(L,t) = F_1(t) - T_i \qquad t > 0 \tag{2-6}$$

$$\frac{\partial \theta(0,t)}{\partial x} = 0 \qquad t > 0 \tag{2-7}$$

Initial temperature condition

$$\theta(x,0) = 0 \qquad 0 \le x \le L \tag{2-8}$$

With the established solution form of Duhamel's method, the solution is calculated as:

$$\theta(x,t) = F(0)\overline{\theta}(x,t) + \int_0^t \frac{d(F(\tau) + T_i)}{d\tau} \overline{\theta}(x,t-\tau)d\tau = T_i + \int_0^t \frac{dF(\tau)}{d\tau} \overline{\theta}(x,t-\tau)d\tau \tag{2-9}$$

$F(\tau)$ is the temperature boundary condition at $x = L$.

$\overline{\theta}(x,t)$ is the solution to the homogeneous problem, where $\overline{\theta}(L,t) = 1$. The auxiliary problem is:

$$\frac{\partial^2 \overline{\theta}}{\partial x_2} = \frac{1}{\alpha} \frac{\partial \overline{\theta}}{\partial t} \qquad 0 \le x \le L, \quad t \ge 0 \tag{2-10}$$

Boundary condition:

$$\overline{\theta}(L,t) = 1 \qquad t > 0 \tag{2-11}$$

$$\frac{\partial\bar{\theta}(0,t)}{\partial x}=0 \qquad t>0 \tag{2-12}$$

Initial temperature condition

$$\bar{\theta}(x,0)=0 \qquad 0\le x\le L \tag{2-13}$$

The procedure to solve this auxiliary problem is attached in Appendix A. The solution to the auxiliary problem is:

$$\bar{\theta}=\sum_{n=1}^{\infty}\frac{4\cdot(-1)^{n}}{(2n-1)\pi}\cos[\frac{(2n-1)\pi}{2a}x]\cdot\exp(-\alpha\frac{(2n-1)^{2}\pi^{2}}{4a^{2}}t)+1 \tag{2-14}$$

Substitution of Eqn. (2-14) into Eqn. (2-9), and noting that $\theta=T-T_{i}$, the solution for the slab temperature distribution is:

$$T(x,t)=\int_{0}^{t}\frac{dF(t)}{d\tau}\left(\sum_{n=1}^{\infty}\frac{4\cdot(-1)^{n}}{(2n-1)\pi}\cos[\frac{(2n-1)\pi}{2a}x]\cdot\exp(-\alpha\frac{(2n-1)^{2}\pi^{2}}{4a^{2}}t)+1\right)d\tau+T_{i}$$

$$\tag{2-15}$$

2.1.2 Single-layered model with two temperature boundary conditions

Another heat conduction model was built, as shown in Fig. 2-2. in this model, both the boundary conditions are temperature boundary conditions. In the second model, the adiabatic boundary condition at $x=0$ is changed into another temperature boundary condition.
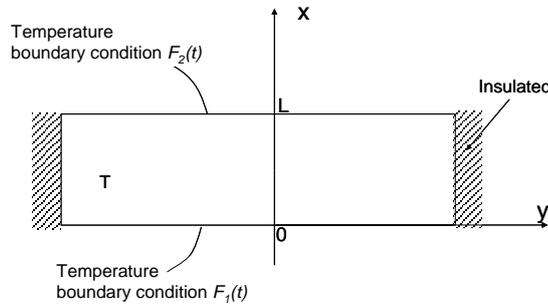
Figure 2- 2 The heat conduction model with two temperature boundary conditions

The governing equation of the two-time-dependent-boundary-condition problem is the same as the heat transfer problem in Fig. 2-1. It had no heat source within the sample and is modeled as a one-dimensional problem, due to the small cross-sectional thickness of the slab. Then its governing equation is:

$$\frac{\partial^2 T}{\partial x_2} = \frac{1}{\alpha}\frac{\partial T}{\partial t} \qquad 0 \le x \le L, \quad t \ge 0 \tag{2-16}$$

Boundary condition:

$$T(0,t) = F_1(t) \qquad t > 0 \tag{2-17}$$

$$T(L,t) = F_2(t) \qquad t > 0 \tag{2-18}$$

Initial condition

$$T(x,0) = T_i \qquad 0 \le x \le L \tag{2-19}$$

The problem is also solved by Duhamel's method as well, and the analytical solution is

$$
\begin{aligned}
T(x,t) \\
= \frac{2T_i}{L}\sum_{m=1}^{\infty}\int_{x'=0}^{L} e^{(-\alpha\beta_m^2 t)} \cdot \sin(\beta_m x)\cdot\sin(\beta_m x')dx' + \frac{2\alpha}{L}\sum_{m=1}^{\infty}\int_{\tau=0}^{t}\beta_m \cdot e^{(-\alpha\beta_m^2(t-\tau))}\cdot\sin(\beta_m x)\cdot F_1(\tau)d\tau \\
-\frac{2\alpha}{L}\sum_{m=1}^{\infty}\int_{\tau=0}^{t}\beta_m \cdot e^{(-\alpha\beta_m^2(t-\tau))}\cdot\sin(\beta_m x)\cdot\cos(\beta_m L)\cdot F_2(\tau)d\tau
\end{aligned}
$$

$$\tag{2-20}$$

where $\cos(\beta_m L) = 1$

Therefore, the eigenvalue is

$$\beta_m = m\pi\big/L \tag{2-21}$$

With this analytical solution, the temperature distribution during the experiment at any position of the sample could be predicted with the proper properties of the material.

Fig. 2-3 shows the comparison of the two conduction models. When $F_1(t) = F_2(t) = F(t)$, with the symmetry theory, the temperature distribution of Fig. 2-3(a) is the same as the temperature distribution in the box shown in Fig. 2-3(b).

<div align="center">(a)   (b)</div>
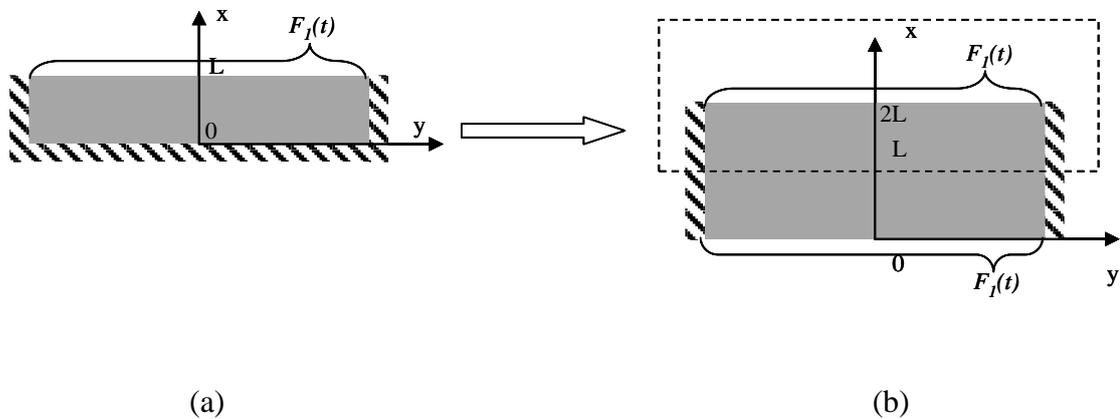
<div align="center">**Figure 2- 3** The comparison of two heat conduction models</div>

The heat transfer problem of Eqns. (2-16) to (2-19) has more flexible boundary conditions. Both the boundary conditions are time-dependent temperature boundary conditions. With proper experimental equipment, saying two heat sources and two temperature boundary condition measurements, this problem would be easy to perform and could give a better model for the experiment problem, since the boundary condition at $x = 0$ was actually measured by experiment equipment instead of assuming an ideal boundary condition. As for this research, the experiment equipment is limited; hence only one time-dependent temperature boundary condition was applied in the experiment. The model in Fig. 2-3(b) was used for single-layered problem.

2.2 Two-layered model

Two-layered model is the heat conduction model with two layers of slabs in perfect contact with each other. This problem is solved by Green's function method.

2.2.1 Green's function

The most commonly used method to solve heat conduction problem is the separation of variables. It is the most efficient solution techniques for some kind of PDE problems. However, the heat conduction problem of two-layered model could not be solved by this classic method alone due to the nonlinear temperature boundary condition. Green's function [49], accompanied with orthogonal expansion technique, was used to solve this two-layered conduction problem with time-variable temperature boundary condition.

Green's function method deals with general kinds of heat conduction problems, and tries to seek a form that gives the solution in terms of all the data, such as the boundary condition, initial condition and any other homogeneous term in the PDE.

Green's function method introduced the idea of heat source. The boundary conditions and any inhomogeneous factors are represented in form of heat sources. The temperature distribution in an object was decided by the heat source within this object. If temperature distribution caused by every heat source could be decided, the temperature distribution in the real object could be decided by the superposition of all the temperature distribution caused by every heat source.

Normally, the non-zero solution of linear partial differential equation is from nonhomogeneous boundary conditions, or non-zero initial conditions or

nonhomogeneous governing equation. As for the effect of these nonhomogeneous elements, the basic idea of Green's function is to study the nonhomogeneous factor one by one. Each of the nonhomogeneous factors was assumed as a heat source in a homogenous problem. The solutions from these homogeneous problems are called Green's function. By adding the Green's function (the solution of each heat source problem), the solution of the original problem could be decided.

It gives the solution to a general three-dimensional nonhomogeneous boundary-value problem, which is:

$$\nabla^2 T(r,t) + \frac{1}{k}g(r,t) = \frac{1}{\alpha}\frac{\partial T(r,t)}{\partial t} \qquad in\ region\ R \qquad t > 0 \qquad (2\text{-}22)$$

$$k_i\frac{\partial T}{\partial r_i} + h_i T = h_i T_{\infty i} \equiv f_i(r,t) \qquad on\quad S_i \qquad t > 0 \qquad (2\text{-}23)$$

$$T(r,t) = F(r) \qquad for\quad t = 0\quad in\ region\ R \qquad (2\text{-}24)$$

This problem was solved by considering its auxiliary problem of the same region R:

$$\nabla^2 G(r,t|r',\tau) + \frac{1}{k}\delta(r - r')\delta(t - \tau) = \frac{1}{\alpha}\frac{\partial G(r,t)}{\partial t} \qquad in\ region\ R \quad t > \tau \qquad (2\text{-}25)$$

$$k_i\frac{\partial G}{\partial r_i} + h_i G = 0 \qquad on\quad S_i \qquad t > \tau \qquad (2\text{-}26)$$

The solution is:

$$\begin{aligned}
T(r,t) = &\int G(r,t|r',\tau)\big|_{\tau=0} F(r') \\
&+ \frac{\alpha}{k}\int_{\tau=0}^{t} d\tau \int_R G(r,t|r',\tau)g(r',\tau)dv' \\
&+ \alpha\int_{\tau=0}^{t} d\tau \sum_{i=1}^{N} \int_{s_i} G(r,t|r',\tau)\big|_{r'=r_i} \frac{1}{k_i} f_i(r',\tau)ds_i'
\end{aligned} \qquad (2\text{-}27)$$

For the problem described in this thesis, it is required that the problem is fit into the form of the general problem. The two-layered heat conduction problem is one-dimensional and the coordinates are Cartesian coordinates. One-dimensional Laplacian operator and one-dimensional delta function was applied to the governing equation. Green's function $G(r,t|r',\tau)$ is turned into the form $G(x,t|x',\tau)$. There are two boundary conditions in a one-dimensional conduction problem; therefore, there are two summations in the third part of Eqn. (2-27). The solution of one-dimensional case is reduced to:

$$
\begin{aligned}
T(x,t) = & \int_L G(x,t|x',\tau)\Big|_{\tau=0} F(x')dx' \\
& + \frac{\alpha}{k}\int_{\tau=0}^t d\tau \int_R G(x,t|x',\tau)g(x',\tau)dx' \\
& + \alpha\int_{\tau=0}^t d\tau \sum_{i=1}^2 \int_{s_i} G(x,t|x',\tau)\Big|_{x'=x_i} \frac{1}{k_i} f_i
\end{aligned}
\tag{2-28}
$$

The first term on the right-hand side of the above equation is the effect from the initial temperature condition $F(x')$. In this research, it is represented by constant temperature T_i that was measured by thermocouple. Green's function at $\tau = 0$ is multiplied by the initial temperature condition and integrated over the thickness L. The second term is for the contribution of the energy generation $g(r,t)$ on the temperature distribution. The last term is for the contribution of the nonhomogeneous terms $f_i(r',\tau)$ of the boundary conditions on the temperature distribution. In this research the first kind of boundary condition—the temperature boundary condition was applied. According to the Eqn. (2-26), it requires $k_i = 0$ and $h_i = 1$. When k_i equals zero, it could not be applied to the solution--Eqn. (2-28) directly, since the zero value k_i could not be placed as denominator. Eqn. (2-26) was changed to another form into Eqn. (2-29).

$$-\frac{\partial G}{\partial r_i}/h_i = G/k_i \qquad on \quad S_i \quad t > \tau \tag{2-29}$$

Substituting the one dimensional version of Eqn. (2-29) into (2-28), with some simplification, the solution to the problem was changed into the form:

$$T(x,t) = T_i \int_L G(x,t|x',\tau)dx' + \alpha \int_{\tau=0}^t d\tau \left[-\frac{\partial G}{\partial x'}\bigg|_{x'=0} F_1(\tau) - (-\frac{\partial G}{\partial x'}\bigg|_{x'=L})F_2(\tau) \right] \tag{2-30}$$

By working on the homogeneous situation of this problem, we could calculate the Green's function $G(x,t|x',\tau)$ and its derivative. The Green's function is the kernel part of this method and the determination process is shown in details in Appendix A.

2.2.2 Application of Green's function method to the two-layered sample

The most efficient way to deal with multi-layer problem is the application of Green's function method. It deals with all non-homogeneous problems in the same manner.
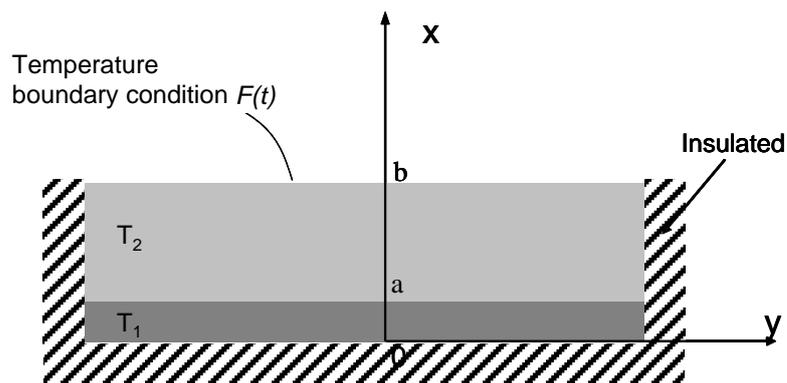
Figure 2- 4 Two-layered model

Figure 2-4 shows the schematic of the conduction model for two-layered samples, which is called two-layered model. The body is composed of two layers. Properties of layer one are described with subscript 1; while that of

layer two is described with subscript 2. The two layers are assumed to have perfect contact with each other. McDonald *et al.* [50] found that the thermal contact resistance between thermal-sprayed droplets and substrate was of the order of 10^{-7} m^{2}-K/W. The thickness of a typical coating would be of order 10^{-3} m [11, 12], and the thermal conductivity of thermal-sprayed materials (ceramics, metals, metal alloys) is normally within the magnitude range of 0.1 W/m-K to 500 W/m-K [41, 43, 52], and the thermal conductivity of the test materials studied this thesis was within the range of 0.14 W/m-K (PMMA) [52] to 401 W/m-K (copper) [45]. The thermal resistance through the coating "R" is decided by thickness "t" and thermal conductivity "k" as $R = t / k$. Though calculation, the thermal resistance through the coating layer is within the range from 10^{-5} m^{2}-K/W to 10^{-2} m^{2}-K/W, which is much greater than the contact resistance (10^{-7} m^{2}-K/W) between layers. Therefore, the much smaller contact resistance between the coating and substrate (10^{-7} m^{2}-K/W) is negligible compared with the thermal resistance of the coating layer (10^{-5} m^{2}-K/W to 10^{-2} m^{2}-K/W). Hence, the two layers could be assumed to be in perfect contact in the two-layered model to simulate thermal sprayed samples.

The origin is built from the bottom of the lower layer. From the origin, the thickness of layer one is "a", the total thickness of the composite body is "b". The size of the sample in y direction is much bigger than the size in x direction, and the surface in y direction is insulated. Therefore, the problem is one-dimensional. No energy source or sink exists inside the body. The temperature in the body is uniform before the temperature gradient is introduced. The two layers have different properties, such as thermal diffusivity. Thermal diffusivity for each layer was assumed to be constant during the experiment. The bottom surface of the body is insulated; the top surface has a time variable boundary condition after time 0.

The governing equations for the temperature distribution in the composite medium are:

$$\frac{\partial^2 T_1}{\partial x^2} = \frac{1}{\alpha_1} \frac{\partial T_1}{\partial t} \quad 0 \le x \le a \quad t \ge 0 \tag{2-31}$$

$$\frac{\partial^2 T_2}{\partial x^2} = \frac{1}{\alpha_2} \frac{\partial T_2}{\partial t} \quad a \le x \le b \quad t \ge 0 \tag{2-32}$$

The boundary and initial conditions are:

$$\frac{\partial T_1(0,t)}{\partial x} = 0 \quad x = 0 \quad t \ge 0 \tag{2-33}$$

$$T_1(a,t) = T_2(a,t) \quad x = a \quad t \ge 0 \tag{2-34}$$

$$\frac{\partial T_1(a,t)}{\partial t} = \frac{k_2}{k_1} \frac{\partial T_2(a,t)}{\partial t} \quad x = a \quad t \ge 0 \tag{2-35}$$

$$T_2(a,t) = F(t) \quad x = b \quad t \ge 0 \tag{2-36}$$

The boundary conditions are adiabatic condition at $x = 0$, and time-variable temperature boundary condition at $x = b$. Eqns. (2-34) and (2-35) are the interface boundary condition with perfect contact, meaning equal temperature and equal heat flux separately. The initial condition of both layers was assumed as the same.

$$T_1(x,0) = T_i \quad 0 \le x \le a \quad t = 0 \tag{2-37}$$

$$T_2(x,0) = T_i \quad a \le x \le b \quad t = 0 \tag{2-38}$$

This is a problem with nonhomogeneous boundary condition. To solve the problem, the first step is to transform this problem into several simpler problems with homogeneous boundary conditions.

The original problem has nonhomogeneous boundary condition at $x = b$. In order to transform this time-dependent problem into one with homogeneous boundary conditions, we develop the temperature profile solution of the

system, $T_j(x,t)$ (j = 1, 2, representing the layer number) by applying superposition of two simpler problems in the following form:

$$T_j(x,t) = \theta_j(x,t) + \psi_j(x) \cdot F_j(t) \qquad j = 1,2 \tag{2-39}$$

In Eqn. (2-39) the element $\psi_j(x)$ could be determined by solving a steady-state problem; the element $\theta_j(x,t)$ could be decided by a time-dependent problem, subjected to homogeneous boundary condition. The two problems were solved separately and substituted later into the final solution.

The element $\psi_j(x)$ was decided by the following heat transfer problem. It is a steady-state problem with one non-homogeneous boundary condition. The equation groups are listed:

$$\frac{d^2(\psi_1)}{dx^2} = 0 \tag{2-40}$$

$$\frac{d^2(\psi_2)}{dx^2} = 0 \tag{2-41}$$

The equation group needs four boundary conditions, which are:

$$\frac{d\psi_1(0)}{dx} = 0 \tag{2-42}$$

$$\frac{d\psi_1(a)}{dx} = \frac{k_2}{k_1} \frac{d\psi_2(a)}{dx} \tag{2-43}$$

$$\psi_1(a) = \psi_2(a) \tag{2-44}$$

$$\psi_2(b) = 1 \tag{2-45}$$

$\theta_j(x,t)$ are solutions of the following time-dependent problem, subject to homogeneous boundary conditions.

$$\frac{\partial^2 \theta_j}{\partial x^2} + F_2(t)\frac{d^2\psi_j}{dx^2} = \frac{1}{\alpha_j}[\frac{\partial \theta_j}{\partial t} + \psi_j(x)\frac{dF_2(t)}{dt}]$$

(2-46)

The boundary conditions are:

$$\frac{\partial \theta_1(0,t)}{\partial x} = 0$$

(2-47)

$$\theta_1(a,t) = \theta_2(a,t)$$

(2-48)

$$\frac{\partial \theta_1(a,t)}{\partial x} = \frac{k_2}{k_1}\frac{\partial \theta_2(a,t)}{\partial x}$$

(2-49)

$$\theta_2(b,t) = 0$$

(2-50)

In the following part, ψ_j and θ_j are solved. Integrating Eqn. (2-40) and Eqn. (2-41), it is obtained that:

$$\psi_1 = c_1 x + c_2$$

(2-51)

$$\psi_2 = c_3 x + c_4$$

(2-52)

Substitute the assumed form of equation in to the boundary conditions to decide the coefficients $c_1,$ $c_2,$ c_3 and c_4.

$$\frac{d\psi_1(x)}{dx} = c_1$$

(2-53)

$$\frac{d\psi_2(x)}{dx} = c_3$$

(2-54)

When $x = 0$, the coefficient c_1 could be calculated.

$$\frac{d\psi_1(0)}{dx} = 0$$

(2-55)

From boundary conditions--Eqns. (2-47) to (2-50), coefficient c_1 could be easily decided.

$$c_1 = 0 \qquad (2\text{-}56)$$

With the knowledge of c_1, substitute the assumption, we could get:

$$c_2 = c_3 a + c_4 \qquad (2\text{-}57)$$

By boundary condition (2-11), we could get:

$$\frac{k_2}{k_1} c_3 = 0 \qquad (2\text{-}58)$$

Therefore,

$$c_3 = 0 \qquad (2\text{-}59)$$

$$c_2 = c_4 = 1 \qquad (2\text{-}60)$$

Since all the coefficients were decided, the function $\psi_1(x)$ and $\psi_2(x)$ were available.

$$\psi_1(x) = 1 \qquad (2\text{-}61)$$

$$\psi_2(x) = 1 \qquad (2\text{-}62)$$

The next step is to solve function θ_1 and θ_2. The two functions were decided by the following equation groups. It is known from Eqn. (2-61) and Eqn. (2-62) that

$$\frac{d^2 \psi_j}{dx^2} = 0 \qquad (2\text{-}63)$$

Therefore,

$$\frac{\partial^2 \theta_j}{\partial x^2} - \frac{\psi_j(x)}{\alpha_j}\frac{dF_2(t)}{dt} = \frac{1}{\alpha_j}\frac{\partial \theta_j}{\partial t} \qquad (2\text{-}64)$$

Eqn. (2-64) could also be represented as:

$$\frac{\partial^2 \theta_1}{\partial x^2} - \frac{\psi_1(x)}{\alpha_1}\frac{dF_2(t)}{dt} = \frac{1}{\alpha_1}\frac{\partial \theta_1}{\partial t} \qquad (2\text{-}65)$$

$$\frac{\partial^2 \theta_2}{\partial x^2} - \frac{\psi_2(x)}{\alpha_2}\frac{dF_2(t)}{dt} = \frac{1}{\alpha_2}\frac{\partial \theta_2}{\partial t} \qquad (2\text{-}66)$$

To apply the Green's function method to solve this two-layered problem, the equations are rearranged to the following form.

$$\alpha_1 \frac{\partial^2 \theta_1}{\partial x^2} + [\frac{\alpha_1}{k_1} g_1] = \frac{\partial \theta_1}{\partial t} \qquad (2\text{-}67)$$

$$\alpha_2 \frac{\partial^2 \theta_2}{\partial x^2} + [\frac{\alpha_2}{k_2} g_2] = \frac{\partial \theta_2}{\partial t} \qquad (2\text{-}68)$$

Where:

$$g_1 = \frac{-k_1}{\alpha_1}\frac{dF(t)}{dt} \qquad (2\text{-}69)$$

$$g_2 = \frac{-k_2}{\alpha_2}\frac{dF(t)}{dt} \qquad (2\text{-}70)$$

$$F_2 = T_i - F(0) = D \qquad (2\text{-}71)$$

T_i is the initial temperature.

$$\theta_1(x,t) = \int_0^a G_{11}(x,t|x',t)\big|_{\tau=0} \cdot Ddx' + \int_a^b G_{12}(x,t|x',t)\big|_{\tau=0} \cdot Ddx'$$

$$= \int_{\tau=0}^t d\tau\{\int_0^a G_{11}(x,t|x',t)\cdot[\frac{\alpha_1}{k_1} g_1(x',\tau)]dx' + \int_a^b G_{12}(x,t|x',t)\cdot[\frac{\alpha_2}{k_2} g_2(x',\tau)]dx'\}$$

$$(2\text{-}72)$$

$$N_n = \frac{k_1}{\alpha_1}\int_0^a \psi_{1n}{}^2(x')dx' + \frac{k_2}{\alpha_2}\int_a^b \psi_{2n}{}^2(x')dx' \qquad (2\text{-}73)$$

$$G_{11}(x,t|x',\tau) = \sum e^{-\beta_n^{2}(t-\tau)} \frac{k_1}{\alpha_1} \frac{\psi_{1n}(x)\psi_{1n}(x')}{N_n} \tag{2-74}$$

$$G_{12}(x,t|x',\tau) = \sum e^{-\beta_n^{2}(t-\tau)} \frac{k_2}{\alpha_2} \frac{\psi_{1n}(x)\psi_{2n}(x')}{N_n} \tag{2-75}$$

$$\psi_{1n} = A_{1n} \sin(\frac{\beta_n}{\sqrt{\alpha_1}}x) + B_{1n} \cos(\frac{\beta_n}{\sqrt{\alpha_1}}x) \tag{2-76}$$

$$\psi_{2n} = A_{2n} \sin(\frac{\beta_n}{\sqrt{\alpha_2}}x) + B_{2n} \cos(\frac{\beta_n}{\sqrt{\alpha_2}}x) \tag{2-77}$$

ψ_{1n} and ψ_{2n} are solved by the related eigenvalue problem, therefore they are regulated by the following equations.

$$\psi_{2n}(x=b) = 0 \tag{2-78}$$

$$\psi_{1n}(x=a) = \psi_{2n}(x=a) \tag{2-79}$$

$$\frac{\partial \psi_{1n}(a)}{\partial x} = \frac{k_2}{k_1} \frac{\partial \psi_{2n}(a)}{\partial x} \tag{2-80}$$

$$\frac{\partial \psi_{1n}(x=0)}{\partial x} = 0 \tag{2-81}$$

The coefficients are solved.

$$A_{1n} = 0 \tag{2-82}$$

$$A_{2n} = -B_{2n} \arctan(\frac{\beta_n}{\sqrt{\alpha_2}}b) \tag{2-83}$$

$$B_{1n} = B_{2n}[-\arctan(\frac{\beta_n}{\sqrt{\alpha_2}}b) \frac{\sin(\frac{\beta_n}{\sqrt{\alpha_2}}a)}{\cos(\frac{\beta_n}{\sqrt{\alpha_1}}a)} + \frac{\cos\left(\frac{\beta_n}{\sqrt{\alpha_2}}a\right)}{\cos\left(\frac{\beta_n}{\sqrt{\alpha_1}}a\right)}] \tag{2-84}$$

β_n is calculated by the following equation.

$$\left(\sin(\frac{\beta_n b}{\sqrt{\alpha_2}}) \cdot \tan^{-1}(\frac{\beta_n a}{\sqrt{\alpha_2}}) - \cos(\frac{\beta_n a}{\sqrt{\alpha_2}})\right) \cdot \tan(\frac{\beta_n a}{\sqrt{\alpha_1}})$$
$$= -\frac{k_2}{k_1}\sqrt{\frac{\alpha_1}{\alpha_2}} \cdot \left(\cos(\frac{\beta_n a}{\sqrt{\alpha_2}}) \cdot \tan^{-1}\left(\frac{\beta_n b}{\sqrt{\alpha_2}}\right) + \sin(\frac{\beta_n a}{\sqrt{\alpha_2}})\right)$$

(2-85)

B_{2n} is the only unknown coefficient, and solved by the application of the initial temperature condition. With the knowledge of all the coefficients, ψ_i and θ_i are solved. Substitute them to Eqn. (2-39), this problem is solved. The solution is listed in Eqns. (2-86) to (2-89).

$$T_1 = \theta_1(x,t) + F(t) \tag{2-86}$$

where:

$$\theta_1(x,t) =$$
$$-\frac{k_1}{\sqrt{\alpha_1}}\sum_{n=1}^{\infty}\frac{C1^2}{Q_n\beta_n}\sin(\beta_n\frac{a}{\sqrt{\alpha_1}})\int_0^t \frac{dF(t)}{d\tau}e^{(-\beta_n^2(t-\tau))}d\tau\cos(\frac{\beta_n x}{\sqrt{\alpha_1}})$$
$$-\frac{k_2}{\sqrt{\alpha_2}}\sum_{n=1}^{\infty}\frac{C1C3}{Q_n\beta_n}\int_0^t \frac{dF(t)}{d\tau}e^{(-\beta_n^2(t-\tau))}d\tau\cos(\frac{\beta_n x}{\sqrt{\alpha_1}})$$
$$+\frac{Dk_1}{\sqrt{\alpha_1}}\sum_{n=1}^{\infty}\frac{C1^2 e^{(-\beta_n^2 t)}}{Q_n\beta_n}\sin(\frac{\beta_n a}{\sqrt{\alpha_1}})\cos(\frac{\beta_n x}{\sqrt{\alpha_1}})$$
$$+\frac{Dk_2}{\sqrt{\alpha_2}}\sum_{n=1}^{\infty}\frac{C1C3e^{(-\beta_n^2 t)}}{Q_n\beta_n}\int_0^t \frac{dF(t)}{d\tau}e^{(-\beta_n^2(t-\tau))}d\tau\cos(\frac{\beta_n x}{\sqrt{\alpha_1}})$$

(2-87)

The constants involved in the equations were:

$$Q_n = Q_1 + \frac{k_1}{\alpha_1}(Q_2 + Q_3)$$

$$Q_1 = \frac{k_1}{\alpha_1} C1^2 \left[\frac{a}{2} + \sin(\frac{2\beta_n a}{\sqrt{\alpha_1}}) \cdot \frac{\sqrt{\alpha_1}}{4\beta_n} \right]$$

$$Q_2 = \frac{(b-a)}{2}(C2^2 + 1) - \frac{C2\sqrt{\alpha_2}}{2\beta_n} \cdot \left[\cos(\frac{2\beta_n b}{\sqrt{\alpha_2}}) - \cos(\frac{2\beta_n a}{\sqrt{\alpha_2}}) \right]$$

$$Q_3 = \frac{(C2^2 - 1)\sqrt{\alpha_2}}{4\beta_n} \left[\sin(\frac{2\beta_n b}{\sqrt{\alpha_2}}) - \sin(\frac{2\beta_n a}{\sqrt{\alpha_2}}) \right]$$

(2-88)

Where:

$$C1 = \frac{\cos\frac{\beta_n a}{\sqrt{\alpha_2}}}{\cos\frac{\beta_n a}{\sqrt{\alpha_1}}} - \tan^{-1}(\frac{\beta_n b}{\sqrt{\alpha_2}}) \frac{\sin\frac{\beta_n a}{\sqrt{\alpha_2}}}{\cos\frac{\beta_n a}{\sqrt{\alpha_1}}}$$

$$C2 = -\tan^{-1}\frac{\beta_n b}{\sqrt{\alpha_2}}$$

(2-89)

$$C3 = (\sin\frac{\beta_n b}{\sqrt{\alpha_2}} - \sin\frac{\beta_n a}{\sqrt{\alpha_2}}) - C2(\cos\frac{\beta_n b}{\sqrt{\alpha_2}} - \cos\frac{\beta_n a}{\sqrt{\alpha_2}})$$

$$D = T_i - F(t) \quad t = 0$$

The β_n involved in the solution was calculated by the following implicit expressions:

$$\left(\sin(\frac{\beta_n b}{\sqrt{\alpha_2}}) \cdot \tan^{-1}(\frac{\beta_n a}{\sqrt{\alpha_2}}) - \cos(\frac{\beta_n a}{\sqrt{\alpha_2}}) \right) \cdot \tan(\frac{\beta_n a}{\sqrt{\alpha_1}})$$

$$= -\frac{k_2}{k_1}\sqrt{\frac{\alpha_1}{\alpha_2}} \cdot \left(\cos(\frac{\beta_n a}{\sqrt{\alpha_2}}) \cdot \tan^{-1}\left(\frac{\beta_n b}{\sqrt{\alpha_2}}\right) + \sin(\frac{\beta_n a}{\sqrt{\alpha_2}}) \right)$$

(2-90)

It should be noted that the temperature evolution of the second layer T_2 could also be decided by this analytical solution developed above. However, for the thermal diffusivity measurement method developed by this thesis, only T_1 --temperature of the first layer, was needed to determine the thermal diffusivity for the coating. Therefore, the solution for T_2 is not shown in this thesis.

2.3 Summary of mathematical model

In this chapter, heat conduction problems were solved by analytical method. The method of separation of variables is the basic method to deal with partial differential equations. The heat conduction model in this chapter has inhomogeneous and time-dependent boundary conditions, so that more work is needed before the basic method could be applied. For single-layered model, Duhamel's method was applied. For two-layered model, Green's function method was applied. The problem was transformed into several simpler problems and solved by the basic separation of variable method.

This conduction problem has non-homogeneous boundary condition at the outer surface, which was transformed into a problem with homogeneous boundary conditions. This transformation would add a heat generation term into the governing equation. The orthogonal expansion technique, coupled with Green's functions, was used to solve the resulting governing equations for the temperature distribution in the composite medium.

In this chapter, the solution to the single-layered and two-layered conduction problem are calculated and shown in Eqns. (2-20) (2-21) and in Eqns. (2-86) to (2-90). From these equations, it could be seen that the thermal diffusivity values (α in single-layered solution and α_1, α_2 in two-layered solution) play a crucial role in the solution. With the knowledge of thermal diffusivity and the other elements, (such as thickness of the substrate and coating, thermal diffusivity and thermal conductivity of the substrate), temperature profiles could be developed. Vice versa, if the temperature profile is known, and if one of the thermal diffusivity value is the only unknown, thermal diffusivity could be decided by the knowledge of temperature profile. In the thesis, an experiment was designed to measure the temperature profile, which was used to decide the thermal diffusivity value later. Chapter 3

describes the experimental equipment, experimental procedure and the sample preparation techniques.

Chapter 3: Experimental equipment and experiment procedure

The sample, wrapped with insulation (Styrofoam), was kept at room temperature initially. The sample was laid on a hot plate, which was set at a constant temperature (i.e. 50°C to 100°C based on different experiments). The hot plate would create a temperature gradient in the sample, and induce a heat conduction process within the sample. The temperature variation at top surface of the sample was recorded by thermocouples and transferred to a monitor by a data acquisition system (DAS).

The sample tested was either a single-layered slab or two-layered slab. Single-layered samples were of different materials, including aluminum, copper, low carbon steel, PMMA, and PYREX. They were cut directly from the bulk materials into slab shapes. The two-layered slab samples were prepared by flame spraying, plasma spraying or cold spraying , including titanium dioxide (TiO_2) on low carbon steel substrate, TiO_2 on copper substrate, yttria-stabilized zirconia (YSZ) on low carbon steel substrate, and nanostructured TiO_2 on Pyrex substrate.

3.1 Experimental equipment setup

The experimental assembly is shown in Fig.3-1. The equipment assemblies included hot plate that was used to heat the samples, a data acquisition system that was used to record the temperature data during the heat conduction process, and a monitor on which temperature profiles were observed.
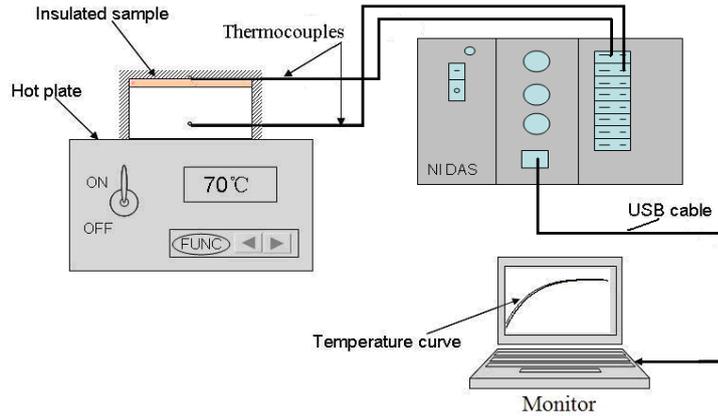
Figure 3- 1 Experiment assembly

The heat source used in the experiment is a hot plate (Type 2600, Thermolyne, Dubuque, IA, USA).   The hot plate has a flat surface and could provide adjustable temperatures.

The flat surface on the hot plate could ensure good contact with the flat samples. The size of the flat surface is 150 mm x 150 mm. The temperature controller of the hot plate is on/off (analog) type; a thermocouple was inserted under the flat surface of the hot plate to monitor its temperature, and provided feedback to the equipment. In this way, the hot plate could be maintained at a constant temperature as set on the LED display window.

The tested sample shown in Fig. 3-1 is a two-layered sample. The upper thin layer represents the coating layer, and the lower thick layer represents the substrate layer. If the tested sample is single-layered, the sample in the assembly graph-Fig. 3-1 is simply one-layered. The insulating material Styrofoam was wrapped on the sample to keep the boundaries adiabatic. Section 3.5.1 describes the insulating procedure in details. Considering that the position of the thermocouple was in the center hot surface, the temperature in the center of the hotplate was closer to the temperature displayed in the LED window. On the entire surface of the hot plate, when the sample was heated on the hot plate, it is hard to guarantee that the sample was heated uniformly. In Chapter 2, the mathematical model used uniform temperature on

the boundary as boundary condition. Compared with the hot plate size (150mm x 150mm), relatively small surface area (40mm x 40mm) of the samples would reduce the error from uneven temperature. Therefore, in the experiment, the samples were prepared with a smaller size and were placed in the center of the heating zone of the hot plate. It should be noticed that the length and width (40mm x 40mm) of the sample are small compared with the size of the hot plate. When compared with the thickness of the sample (3mm - 9mm), the length and width of the sample are large. The ratio of the length and width of the sample to the thickness of the sample is around 10:1. This makes the sample 1-demensional. The one-dimensional assumption is also explained by Biot Number theory. The Biot Number [49] is represented by Eqn. (3-1).

$$Bi = \frac{hL_c}{k} = \frac{(L_c / kA_{surface})}{(1 / hA_{surface})} = \frac{(internal\ thermal\ resistance)}{(external\ thermal\ resistance)} \quad (3\text{-}1)$$

where:

h is the convective heat transfer coefficient

$A_{surface}$ is the surface area

L_c is the characteristic length, defined as $L_c = \dfrac{V_{body}}{A_{surface}}$

k is the thermal conductivity of the material.

Referred to Eqn. (3-1), the external thermal resistance is infinite on the side surfaces (in Figs. 2-1, 2-2, 2-4), since there is no convection ($h = 0$) at the boundaries due to existence of the insulating materials. The internal thermal resistance of the sample is calculated roughly. According to the size of the sample (6mm x 40mm x 40mm), $L_c = 3.4$. The tested samples its thermal conductivity within the range of 0.14 W/m-K (PMMA) [52] to 401 W/m-K

(copper) [45]. Surface area is $0.004m^2$. From Eqn. (3-1), the internal thermal resistance range is from 2.1K/W to 6070K/W. Compared with infinite external thermal resistance, Bi number is 0. Therefore, the sample is partially lumped [49] in the horizontal directions. Due to the existence of heat source at the bottom, the sample had sharp temperature gradient in x direction. The above explanation verifies the 1-D conduction assumption used in Chapter 2.

The experiments were conducted several times with different boundary conditions, to test its repeatability. Temperature boundary condition is easy to be manipulated and variation of temperature boundary condition is effective. Therefore, different temperature conditions were obtained by simply adjusting the temperature set on the hot plate.

In this research project, experiments were carried with the hot plate fixed at a certain temperature. Higher temperature could create greater temperature gradient. However, if the temperature was set above 100°C, the insulator, which was used to wrap the sample to create adiabatic boundary condition, started to deform. Tests were performed by setting the temperature on the hot plate to 50°C, 60°C, 70°C, 80°C and 90°C, separately. Temperatures higher than 100°C would result in melting and deformation of the insulation.

The data acquisition system (Model SCXI-1000, National Instruments, Austin, TX, USA) could take 8 measurements of temperature, show data in real-time form, and export temperature data to Excel file. In this research up to 4 channels were used simultaneously. During the experiment, the temperature was taken at a frequency of 10 Hz.

The data taken by the data acquisition system were shown in a monitor, which was connected with the DAS by a USB cable. After the temperature profiles were collected, the data was transferred into an Excel file.

3.2 Experimental sample preparation

As mentioned at the beginning of the chapter, two types of samples were tested, namely single-layered samples and two-layered samples. For single-layered samples, copper and aluminum were studied as metal materials with high thermal diffusivity values. PMMA and PYREX were studied due to their low thermal diffusivity values. Alumina (AF6, Refractron Technologies Corp, NY, USA) was studied as a porous sample. For the two-layered experiments, TiO_2 on a copper substrate and TiO_2 on a low carbon steel substrate were studied to observe the effect of substrate on the coating thermal diffusivity results. YSZ on low carbon steel was chosen to study the effect of low diffusivity coating on high diffusivity substrate.

Single-layered samples were simply cut from a bulk material. The two-layered samples were prepared by spraying a coating on the single-layered material, which was called substrate. Two kinds of spraying technique were involved in this study, namely cold spraying and flame spraying.

3.2.1 Preparation before spraying

Before flame spraying and cold spraying was conducted, some preparation procedure was needed, including particle sieving and grit blasting for the substrate.

In the spraying industry, a fine balance between particle size, density, temperature and velocity are important criteria to achieve the desired coating. Therefore, the coatings were fabricated according to recipes proposed by the supplier or the established by the lab to achieve best coating quality.

In this research, before being sprayed, powders were sieved by a powder siever (TYLER Ro-Tap® 8" RX-29, W.S. Tyler, Alberta, Canada), shown in Fig. 3-2. Table 3-1 shows the information of coating materials, powder sizes and product information.

Figure 3- 2 Photograph of Tyler powder seiver

Powder material	Spray technique	Particle size	Company	Product No.
TiO_2	Flame spray	-88+7.8μm	Sulzer Metco	Metco 102
YSZ	Air plasma spray	-176+11μm	Sulzer Metco	Sulzer Metco 2460 NS
Nano TiO_2	Flame spray	Nano size	Altair Nanotechno-logies	Altairnano $TiCP_2$-P-01-0506 28-289
Copper	Cold spray	-45+5μm	Centerline SST	SST-C5003

Table 3- 1 Powder information and size

Both two-layered samples and single-layered samples were trimmed into a slab shape to be suitable for the experiment. The size of both single-layered samples and substrates for two-layered samples are listed in Table 3-2.

	Material	flat surface	thickness
Single-layered sample	PMMA	39mm x 39mm	3mm
Single-layered sample	PMMA	40mm x 40mm	6mm
Single-layered sample	copper	36mm x 15mm	3mm
Single-layered sample	copper	38mm x 33 mm	9mm
Single-layered sample	Aluminum	42mm x 26mm	3mm
Single-layered sample	Aluminum	40mm x 30mm	5mm
Single-layered sample	30% porous Al_2O_3	41mm x 40mm	8mm
Single-layered sample	PYREX	35mm x 35mm	3mm
Single-layered sample	PYREX	35mm x 35 mm	6mm
Substrate	Low carbon steel	34mm x 32 mm	6.29mm
Substrate	PYREX	35mm x 32mm	3mm
Substrate	PYREX	35mm x 30mm	6mm
Substrate	Copper	33mm x 33mm	9.42mm

Table 3- 2 Size for single-layered samples and substrate for two-layered samples

To ensure proper bonding between the coating and substrate, before coating was sprayed onto the substrate, the substrate should be grit blasted before all the spraying process. Grit blasting is to spray a large number of abrasive pellet particles on to the substrate. This procedure would not only create a rough surface to promote adhesion of the coating, but also remove the surface oxides and contaminants. In this research, a grit-blaster (TRINCO™ MODEL 30, Trinco Tool Company, Fraser, United States) was used and the #24 alumina served as the grit particles, shown in Fig. 3-3.

Figure 3- 3 Photograph of Trinco grit-blaster

Before the spraying process, the grit blasted substrate was fixed on a holder. The parameters were set on the spraying equipment according to the recipes, which are listed in Table 3-3. The torches, operated by a programmed robot (HP 20, MOTOMAN, West Carrollton, Ohio, United States) shown in Fig. 3-4, passed rapidly across the substrate.

3.2.2 Spraying parameters

In this research the air plasma spraying was performed by 3MBM ThermoSpray Gun (Sulzer Metco, Inc., Westbury, NY, USA), whose spraying parameters are listed in Table 3-3. The flame spraying was performed by 6P-II flame spray torch (Sulzer Metco, Westbury, NY, USA), whose spraying parameters are listed in Table 3-4. The cold spraying was performed by centerline cold spray torch (SSM-P3800-001, Centerline, ON, Canada) was applied, whose spraying parameters are listed in Table 3-5.

Figure 3- 4 Photograph of programmed robot

3.3 Thermocouple arrangement

Thermocouples were attached on the sample before the heat conduction experiment started. Initial temperature and temperature variation during the entire conduction process were monitored. The thermocouples were attached on the sample on its surface or into the sample by drilling a hole into the sample. Fig. 3-5 shows the possible positions on a single-layered sample where the thermocouple would be attached. As shown in the figure, the bottom surface of the sample was heated by a hot plate, while all the other surfaces were insulated.

Primary Gas	Argon
Secondary Gas	Hydrogen
Ar flow rate	90 SCFH
H2 flow rate	20 SCFH
Ar pressure	75 psig
H2 pressure	100 psig
Carrier gas pressure	60 psig
Carrier gas flow rate	14 SCFH
Standoff distance	2.5 in
Current	500A
Voltage	60V

Table 3- 3 Air plasma spraying parameters for YSZ coating on low carbon steel substrate

Powder feed rate	35%
Air Pressure (psi)	124
Air Temperature (°C)	400
Stand-off distance (mm)	10
Torch speed (mm/s)	5

Table 3- 4 Cold spraying parameters for copper coating

Considering the symmetry effect, the possible thermocouple positions on the left surface would have the same effect as the right, the front and the

back ones. Therefore, the thermocouple arrangement is shown only on the visible surfaces and bottom of the sample.

Coating Material	Conventional TiO$_2$	Nanostructure TiO$_2$
Powder feed rate (FMR)	90	110
Number of passes	15	9
Carrier gas flow rate (SCFH)	20	
Vibrating air pressure (psi)	70	
Torch stand-off distance (mm)	100	
Compressed air pressure (psi)	None	
Acetylene flow rate (NLPM)	22	
Oxygen flow rate (NLPM)	35	
Torch speed (mm/s)	400	
Increment (mm)	3	

Table 3- 5 Flame spraying parameters for other two-layered samples

There are seven possible positions for the thermocouple including position A to G. Their shortcomings, advantages and compatibility with the mathematical model are compared in the next graph. Positions "*A*", "*F*" and "*E*" with 1 mm diameter and 8 mm depth were applied on the sample.
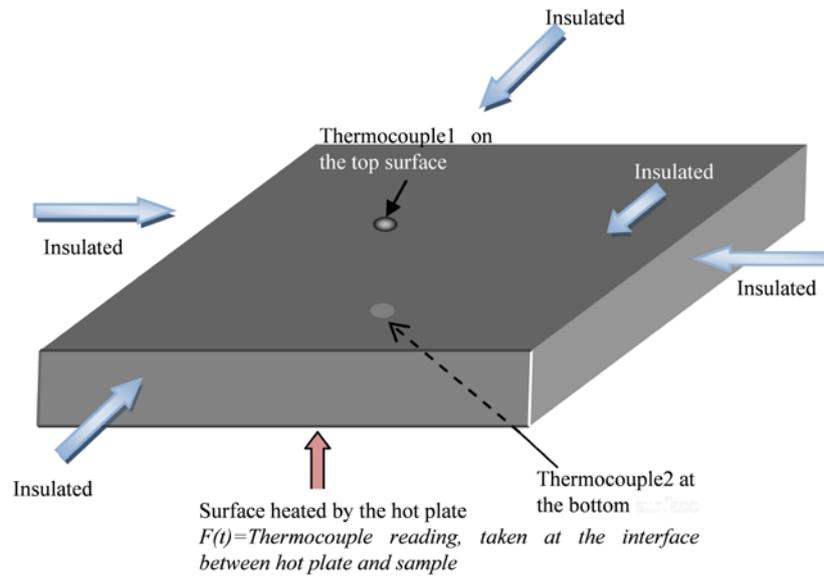
Figure 3-5 Possible positions on a single-layered sample where thermocouples would be attached

On the top surface, thermocouples could be attached, since this was a one-dimensional problem, "A" and "B" were supposed to have the same temperature profile from the model prediction. But considering the experiments were not as ideal as assumed, there would be heat loss from sides of the sample. Position "B" might have more error. Compared with position "B", position "A" is at the center of the sample, which would be more representative for the temperature on the top surface. With the same reasoning, position "F" is better than other positions on the bottom.

Position "C" is on top of the right side surface. Similar to the disadvantage of position "B", for a one-dimensional problem, the sides would have more heat loss, which was not considered in the model; therefore, position on the side would suffer more error. And also, the one-dimensional model would be sensitive to the position at the vertical direction. Thermocouple has to be welded on to the sample, since temporary attachment would result thermocouple movement during the repeated experiments. Due to the limitation of this position, "C" was not considered in the experiment.

To solve the disadvantage of position "C", two other positions, namely "E" and "D", were considered. On the front surfaces, possible positions "E" and "D" represent thermocouple holes. It means a hole drilled into the sample from the side surface. Thermocouple would be inserted into the thermocouple hole to take temperature data. Thermocouple hole in a transparent single layer PMMA and thermocouple junction is shown in Fig. 3-5 to demonstrate the attachment.

Position "*A*" is at the center top of the sample, which represented the temperature on the top surface. Position "*E*" represents thermocouple holes drilled from the side of the sample. A thermocouple was inserted into the thermocouple hole to take temperature data. To demonstrate the attachment, thermocouple hole in a transparent single layer PMMA and thermocouple junction is shown in Fig. 3-5. Position "*F*" is at the center of the bottom of the sample, which represented the temperature on the bottom surface.

The thermocouple hole would keep the thermocouple at a fixed position to avoid inaccurate information for the position. And also, the depth of the thermocouple hole would bring the position of thermocouple closer to the center of the sample, therefore, to ease the error brought by the heat loss from the sides. From this point, the hole should be drilled close to the center of the sample. However, deeper hole requires bigger diameter, because the wire cover of the thermocouple needs to be inserted into the hole in this case. A wide and deep hole would undermine the assumption of bulk material, which was made in the prediction model in Chapter 2. Therefore, the depth of the thermocouple hole should be able to fix the thermocouple. Thermocouple junction would fall out easily from a shallow hole. The diameter of the hole should have the thermocouple junction fit in. Therefore, thermocouple holes with 1mm diameter, drilled by # 60 driller, and depth of 8 mm were used for all the samples.

Another concern of using thermocouple hole is that, there would be air gap between the inner wall of the hole and the thermocouple junction. If this is the case, the temperature data taken by thermocouple would be lower than the actual temperature. This problem was solved by adding some thermal paste (SPF-350, FangYong, Taiwan), also known as thermal grease, into the thermocouple hole. Thermal paste was used in this research. It has a thermal conductivity of 1.5 W/(m-K), which is much more conductive than air which has a thermal conductivity of 0.024 W/(m-K) [51]. The thermal grease was applied to fill air gaps existed between the inner wall of thermal couple hole and the thermocouple junction to ensure even and quick temperature measurement by the thermocouple.
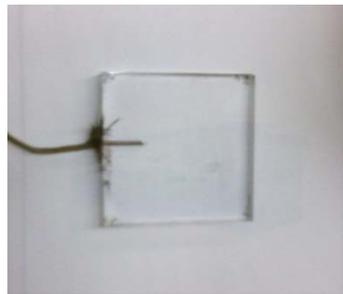
Figure 3- 6 Thermocouple hole in PMMA and thermocouple junction

3.4 Temperature boundary conditions

As mentioned in Section 3.1, the hot plate was used to provide temperature gradient. Boundary condition information was essential to this problem. With the wrong boundary condition, the model could not predict the correct temperature profile. In Fig. 2-2 and Fig. 2-3, the partial differential equation for the one-dimensional and transient conduction problem needs two boundary conditions. The first one was adiabatic boundary condition, and the second one was time variable boundary condition. The first adiabatic boundary condition could be taken care of by wrapping the sample with insulating material. The time variable boundary condition needs more concern. The heat source was hot plate, but the method for taking the temperature

measurement could be different. For this temperature boundary condition, three boundary taking methods were considered in this research, and they are referred as Type A, Type B and Type C and explained in the following paragraphs.

Type A: Constant temperature boundary condition

Temperature boundary Type A was taken as constant temperature boundary condition. Since the temperature on the hot plate could be set at a constant temperature, the temperature set on the hot plate could be used as a fixed temperature boundary condition. Referring to temperature boundary condition Eqn. (2-2) for one-layered model or Eqn. (2-36) for two-layered model, the temperature boundary could be represented by a constant.

The thermocouple and boundary condition arrangement is shown in Fig. 3-7. Only one thermocouple was attached on the top of the sample to take the temperature profile which would be matched later. The sample was wrapped all over with insulating material except the bottom surface. The exposed surface of the sample would be pressed hard on the hot plate to have close contact with the hot plate and to get the temperature gradient.
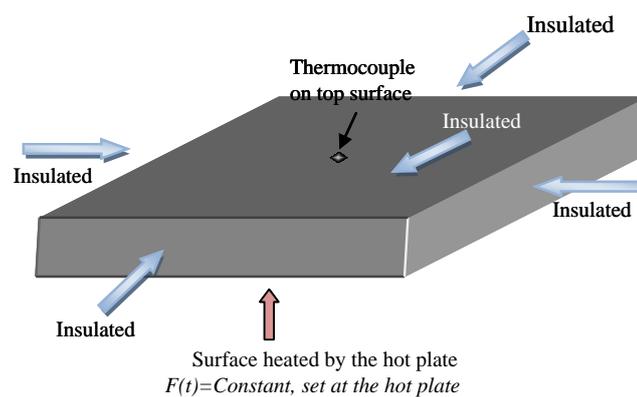
Figure 3- 7 Type A of temperature boundary condition and thermocouple
    arrangement

The advantage of this method is that the boundary condition is easy to obtain, which makes the experiment process simple as well. And also, without

the time variable boundary condition, the model is greatly simplified, the analytical and MATLAB code would be most simplified. It should be noted that even though the boundary condition is constant, the conduction problem is still transient. Since the uniform initial temperature was disturbed by an extra heat source. This problem would turn into a static problem when the temperature throughout the sample reaches to the temperature of the heat source.

Type B Boundary condition measured by thermocouple at the contact surface

Temperature boundary condition Type B is to insert a thermocouple between the hot plate and the sample. Therefore, the temperature fluctuation was recorded by data acquisition system. The thermocouple and boundary condition arrangement is shown in Fig. 3-8. In this method two thermocouples were applied. A thermocouple was attached on the top surface of the sample to take comparison temperature profile, same as the Section 3.4.1. While another thermocouple, thermocouple 2 was attached at the bottom of the sample to take temperature boundary condition.
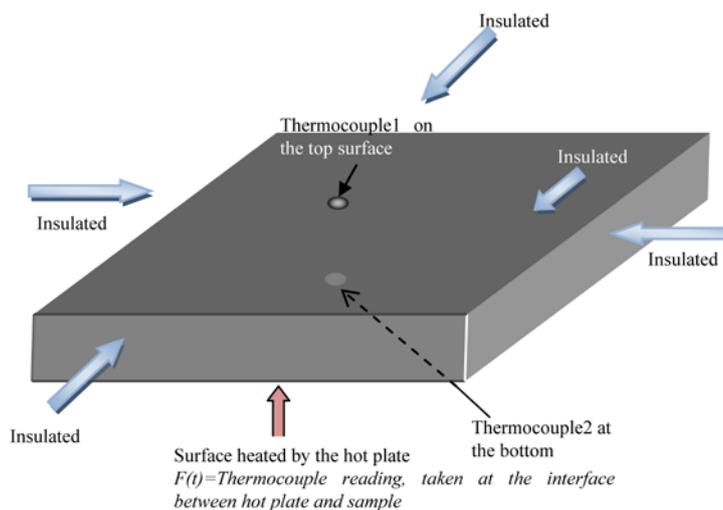
Figure 3- 8 Type B of temperature boundary condition and thermocouple arrangement

Type C Boundary condition measured within thermocouple hole

Type C of boundary condition used the thermocouple hole mentioned in Section 3-4 to take temperature data as the temperature boundary condition. The advantage of this method is temperature boundary condition data could be measured more accurately. As shown in Fig. 3-9, a thermocouple was drilled from the edge of the sample close to the surface; the hole is 8 mm deep and 1 mm wide. With thermal grease filled in the gap, thermocouple 2 was inserted into the thermocouple hole to take temperature in the hole. A boundary condition has to be at the boundary of the body, therefore the temperature taken by thermocouple 2 cannot be used directly. In Fig. 3-10 the original body of sample was divided into two parts by dash lines. The body part under the dash line was regarded as heat source (pink part), which had perfect contact with the body (grey part). In this way, the temperature taken by thermocouple 2 is the boundary of the grey part, where thermal conduction calculation would be applied.
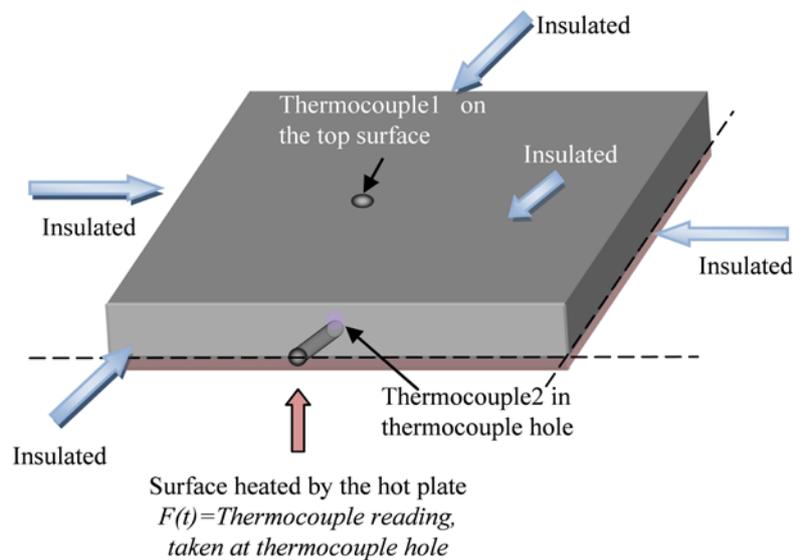
Figure 3- 9 Type C of temperature boundary condition and thermocouple arrangement

The disadvantage is that a thermocouple hole has to be drilled from the edge of the sample. This does not only demand more work in the sample

preparation, but also require thicker sample to be able to leave space for the hole.

For two-layered samples, the sample thickness should be considered to decide the position of thermocouple hole. Normally, substrate has greater thickness and better quality than the coating deposited. Therefore, it is more reasonable to have the thermocouple hole drilled from the edge of the substrate to leave more space for the conduction process. The substrate surface is always the surface being heated in this research to protect the coating from drilling destruction, as shown in Fig. 3-10.
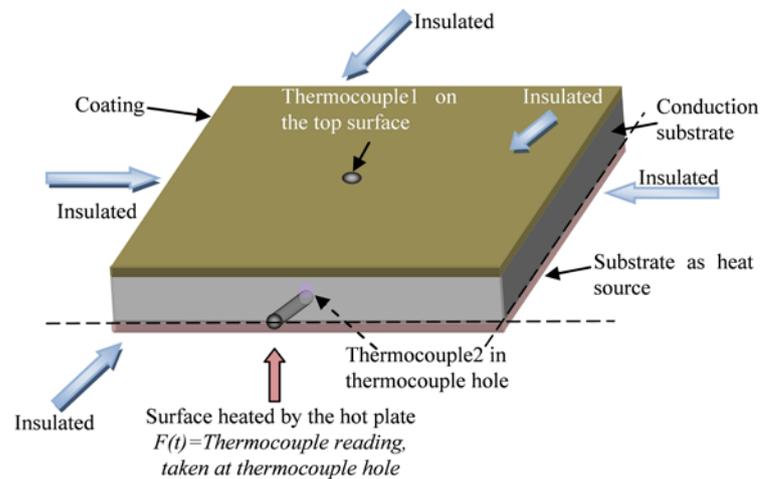
Figure 3- 10 Type C of temperature boundary condition and thermocouple arrangement for two-layered sample

The temperature boundary condition $F(t)$ for type B and type C was not constant. $F(t)$ was from the thermocouple reading and measured the temperature evolution at the position specified for boundary condition type B and type C. Even though the hot plate was set at a constant temperature, the sample, which was in contact with the hot plate, would not immediately have the same surface temperature as the hot plate. Therefore, the thermocouple reading $F(t)$ was a time variable temperature boundary condition.

3.5 Experimental procedure

After the experimental equipments were installed, which were described in Section 3.1 (including preheating of the hot plate and the adjustment of the data acquisition system) and the boundary condition choices were made, the heat conduction experiments were ready to be conducted.

3.5.1 Uniform initial temperature

First, the sample tested should be kept at a uniform and constant initial temperature. To guarantee this initial condition being uniform and constant, Styrofoam, thermocouple(s) and data acquisition system were used. Thermocouple(s) was/were attached on the sample according to the thermocouple and boundary condition arrangement. Styrofoam was cut into the shape that could be used to wrap the sample all over, leaving only one surface (bottom surface) exposed. The exposed surface (bottom surface) was laid on another piece of Styrofoam, which was referred as base Styrofoam, to keep uniform initial temperature within the sample. The exposed surface would be heated later on the hot plate during the experiment. Data acquisition system was used to measure the initial temperature at a frequency of 10 Hz.A typical initial temperature measurement graph is shown in Fig. 3-11.

The temperature evolution was monitored, and the experiment could not be further conducted until the measured temperature became constant, which means a uniform initial temperature was built within the sample. "Temperature_0" represents temperature measured by thermocouple inserted in the thermocouple hole, and the "Thermocouple_2" represents the temperature taken by thermocouple attached on top surface of the sample.
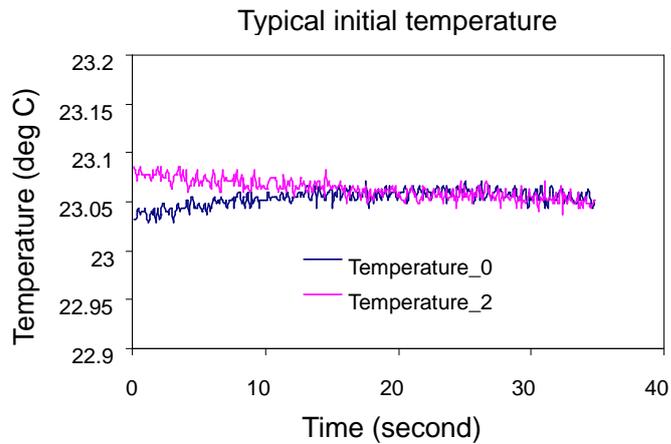
Figure 3- 11 Typical initial temperature measurement

3.5.2 Temperature evolution Observation

Once the initial uniform temperature was built, the sample wrapped with the insulating Styrofoam, was lifted up from the base Styrofoam. The exposed surface of the sample was immediately laid on the hot plate, which was set at a constant temperature, to have heat balance of the tested sample disturbed. To make sure the temperature evolution within the sample being recorded, data acquisition system was turned on before the sample was laid on the hot plate. The measurement time was normally set as 60 seconds. A typical temperature evolution profile is shown in Fig. 3-12. In Fig. 3-12, the temperature profiles were horizontal from the beginning till 4.5 second. This period was before the sample was laid on the hot plate, and this period could also provide the initial condition for the sample.

All the data needed for program were collected during the experiment. However, the temperature profile could not be applied directly. The data process procedure would be described in Chapter 4.
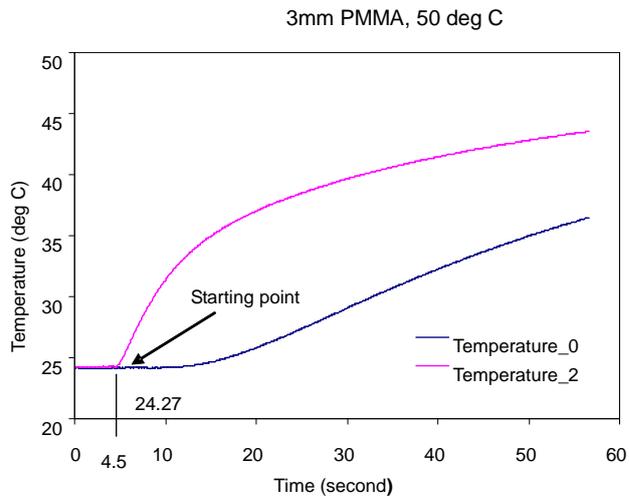
Figure 3- 12 Typical temperature evolution during the conduction process

Chapter 4: Algorithm implementation and thermal diffusivity measurement method

A thermal diffusivity measurement method was developed on both single-layered samples and two-layered samples. Since the mathematical model was developed and experiment data were ready, a MATLAB code was written to predict the temperature on the sample surface. Without knowing the thermal diffusivity of a material, thermal diffusivity value was assumed and put into the MATLAB code to predict the temperature. Then the temperature data measured in the experiment were compared with the predicted temperature. If the predicted temperature profile agreed with the experimental temperature profile, it means the assumed thermal diffusivity property is correct. If the predicted temperature profile did not agree with the experimental temperature profile, another guessed thermal diffusivity value was put into the mathematical model to see whether the predicted temperature curve could result a match with the experiment temperature curve. The guess-matching processes were repeated until a match was achieved. This procedure is called the tuning method in this thesis. The thermal diffusivity measurement method is explained in details in Section 4.1.

A MATLAB code was written to predict the temperature profile. The algorithm for single-layered model is relatively easy, since its solution is explicit. The two-layered model is in implicit expression, several steps were taken to solve the problem.

Here is the solution for one-layered model in explicit form, which was obtained in Chapter 2.

$$T(x,t)$$

$$= \frac{2T_i}{L} \sum_{m=1}^{\infty} \int_{x'=0}^{L} e^{(-\alpha\beta_m^2 t)} \cdot \sin(\beta_m x) \cdot \sin(\beta_m x') dx'$$

$$+ \frac{2\alpha}{L} \sum_{m=1}^{\infty} \int_{\tau=0}^{t} \beta_m \cdot e^{(-\alpha\beta_m^2(t-\tau))} \cdot \sin(\beta_m x) \cdot F(\tau) d\tau$$

$$- \frac{2\alpha}{L} \sum_{m=1}^{\infty} \int_{\tau=0}^{t} \beta_m \cdot e^{(-\alpha\beta_m^2(t-\tau))} \cdot \sin(\beta_m x) \cdot \cos(\beta_m L) \cdot F(\tau) d\tau$$

(4-1)

The solution for two-layered model is in implicit form and includes five parts, which are Eqns. (4-2) to (4-6).

$$T_1 = \theta_1(x,t) + F(t) \tag{4-2}$$

where:

$$\theta_1(x,t) =$$

$$-\frac{k_1}{\sqrt{\alpha_1}} \sum_{n=1}^{\infty} \frac{C_1^2}{Q_n \beta_n} \sin(\beta_n \frac{a}{\sqrt{\alpha_1}}) \int_0^t \frac{dF(t)}{d\tau} e^{(-\beta_n^2(t-\tau))} d\tau \cos(\frac{\beta_n x}{\sqrt{\alpha_1}})$$

$$-\frac{k_2}{\sqrt{\alpha_2}} \sum_{n=1}^{\infty} \frac{C_1 C_3}{Q_n \beta_n} \int_0^t \frac{dF(t)}{d\tau} e^{(-\beta_n^2(t-\tau))} d\tau \cos(\frac{\beta_n x}{\sqrt{\alpha_1}})$$

$$+\frac{Dk_1}{\sqrt{\alpha_1}} \sum_{n=1}^{\infty} \frac{C_1^2 e^{(-\beta_n^2 t)}}{Q_n \beta_n} \sin(\frac{\beta_n a}{\sqrt{\alpha_1}}) \cos(\frac{\beta_n x}{\sqrt{\alpha_1}})$$

$$+\frac{Dk_2}{\sqrt{\alpha_2}} \sum_{n=1}^{\infty} \frac{C_1 C_3 e^{(-\beta_n^2 t)}}{Q_n \beta_n} \int_0^t \frac{dF(t)}{d\tau} e^{(-\beta_n^2(t-\tau))} d\tau \cos(\frac{\beta_n x}{\sqrt{\alpha_1}})$$

(4-3)

The constants involved in the equations are:

$$Q_n = Q_1 + \frac{k_1}{\alpha_1}(Q_2 + Q_3)$$

$$Q_1 = \frac{k_1}{\alpha_1} C_1^2 \left[\frac{a}{2} + \sin(\frac{2\beta_n a}{\sqrt{\alpha_1}}) \cdot \frac{\sqrt{\alpha_1}}{4\beta_n} \right]$$

$$Q_2 = \frac{(b-a)}{2}(C_2^2 + 1) - \frac{C_2 \sqrt{\alpha_2}}{2\beta_n} \cdot \left[\cos(\frac{2\beta_n b}{\sqrt{\alpha_2}}) - \cos(\frac{2\beta_n a}{\sqrt{\alpha_2}}) \right]$$

$$Q_3 = \frac{(C_2^2 - 1)\sqrt{\alpha_2}}{4\beta_n} \left[\sin(\frac{2\beta_n b}{\sqrt{\alpha_2}}) - \sin(\frac{2\beta_n a}{\sqrt{\alpha_2}}) \right]$$

(4-4)

where:

$$C_1 = \frac{\cos\dfrac{\beta_n a}{\sqrt{\alpha_2}}}{\cos\dfrac{\beta_n a}{\sqrt{\alpha_1}}} - \tan^{-1}(\frac{\beta_n b}{\sqrt{\alpha_2}})\frac{\sin\dfrac{\beta_n a}{\sqrt{\alpha_2}}}{\cos\dfrac{\beta_n a}{\sqrt{\alpha_1}}}$$

$$C_2 = -\tan^{-1}\frac{\beta_n b}{\sqrt{\alpha_2}}$$

$$C_3 = (\sin\frac{\beta_n b}{\sqrt{\alpha_2}} - \sin\frac{\beta_n a}{\sqrt{\alpha_2}}) - C_2(\cos\frac{\beta_n b}{\sqrt{\alpha_2}} - \cos\frac{\beta_n a}{\sqrt{\alpha_2}})$$

$$D = T_i - F(t) \quad t = 0$$

(4-5)

The β_n involved in the solution was calculated by the following implicit expressions:

$$\left(\sin(\frac{\beta_n b}{\sqrt{\alpha_2}}) \cdot \tan^{-1}(\frac{\beta_n a}{\sqrt{\alpha_2}}) - \cos(\frac{\beta_n a}{\sqrt{\alpha_2}}) \right) \cdot \tan(\frac{\beta_n a}{\sqrt{\alpha_1}})$$

$$= -\frac{k_2}{k_1}\sqrt{\frac{\alpha_1}{\alpha_2}} \cdot \left(\cos(\frac{\beta_n a}{\sqrt{\alpha_2}}) \cdot \tan^{-1}\left(\frac{\beta_n b}{\sqrt{\alpha_2}}\right) + \sin(\frac{\beta_n a}{\sqrt{\alpha_2}}) \right)$$

(4-6)

In the solution of both one-layered model and two-layered model, a curve fitting and an integration procedure were used. It is described in Section 4.2 of this chapter. The two-layered solution, however, had implicit form and need to be studied in detail. Section 4.3 in this chapter focuses on explaining the algorithm of two-layered model solution.

4.1 Development of thermal diffusivity measurement method

The tuning method to measure thermal diffusivity was developed. Fig. 4-1 gives a detailed flow chart for this method. If the correct properties were input into the mathematical model, the experiment temperature curve collected by the data acquisition system should be matched by the predicted temperature curve developed by the analytical model. Therefore, with a

known temperature profile (experimental data) at a test position, a repeated guessing process of the thermal diffusivity value was used to match the predicted temperature profile with the known experiment temperature profile.

Hot plate was set at a constant temperature. Data acquisition system saved the temperature data during the experiment; temperature boundary condition curve and experiment temperature curve were generated. The temperature boundary condition curve was put into the mathematical program, while the experiment temperature curve was set as a comparison standard for the predictions to be matched. In the mathematical model part, a thermal diffusivity value was assumed and put into the MATLAB code as a known parameter. Other parameters, such as thickness of the coating "a", thickness of the whole sample "b", properties of the substrate, etc. were known beforehand or measured. The boundary condition was collected by the data acquisition system from the experiment part, processed and transformed into polynomial function, as described in Chapter 3. Temperature on top of the coating surface was calculated to create a predicted temperature curve.

The experiment temperature curve obtained from the experiment part was set as a standard to be matched by the predicted temperature curve. If the match was a success, it meant the thermal diffusivity value put into the mathematical model was correct. The determination process was finished. If the two curves did not match each other, it meant the thermal diffusivity value put into the model was not correct, and another assumption was needed. If the predicted temperature by a guessed thermal diffusivity value is lower than the experiment temperature curve, a higher guessed value should be given into the mathematical model. The other way round, if a guessed value gives a higher temperature prediction curve, a lower guessed thermal diffusivity value should be used.
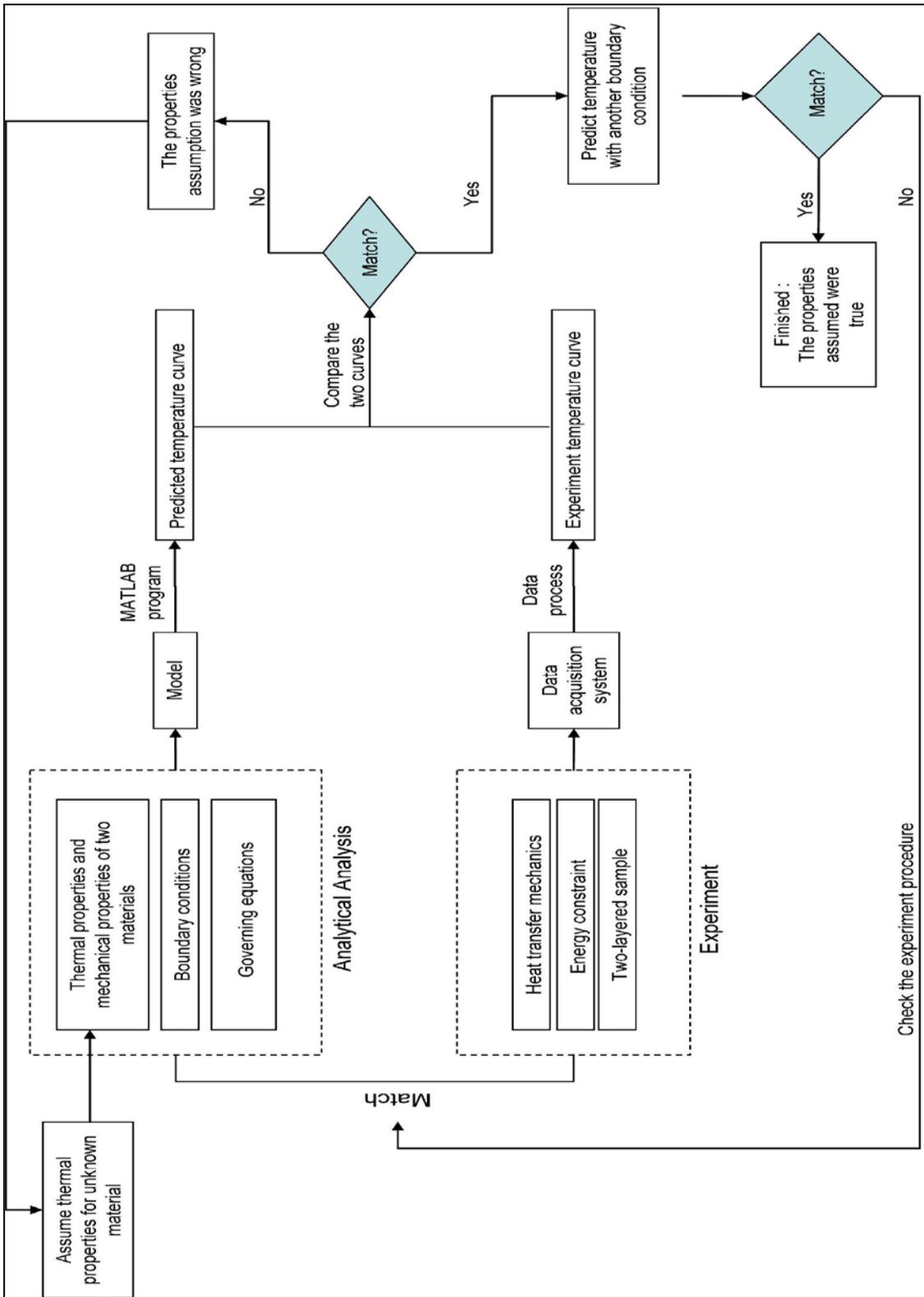
Figure 4- 1 Thermal diffusivity measurement method flow chart

For a new assumption of thermal diffusivity, the mathematical prediction process would be restarted by using the same temperature boundary condition. This assumption and matching process was kept until a match between the experimental and model temperature profiles were achieved, which meant the thermal diffusivity value was found.

4.2 Experiment temperature boundary condition as a polynomial function — curve fitting procedure

The MATLAB code was written based on Eqn. (4-1) for single-layered model and on Eqns. (4-2) to (4-6) for the two-layered model. It could be seen that the temperature boundary condition was represented by $F(t)$. As mentioned in Chapter 3, the experimental temperature data were recorded into EXCEL files in form of series. Therefore, the experimental boundary condition should be changed into a function – "$F(t)$" to be fit into the solutions.

An easy way to describe the series with function is to fit the series into polynomial curves. In this thesis, a five-degree polynomial function was used to perform the curve fitting. A typical temperature data was collected as shown in Fig. 4-2(a). In this figure, before the starting point at (24.27 °C, 4.5 second), the temperature data collected by the two thermocouples were equal and mostly constant. It was because during this time of experiment, the sample was wrapped all over with insulating materials and kept at uniform initial temperature. After the starting point (24.27 °C, 4.5 second), the sample was placed on the hot plate and heated as described in Chapter 3. The thermocouples started to sense the temperature change. To fit into a

mathematical model, the temperature boundary condition should better be a smooth function. Therefore, the data before the starting point was cut off, shown in Fig. 4-2 (b). A curve fitting process was reflected in this figure in a form of $F(t) = at^5 + bt^4 + ct^3 + et^2 + ft + g$, where *a, b, c, e, f* and *g* are the coefficients for the curve fit polynomial, *t* represents time.

In Fig. 4-2, R^2 is the R squared value, which is called the correlation coefficients. It describes the goodness of fit of the polynomial to the raw temperature data. A R^2 of value 1.0 means that the polynomial fits the raw temperature data perfectly. The mathematic definition of correlation coefficients is shown in Eqn. (4-7), where $f(i)$ represents the curve fitting function and y_i represents the raw data. In this thesis, to give good fit to the temperature data, the R^2 was checked and ensured to be greater than 0.9. Five-degree polynomial was chosen because it could provide curve fitting results which met the required standard. The least square curve fitting method was used to provide the curve fitting by MATLAB program.

$$R^2 \equiv 1 - \frac{SS_{err}}{SS_{tot}} = 1 - \frac{\sum_i (y_i - F(i))^2}{\sum_i (y_i - \frac{1}{n}\sum_i y_i)^2} \qquad (4\text{-}7)$$

In the analytical solution, integration was used frequently. As shown in Eqn. (4-1) and Eqn. (4-3), the integration was within superposition part; therefore unlimited number of integration results would be summated. The accuracy of the integration needs to be ensured due to the superposition calculation. The exact integration could reduce the error significantly.

Part of calculation was done by hands regarding with the integration part in the solution. As discussed before, the boundary condition was represented by polynomial $F(t)$. In the solution, the integration parts are in Eqn. (4-1) and Eqn. (4-3). The form of the most used integrated parts in the thesis is

calculated in Eqn. (4-8).
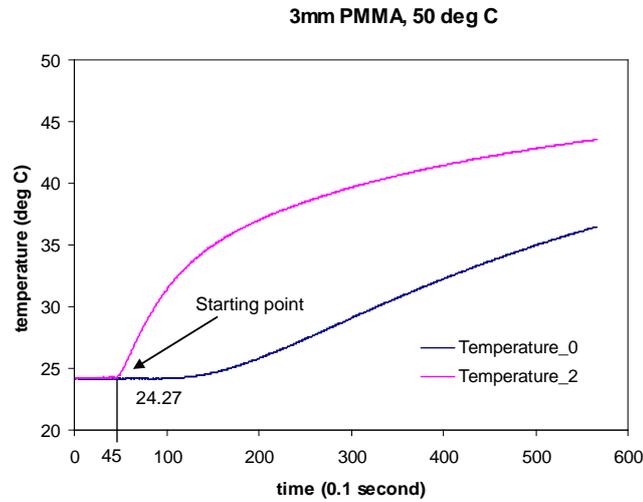
(a)
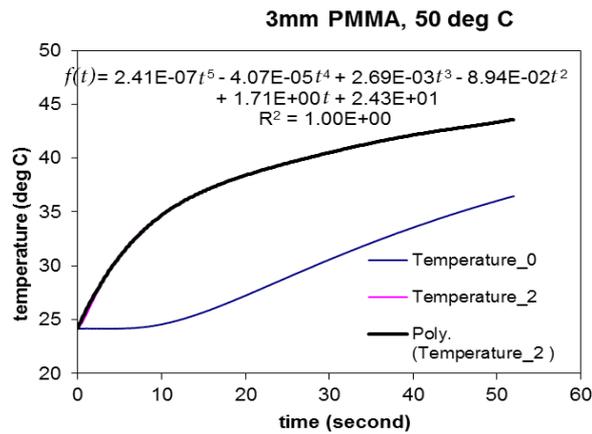
(b)

Figure 4- 2 Fitting the temperature boundary condition into polynomial function (a) a typical temperature data graph (b) the modified temperature data graph

By Eqn. (4-7) the integration could be programmed directly then. Further, the Eqn. (4-1), solution for single-layered sample, could be programmed.

For single-layered conduction problem, this polynomial-Eqn. (4-8) could be programmed to give temperature boundary conditions. For two-layered conduction problem, eigenvalues have to be decided to get the program ready.

$$Int = \int_{\tau=0}^{t} e^{\alpha\beta_m^2(\tau-t)} F(\tau)d\tau = \int_{\tau=0}^{t} e^{\alpha\beta_m^2(\tau-t)} F'(\tau-t)d\tau$$

$$= \int_{\tau-t=-t}^{\tau-t=0} e^{\alpha\beta_m^2(\tau-t)} (A(\tau-t)^5 + B(\tau-t)^4 + C(\tau-t)^3 + E(\tau-t)^2 + F(\tau-t) + G)d(\tau-t)$$

$$= D^{-6}(-120A + 24BD - 6CD^2 + 2ED^3 - D^4F + D^5G)$$

$$- e^{-Dt}[D^{-6}(-120A + 24BD - 6CD^2 + 2ED^3 - D^4F + D^5G)$$

$$- D^{-5}t(120A - 24BD + 6CD^2 - 2ED^3 + D^4F)$$

$$+ D^{-4}t^2(-60A + 12BD - 3CD^2 + ED^3) - D^{-3}t^3(20A - 4BD + CD^2)$$

$$+ D^{-2}t^4(BD - 5A) - D^{-1}t^5A]$$

$$(4\text{-}8)$$

where:

$$D = \alpha\beta_m^2 \tag{4-9}$$

$$A = a \tag{4-10}$$

$$B = 5at + b \tag{4-11}$$

$$C = 10at^2 + 4bt + c \tag{4-12}$$

$$E = 10at^3 + 6at^2 + 3ct + e \tag{4-13}$$

$$F = 5at^4 + 4bt^3 + 3ct^2 + 2et + f \tag{4-14}$$

$$G = at^5 + bt^4 + ct^3 + et^2 + ft + g \tag{4-15}$$

4.3 The algorithm of two-layered solution

Besides the curve fitting process and integration parts, the algorithm for two-layered model is more complex.

Bear in mind that, the idea of the tuning method was to assume the unknown property, then to predict the temperature profile, and to achieve a match with the experimental temperature profile. For two-layered model, the analytical solution was split into 2 parts, namely the eigenvalue part and

temperature profile part. The eigenvalue part is Eqn. (4-6). The rest parts of the solution, Eqns. (4-2) to. (4-5) are the main body of the two-layered solution. Both the eigenvalue part and main body require the assumption of the unknown properties, it should be make sure that the assumption was consistent. It means in the MATLAB program, the assumed thermal diffusivity value should be the same within each temperature predicting solution Eqns. (4-2) to (4-6).

4.3.1 Eigenvalue determination procedure

The MATLAB program was written to obtain the solution β_n. Eigenvalues could be calculated by Eqn. (4-6). This equation was transformed to Eqn. (4-16) to facilitate the calculation. Fig. 4-3 shows a typical graph of eigenvalue calculation. The horizontal axis is β, which is also referred as test numbers for convenience; the vertical axis is $f(\beta)$. Graphs like Fig. 4.3 and their data, which were obtained by MATLAB program, were used to determine the eigenvalue β_n, which could satisfy Eqn. (4-16). Fig. 4-3 (a) shows the whole eigenvalue determination graph. To check it closely, Fig. 4-3 (b) gives an enlarged part of Fig. 4-3 (a). In Fig. 4-3 (b), it could be seen that there are one eigenvalue and one singularity point standing out. The reason for that both eigenvalue and singularity points are marked in the Fig. 4-3 is explained in details in the following paragraph.

$$
\begin{aligned}
f(\beta_n) = \\
\left(\sin(\frac{\beta_n b}{\sqrt{\alpha_2}}) \cdot \tan^{-1}(\frac{\beta_n a}{\sqrt{\alpha_2}}) - \cos(\frac{\beta_n a}{\sqrt{\alpha_2}}) \right) \cdot \tan(\frac{\beta_n a}{\sqrt{\alpha_1}}) \\
+ \frac{k_2}{k_1} \sqrt{\frac{\alpha_1}{\alpha_2}} \cdot \left(\cos(\frac{\beta_n a}{\sqrt{\alpha_2}}) \cdot \tan^{-1}\left(\frac{\beta_n b}{\sqrt{\alpha_2}} \right) + \sin(\frac{\beta_n a}{\sqrt{\alpha_2}}) \right) = 0
\end{aligned}
\qquad (4\text{-}16)
$$

The eigenvalue points are the needed for calculation and the singularity points should be sieved out. During this procedure, there are certain standards

and limitation involved to determine the eigenvalues, which would be explained in details. Eigenvalue could not be decided directly, and the procedure to determine eigenvalues was shown in Fig. 4-4.
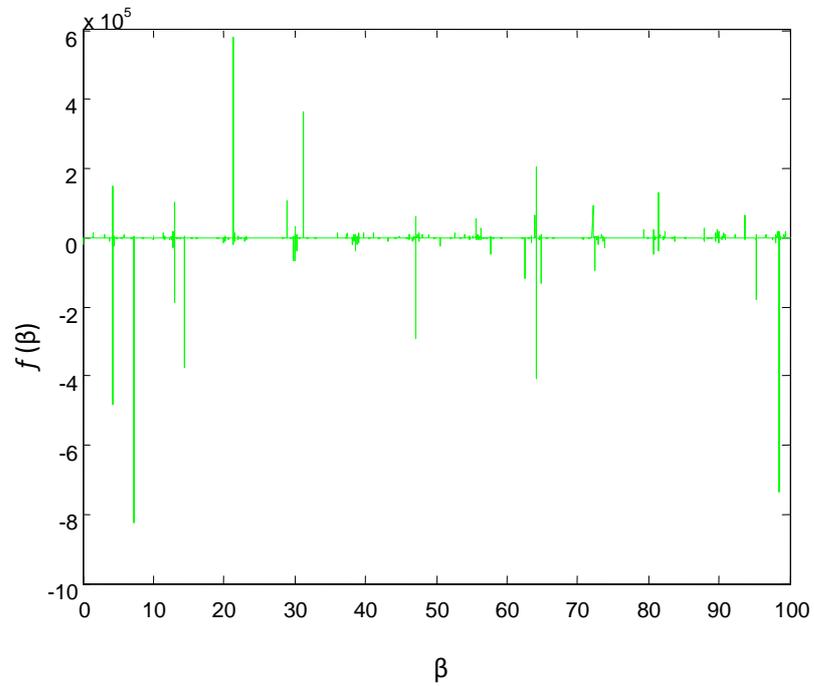
(a) Typical eigenvalue graph
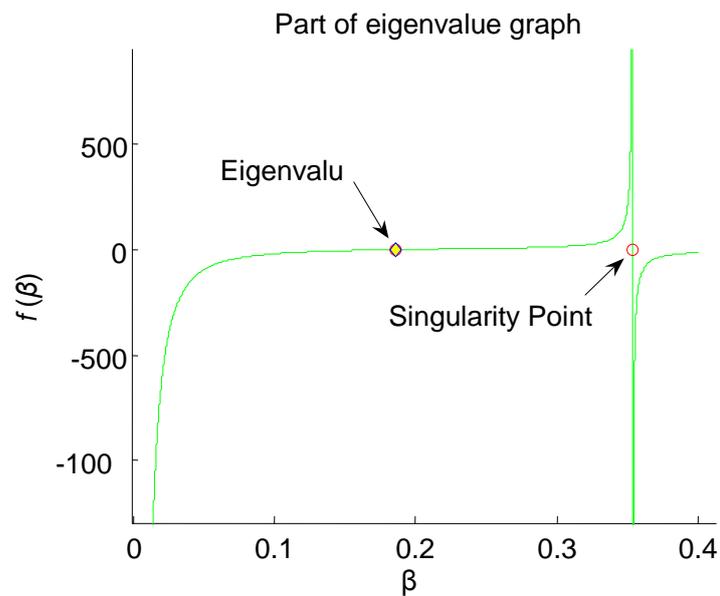
(b) Part of a typical eigenvalue graph

Figure 4- 3 Part of a typical eigenvalue graph
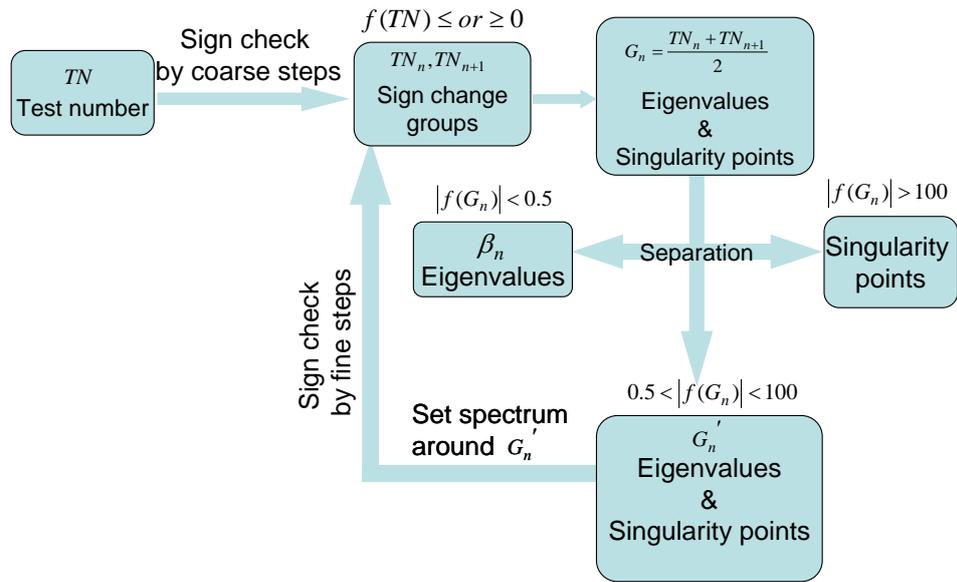
Figure 4- 4 The procedure to decide eigenvalues for two-layered model

Figure. 4-4 shows the procedure to determine eigenvalues. "β'', which is also referred as a number series called Test numbers in this thesis. *TN* are numbers from 0 to 100 of small steps. For example, for a small step of 0.0005, *TN* is a series of numbers [0, 0.0005, 0.0010, 0.0015…100]. The size of the step was decided by the programmer based on the material. Test numbers *TN* were substituted into Eqn. (4-16) to calculate eigenfunction $f(eigenvalue) = 0$. The function $f(TN)$ with TN as its independent variables was graphed to determine eigenvalue as shown in the Fig. 4-2 (a). Then we need to spot the value which could satisfy the function, which means $f(TN) = 0$. To get the eigenvalues with program, the sign of each function $f(TN)$ was checked. If the sign experiences variation between two adjacent test numbers, which means $f(TN_n) \times f(TN_{n+1}) < 0$, it could be inferred that, between the two test numbers, an eigenvalue which satisfy $f(TN) = 0$ exists, or a singularity point (discontinuity point) exists. Based on the existence of tangent function, and by checking the graph of eigenvalue

function, it is known that the singularity points exist in the function. The vertical lines in Fig. 4-3 (a) represent the singularity points. Therefore, $y = f(TN)$ is sectional continuous function.

These points, either singularity points or eigenvalues, were approximated by G_n, which were the average values of two adjacent numbers. This procedure is represented by Eqn. (4-17).

$$G_n = (TN_n + TN_{n+1})/2$$
$$if \quad f(TN(n)) \times f(TN(n+1)) < 0$$
(4-17)

Since the step was small, the approximation had good accuracy. Bear in mind that all the singularity points in function $f(G_n)$ approaches either positive infinity or negative infinity, therefore, G_n the approximation of singularity points would make $f(G_n)$ having a great absolute value. Absolute values of $f(G_n)$ were calculated and used as separation standard to separate the singularity points and eigenvalues in G_n.

Limitations for the absolute value of $f(TN)$ were set to separate the two groups of numbers. In this thesis, the following limitations were established. If $|f(G_n)| < 0.5$, the absolute value is small and close to 0, G_n is an eigenvalue. If $|f(G_n)| > 100$, with such small steps, it is impossible for any number close to G_n having eigenfuction satisfied, therefore, G_n must be a singularity point. If $f(G_n)$ is between the range 0.5 and 100, either way is possible. The G_n in this category would be either singularity points or eigenvalues, and they are further represented by G_n'. Another round of separation is required for section $[G_n' - step, \quad G_n' + step]$ with even finer step.

After the first circle of separation, spectrum was set around $G_n^{'}$, and fine step of 0.00001 was set within the spectrum to carry another round of separation. The numbers within the spectrum with fine step became the new test numbers, and the same procedures, namely checking signs and limitation of absolute values, were involved. The same limitations for values of function $f(TN)$ were applied to separate the singularity points and eigenvalues. This time, the step was small enough to guarantee that all the test numbers fall into the categories of singularity points or eigenvalues. In this way, all the eigenvalues were calculated and represented by β_n. The eigenvalues were also guaranteed by checking the eigenvalue graph as in Fig. 4-3 (b), to make sure the function was satisfied.

4.3.2 Limitation standards of eigenvalues

In the separation process, the absolute value of the function $f(TN)$ was used as the separation standards. Referring to Fig. 4-2, around the eigenvalues, the function $f(G_n)$ should be continuous and close to 0, which is regarded as small absolute value. While, around the singularity point, the function $f(G_n)$ should experience sharp change, and have big absolute value. In this research, small value standard was set as less than 0.5; big value standard was set as greater than 100, by extensive observation. The reason for some $\left| F(G_n) \right|$ falling between 0.5 and 100 was that the step of test number set in the first round was not small enough to spot all the singularity points.

Smaller step would provide more data for program to separate singularity points from eigenvalues; but the separation program would take longer time to run. Coarse step would take shorter program-running-time but provide less data. Coarse step would work for most of the test numbers as in Fig. 4-3(b).

However, for some points, the function values $f(TN)$ would not be distinctive to be separated. The comparison of $f(TN)$ function graph between fine step and coarse step is shown in Fig. 4-4. The two graphs shown were drawn with the same parameters, except the step. It could be seen that for coarse step 0.0005, the graph did not exhibit clear singularity attributes, and the $f(TN)$ value is between 0.5 and 100. With step set finer, the singularity point was obvious, and the absolute value of $f(TN)$ was much greater than 100.
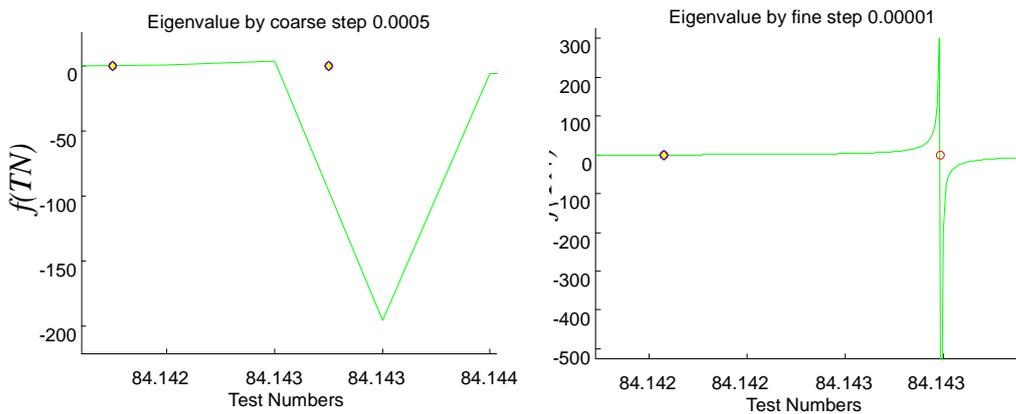
Figure 4- 5 Eigenvalue graph comparison by coarse step 0.0005 and fine step 0.00001

Therefore, the two rounds of separation were applied to determine all the eigenvalues with better efficiency and accuracy. For the first round, coarse step 0.0005 of TN was applied to separate most of the eigenvalues and save time. Finer step of 0.00001 was applied in the second circle within small spectrum for the undecided points.

4.3.3 Evaluation of test number step

As mentioned in the former paragraph, the coarse step was 0.0005, and the fine step was 0.00001 in the program. The step magnitude is calculated by an evaluation procedure. Since $\tan(\pi/2) = \infty$, the step for the argument should be small enough that the tangent function could achieve large absolute value, saying 2000. The step was calculated by Eqn. (4- 18).

$$|\tan(\pi/2 - step)| > 2000 \qquad\qquad (4\text{-}18)$$

Solving this equation, Eqn. (4-19) was obtained.

$$step < 0.005 \qquad\qquad (4\text{-}19)$$

The above function means that step of tangent argument should be smaller than 0.005 to be able to detect large absolute value. The argument for tangent function in Eqn. (4-1) is in the form $\beta_n l/\sqrt{\alpha}$, where β_n was the magnitude of eigenvalues, l is the magnitude the length, and α is the magnitude of thermal diffusivity.

Considering $1\times10^{-8} m^2/s < \alpha < 1\times10^{-4} m^2/s$, magnitude of l is set as $1\text{x}10^{-3}$ (m), and the magnitude of α was set as $1\text{x}10^{-8}$ (m^2/s) according to the samples tested such as copper, aluminum, Pyrex and PMMA. Setting the magnitudes of all the elements into tangent function argument, the magnitude of β_n was calculated in Eqn. (4-20).

$$\beta_n \cdot 0.001 \Big/ \sqrt{1\times10^{-8}} = 0.005 \qquad\qquad (4\text{-}20)$$

Therefore, the coarse step was $\beta_n = 0.0005$.

Similarly, for the fine step, large number was set as 10000. The fine step was calculated to be $\beta_n = 0.00001$.

The test number range was set as 0 to 100. This was decided by convergence check. Larger range of test numbers could provide more eigenvalues. The number of eigenvalues would decide the summation number in the temperature solution. It was found out that within the test number range

[0, 100]; the number of summation was enough to achieve a 99.9 % convergence.

The MATLAB program was used to predict the temperature in the sample. In Chapter 3, three kinds of boundary conditions were introduced. Three experiments by different boundary conditions were carried on two-layered sample. The two-layered program was run to predict the temperature for each experiment.

The MATLAB program was run to predict the temperature on a two-layered sample with known material to check whether the mathematical model could make good prediction.

Chapter 5: Experimental results and heat loss analysis

Temperature measurement experiments were conducted on the samples; temperature data were collected and used to estimate the thermal diffusivity of the material. In this chapter, the experimental figures and test results are shown by graphs or tables.

The temperature profiles of copper sample obtained by different boundary conditions are shown in Section 5.1. The test results were used to identify the better boundary condition for this tuning method. In the meanwhile, the mathematical model was verified. The results were analyzed and explained in Section 5.1.

Section 5.2 to Section 5.6 shows the thermal diffusivity results and experimental figures of all the samples. Each material has its own feature, and has a specific shape in the figures, which is discussed and explained by heat loss analysis in Section 5.7.

5.1 Identification of better temperature boundary condition

Comparison of boundary condition Type A and Type C
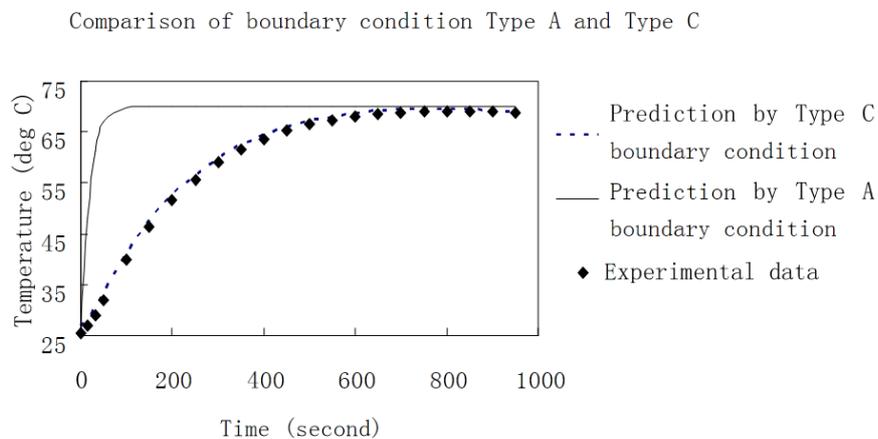
(a)
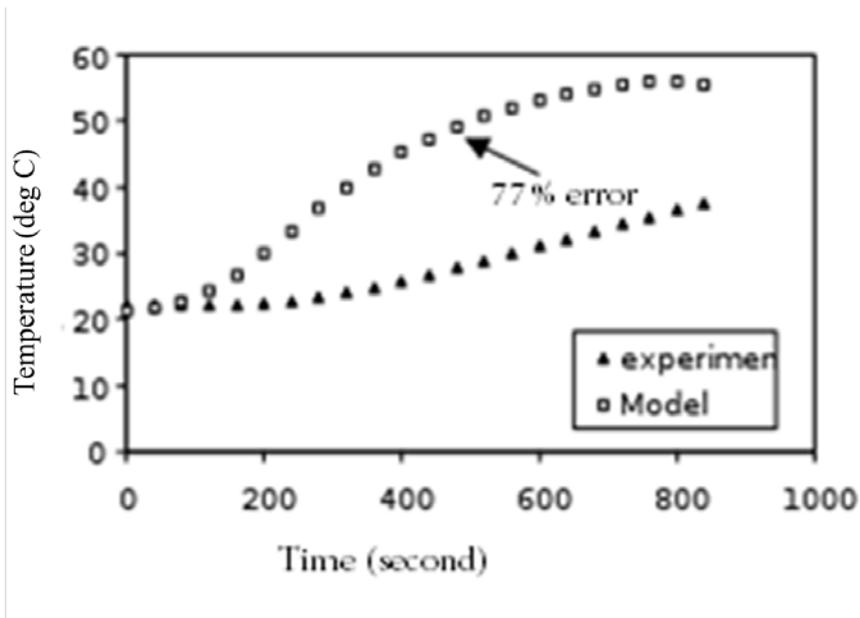
(b)

Figure 5 -1 Temperature prediction by different boundary conditions. (a) is comparison between Type A and Type C; (b) is the temperature prediction compared with experiment prediction by Type B

For boundary condition Type A, instead of measuring the temperature on the hot plate, the boundary temperature was assumed to be the temperature set on the hot plate. However, temperature set on the on/off hot plate would not stay absolutely constant. The actual temperature on the hot plate would fluctuate around the set temperature. Another problem is that even though the sample was pressed hard to have close contact with the hot plate, there would still be thermal resistance between the hot plate and the heated surface of the sample. The temperature on the hot plate was not necessarily the temperature on the bottom surface of the sample. The poor prediction from Type A is due to the imperfect contact between the sample and the hot plate.

For boundary condition Type B, the existence of thermocouple between the sample and the hot plate resulted that the hot plate could not have good contact with the hot plate, and the sample was slightly inclined when heated on the hot plate, as shown in Fig. 5-2. This inclination caused uneven heat flux input into the sample and exposed surface to the environment. Thermocouple

was measuring the temperature of both hot plate and bottom of the sample.
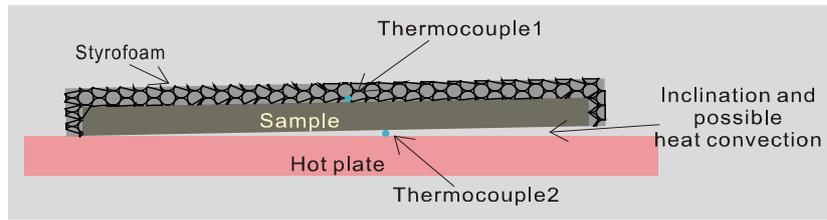
Figure 5 - 2 Inclination caused by boundary condition Type B

After identification of the best boundary condition, the following results (Section 5-2 to Section 5-6) were all calculated by boundary condition Type C.

5.2 Experiments on PMMA

Experiments procedures described in Chapter 3 were conducted on the PMMA single-layered samples. Two PMMA samples of different thickness, 3mm PMMA and 6 mm PMMA samples were tested to study the influence of sample thickness to thermal diffusivity result. Each sample was tested separately when the hot plate was set at 50˚C, 60˚C, 70˚C, 80˚C and 90˚C. The temperature set on the hot plate was referred as "experiment temperature" throughout Chapter 5. For each experiment temperature, experiments were repeated 4 times on both samples. Typical experiment figures, which display the experimental temperature curves and model curves, are shown in the Figs. 5-3 and 5-4.

The sample and the experiment temperature are shown in the caption. The test result, thermal diffusivity value of the test material in unit of m^2/s is also listed in the title behind brackets. The curves are temperature (in unit of Celsius degree) versus time (in unit of second) graph. Within these test figures, the measured temperature boundary condition is shown as Temperature 2. The polynomial curve fitting line is shown as "Poly", and its *R* squared value is listed to check whether it could give good simulation to the temperature boundary condition. The tested position temperature is shown as

"Temperature 0" and compared with the predicted temperature profile, which is represented by a number in the figures, i.e. in Figs. 5-3 and 5-4, the predicted temperature curves are represented by "9.5E-08" and "1.10E-07" respectively. The test results for the 3 mm and 6 mm PMMA samples are listed in Table 5-1.
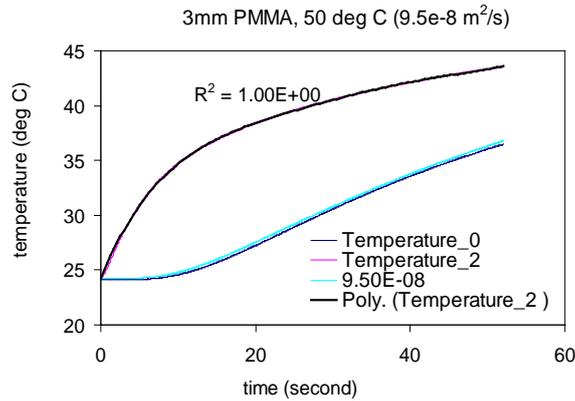
Figure 5 - 3 Typical thermal diffusivity measurement 3 mm PMMA, hot plate set at 50 ˚C
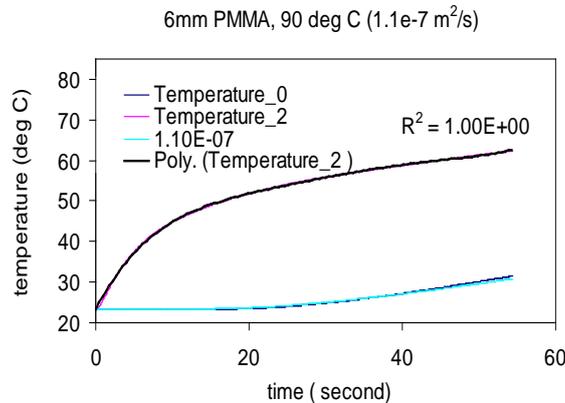
Figure 5 - 4 Typical thermal diffusivity measurement 6mm PMMA, hot plate set at 90˚C

The sensitivity of this thermal diffusivity measurement method to the thickness was studied. From Table 5-1 and the deviation graph-Fig. 5-5, the average thermal diffusivity measured on the 3 mm thick PMMA was $1.02 \times 10^{-7} \pm 2.3 \times 10^{-8}$ m^2/s ($n = 20$, the number of tests); and the average value of thermal diffusivity measured on 6 mm thick PMMA was $1.03 \times 10^{-7} \pm 7 \times 10^{-9}$ m^2/s ($n = 20$). The similarity of the thermal diffusivity results between two separate PMMA samples means that, this tuning method of measuring thermal

diffusivity value could produce dependable results. The thermal diffusivity of PMMA is in the range of 9.6×10^{-8} m^2/s to 1.5×10^{-7} m^2/s [52]. This method successfully predicted the thermal diffusivity of the material PMMA, and showed good repeatability in multiple tests. Tests under the same experiment temperature were repeated four times for both samples. The graph of standard deviation of thermal diffusivity result is also shown in Fig. 5-5.

(a) Calculated thermal diffusivity (m^2/s) results for 3mm PMMA						
temperature set at the hot plate ˚C	50	60	70	80	90	average
1st	9.00×10^{-8}	9.50×10^{-8}	1.10×10^{-7}	9.30×10^{-8}	9.00×10^{-8}	9.56×10^{-8}
2nd	8.90×10^{-8}	8.00×10^{-8}	9.00×10^{-8}	1.00×10^{-8}	9.50×10^{-8}	9.08×10^{-8}
3rd	1.05×10^{-7}	1.05×10^{-7}	1.25×10^{-7}	1.10×10^{-7}	1.00×10^{-7}	1.09×10^{-7}
4th	1.10×10^{-7}	9.50×10^{-8}	1.25×10^{-7}	1.30×10^{-7}	1.00×10^{-7}	1.12×10^{-7}
average	9.85×10^{-8}	9.38×10^{-8}	1.13×10^{-7}	1.08×10^{-7}	9.63×10^{-8}	1.02×10^{-7}
standard deviation	1.06×10^{-8}	1.03×10^{-8}	1.66×10^{-8}	1.61×10^{-8}	4.79×10^{-9}	N/A

(b) Calculated thermal diffusivity (m^2/s) results for 6 mm PMMA						
Temperature set at the hot plate ˚C	50	60	70	80	90	Average
1st	1.05×10^{-7}	1.05×10^{-7}	1.00×10^{-7}	1.05×10^{-7}	1.00×10^{-7}	1.03×10^{-7}
2nd	9.50×10^{-8}	1.00×10^{-7}	1.06×10^{-7}	1.05×10^{-7}	1.00×10^{-7}	1.01×10^{-7}
3rd	1.00×10^{-7}	1.05×10^{-7}	1.05×10^{-7}	1.05×10^{-7}	1.05×10^{-7}	1.04×10^{-7}
4th	1.03×10^{-7}	1.05×10^{-7}	1.03×10^{-7}	1.05×10^{-7}	1.05×10^{-7}	1.04×10^{-7}
Average	1.01×10^{-7}	1.04×10^{-7}	1.04×10^{-7}	1.05×10^{-7}	1.03×10^{-7}	1.03×10^{-7}
Standard deviation	4.35×10^{-9}	2.5×10^{-9}	2.65×10^{-9}	0	2.89×10^{-9}	N/A

Table 5- 1 Thermal diffusivity results of PMMA

Standard deviation for 3 mm PMMA

(a)
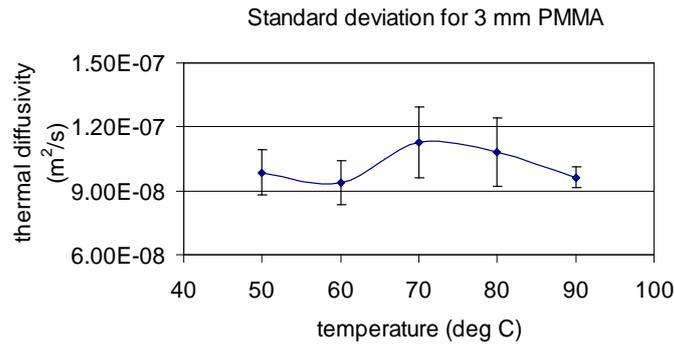
Standard deviation for 6mm PMMA
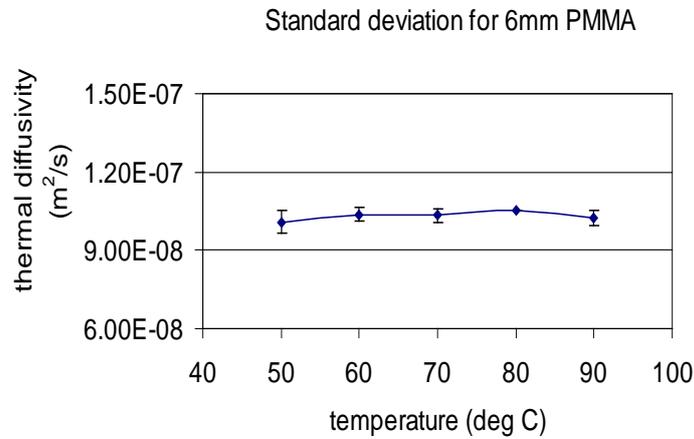
(b)

Figure 5 - 5 Standard deviation for PMMA samples

From Table 5-1 and Fig. 5-5, it could be seen that the thickness of the sample has a clear influence on the thermal diffusivity results decided by the tuning method. For the thinner sample, 3 mm PMMA, the thermal diffusivity results showed relatively more deviation between the experimental tests. The standard deviation for 3 mm PMMA sample ranges from 4.79×10^{-9} m^2/s ($n =$ 20) to 1.66×10^{-8} m^2/s ($n = 20$, the number of tests). For the 6 mm PMMA sample, the thermal diffusivity results appear to be more consistent in multiple tests and its standard deviation was in the range 0 m^2/s to 4.35×10^{-9} m^2/s ($n =$ 20). It is clear that the standard deviation for thick sample is much smaller than the one for thin sample. Smaller deviation means better precision and good repeatability. Therefore, it could be concluded that, with the advantage of better precision, this tuning method to measure thermal diffusivity works

better for thicker samples (6mm).

Based on the good repeatability of this experiment and low deviation result described in Fig. 5-5, for other samples, which were tested later, the average process was omitted, and experiments of different experiment temperature were conducted once to estimate thermal diffusivity results.

5.3 Experiments on metal materials

Comparing with the low diffusivity material PMMA presented in Section 5.2, high thermal diffusivity materials such as copper and aluminum were tested by the tuning method as well. Fig. 5-6 shows the graph for 9.0 mm thick bulk copper plate in 60˚C experiment temperature. Fig. 5-7 shows the graph for 5.9 mm bulk aluminum plate with 80˚C experiment. The best match for 9.0 mm thick bulk copper is the thermal diffusivity value $7 \times 10^{-5} m^2/s$, while the referenced value is 1.12×10^{-4} m^2/s [51]. The best match for 5.9 mm aluminum plate is the thermal diffusivity value 2×10^{-5} m^2/s, while the referenced value is 8.41×10^{-5} m^2/s [51].
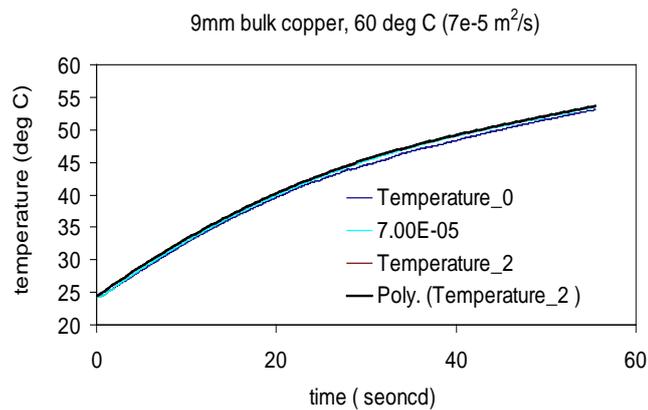
Figure 5 - 6 Test on 9.0 mm bulk copper
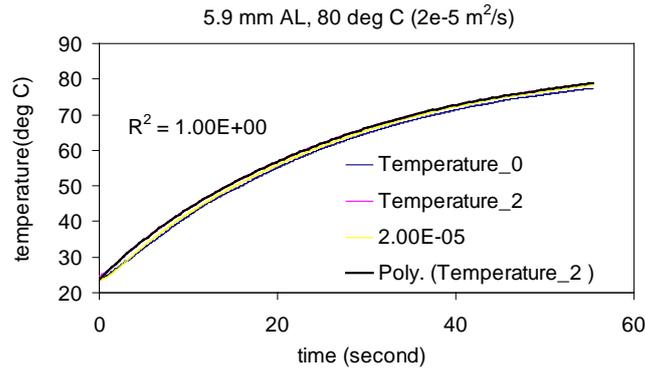
Figure 5 - 7 Test on 5.9 mm aluminum plate

Though the measured thermal diffusivity does not match exactly the established values for these high diffusivity materials, the test results could help to make a rough estimation of the magnitude of the thermal diffusivity. For copper, with the test value as $7\text{x}10^{-5}$ m^2/s and the consideration of heat loss that occurred during the experiment, it is very reasonable to assume that the thermal diffusivity of the material is a bit higher than $7\text{x}10^{-5}$ m^2/s, i.e. ($7\text{x}10^{-5}$ m^2/s – 10^{-4} m^2/s). The test result of the aluminum plate is $2\text{x}10^{-5}$ m^2/s. With the same reasoning with the copper experiment, it was estimated that the thermal diffusivity of the material is a bit higher than $2\text{x}10^{-5}$ m^2/s as well. The true thermal diffusivity value of aluminum is $8.41\text{x}10^{-5}\,m^2$/s, which is within the estimated range i.e. ($2\text{x}10^{-5}$ m^2/s – 10^{-4} m^2/s).

Another fact is that the tested results for aluminum plate were lower than that of the copper plate. By comparison, it could be known that the tested thermal diffusivity value of the aluminum is lower than the tested thermal diffusivity value of copper. In the meanwhile, the true thermal diffusivity value of the aluminum is lower than the true thermal diffusivity value of copper. This means the test result could be used to compare the thermal diffusivity of the materials. If one of the materials was known beforehand, a rough thermal diffusivity range for the other material could be further narrowed.

The reason for the inaccurate thermal diffusivity result was explained by

the heat loss happened during the experiment. High thermal diffusivity materials normally have high thermal conductivity, based on the equation $k = \alpha \rho c_p$. Bear in mind that, one of the boundary conditions used in the model was adiabatic, which means there was no heat flux between the sample and its insulator. In the real world, zero heat flux did not exist during the experiment. Heat loss occurred in the heat transfer process which was governed by the Fourier equation $q'' = -k\dfrac{dT}{dx}$. Therefore, compared with the ideal model used in Chapter 3, greater conductivity value would result more heat loss in the experiment, and reduce the accuracy of this method.

Based on the tests on high thermal diffusivity material copper and aluminum, it is concluded that this tuning method does not suit for high diffusivity materials (10^{-5} m^2/s – 10^{-4} m^2/s) due to the great heat loss in the experiment.

4mm cold sprayed copper, 70 deg C (3e-6 m^2/s)
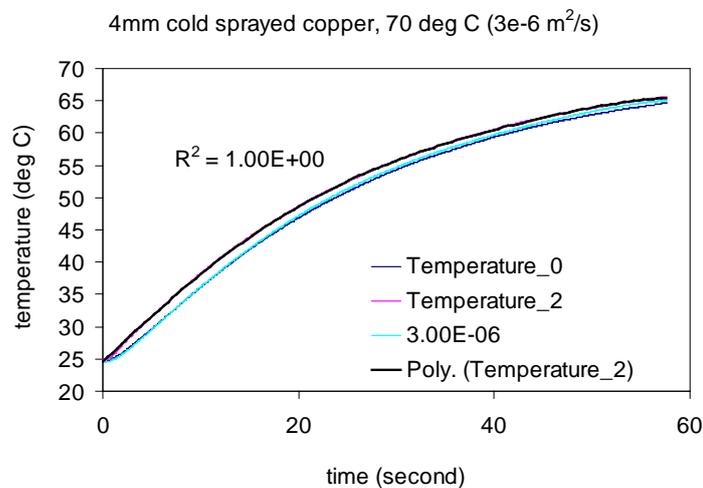
Figure 5 - 8 Tests on 4mm copper coating, fabricated by cold spray

A test was done on a 4 mm thick copper coating and shown in Fig. 5-8. This copper coating was fabricated by cold spraying technique. The copper coating was fabricated on a stainless steel substrate and peeled off afterwards. The thermal diffusivity result for this cold-sprayed copper sample was 3×10^{-6} m^2/s, which was much lower than the thermal diffusivity results 7×10^{-5} m^2/s, calculated by the bulk copper sample experiment. According to the estimation

analysis for copper and aluminum plate, it could be known that it means the thermal diffusivity of the fabricated copper was much lower than the thermal diffusivity of bulk copper. The result difference between the bulk copper sample and cold-sprayed sample means that the thermal properties of materials changed during the cold spray process in the fabrication procedure. Since the temperature (400°C) applied during the cold spray technique was not high enough to cause any oxidations, the reason for the lower thermal diffusivity should be the layered (lamellar) structure of the fabricated coating sample. A SEM test was used to capture the cross-section of the copper coating (Fig. 5-9). ImagePro software was used to estimate the porosity of this coating, which was as high as 0.1%. However, some small cavities existed in the sample, which caused lower thermal diffusivity value. This lower thermal diffusivity result agrees with the test result of analogous results for electrical conductivity by Stoltenhoff [53]. Instead of thermal diffusivity, electrical conductivity of copper coating fabricated by cold spraying method was compared with the electrical conductivity values of bulk copper and other thermal-sprayed copper coatings. It was found that the electrical conductivity of cold-sprayed copper was higher than that of copper coatings fabricated by other thermal spray techniques, namely HVOF and arc spraying. Stoltenhoff [53] found out that cold spraying technique worked better in keeping the original properties of bulk materials than other thermal spraying techniques did. However, the electrical conductivity result was still lower than that of the bulk material itself. The difference of properties between the coating and bulk material could be decreased by adjusting the spraying parameters. But, for most cold-sprayed coatings, the property (such as thermal diffusivity) would differ from that of the bulk material.

The low diffusivity of the cold-sprayed coating is because of air gaps, which were formed during the cold spraying process. The copper powder particles were sprayed to land on each other and endured plastic deformation.

Air was trapped between layers of lamellar coatings, shown in Fig. 5-9. Stoltenhoff *et al.* [53] used the sintering process to increase the electrical conductivity of the cold-sprayed coatings. The sintering process could be used to reduce the gaps within the coating. This process proved that the lower properties of the cold-sprayed copper compared with its bulk material, i.e thermal diffusivity and electrical conductivity, were because of the air gaps that were trapped in the coating.
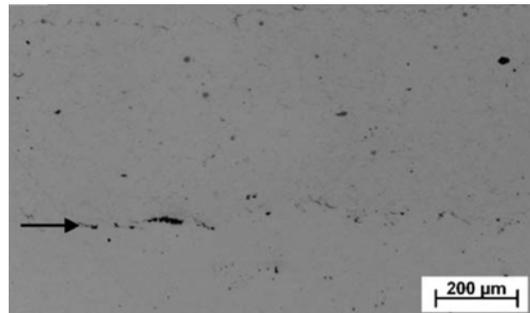
Figure 5 - 9 SEM picture of the cold-sprayed copper coating

5.4 Experiments on porous materials

To study the application of this tuning method to porous sample, 30% porous alumina was tested. Experiments were conducted with the hot plate set at 50˚C, 60˚C, 70˚C, 80˚C and 90˚C.

Temperature set on the hot plate (˚C)	Thermal diffusivity results of Al_2O_3 (m^2/s)
50	6.00×10^{-7}
60	7.00×10^{-7}
70	8.00×10^{-7}
80	8.00×10^{-7}
90	8.00×10^{-7}
average	7.40×10^{-7}

Table 5- 2 Thermal diffusivity table of Al_2O_3

This result of 7.40×10^{-7} m^2/s $\pm 1.4 \times 10^{-7}$ m^2/s ($n = 5$) is also shown in Table 5-2. It should be noted that the thermal diffusivity result obtained by this test is not the thermal diffusivity of bulk Al$_2$O$_3$, but the effective thermal diffusivity of 30% porous Al$_2$O$_3$. The cross-section of porous Al$_2$O$_3$ is shown in Fig. 5-10, the material has many pores. The air in the material greatly reduced the thermal property of the whole material. Therefore, the estimated thermal diffusivity value is much lower than the thermal diffusivity of a traditional Al$_2$O$_3$. The effective thermal conductivity of this material could not simply be decided by the properties of bulk Al$_2$O$_3$ and its porosity. Similar to the cold-sprayed copper coating, the microstructure of Al$_2$O$_3$ is very likely changed during the manufacturing process. This is the reason for the low thermal diffusivity result compared with the bulk Al$_2$O$_3$.
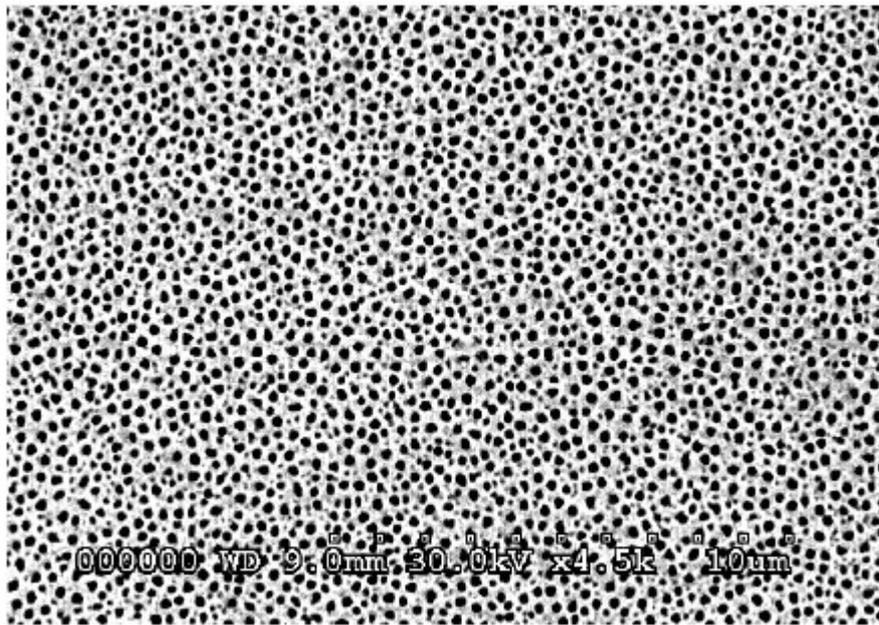
Figure 5 - 10 Cross-section of porous Alumina

5.5 TiO$_2$ on low carbon steel substrate and TiO$_2$ on copper substrate

As mentioned in Chapter 3, TiO$_2$ coatings were fabricated on low carbon steel and copper at the same time. Experimental results of TiO$_2$ on low carbon steel substrate are presented in Section 5.5.1; experimental results of TiO$_2$ on

copper substrate are presented in Section 5.5.2. The purpose of this is to study the effect to the diffusivity results on different substrate. The results of TiO_2 coating on different substrates are compared in Section 5.5.3.

Tests were conducted on two-layered sample TiO_2 on low carbon steel at the temperature 50˚C, 60˚C, 70˚C, 80˚C and 90˚C.

The parameters used in two-layered model are more complex than the single-layered model, and are shown with parameter tables. In these tests of TiO_2 on low carbon steel, two-layered mathematical model was applied accordingly. Substrate low carbon steel was modeled as layer 2 and TiO_2 coating was modeled as layer 1. The layer number is represented by the subscript of properties. Referred to the analytical solution developed in Chapter 2, the primary parameters in Table 5-3 were used in the program.

Parameters for TiO_2 on low carbon steel				
a (mm)	b (mm)	k_1[54] (W/m-K)	k_2[55] (W/m-K)	α_2[55] $10^{-5}(m^2/s)$
0.45	5.74	11.7	51.9	1.65

Table 5- 3 Parameters used in two-layered model for TiO_2 on low carbon steel

The same as TiO_2 on low carbon steel sample. The primary parameters used in the mathematical model are shown in Table 5-4.

Parameters for TiO_2 on copper				
a (mm)	b (mm)	k_1 [56] (W/m-K)	k_2 [52] (W/m-K)	α_2 [52] 10^{-4} (m^2/s)
0.47	8.98	11.7	401	1.12

Table 5- 4 Parameters used in two-layered model for TiO_2 on copper

The two groups of tests on TiO_2, namely TiO_2 on low carbon steel and

TiO$_2$ on copper, were conducted to study the effect of substrate. The coating was TiO$_2$ for both samples, only the substrates were different. One substrate was copper with high thermal diffusivity 1.12×10^{-4} (m^2/s) and high thermal conductivity 401 (W/m-K), and another substrate was low carbon steel with relatively low thermal diffusivity 1.65×10^{-5} (m^2/s) and thermal conductivity 51.9 (W/m-K). The thermal diffusivity test results of TiO$_2$ on both low carbon steel substrate and on copper substrate are shown in Table 5-5.

Thermal diffusivity results of TiO$_2$ (m^2/s)		
Temperature set on the hot plate (˚C)	on low carbon steel substrate	on copper substrate
50	1.80×10^{-7}	5.00×10^{-8}
60	1.50×10^{-7}	5.00×10^{-8}
70	1.50×10^{-7}	8.00×10^{-8}
80	1.50×10^{-7}	8.00×10^{-8}
90	1.50×10^{-7}	5.00×10^{-8}
Average	1.55×10^{-7}	6.2×10^{-8}

Table 5- 5 Thermal diffusivity results of TiO$_2$, tested with TiO$_2$ on low carbon steel and TiO$_2$ on copper

The results show a clear tendency that the thermal diffusivity results of TiO$_2$ on copper substrate are lower than the thermal diffusivity results of TiO$_2$ on low carbon steel substrate. The TiO$_2$ coatings on both the samples were fabricated at the same time. However, the thermal diffusivity results of TiO$_2$ on copper substrate are lower than the thermal diffusivity results of TiO$_2$ on low carbon steel substrate. The influencing factor to the lower results is the high thermal conductivity value of copper substrate. The high thermal conductivity value of copper has resulted large heat loss during the experiment. Reflecting on the results, the TiO$_2$ coating shows lower thermal diffusivity results.

From these groups of experiment, it can be concluded that the substrate could have an influence on the thermal diffusivity results from the test. This is a deficiency of the test method. If the thermal conductivity of the substrate is high, the thermal diffusivity result of the coating would be lower as the consequence of the heat loss from the substrate. On the other hand, for coating on the substrate with low conductivity, the thermal diffusivity result of the coating would be relatively higher and closer to the referenced value, because of lower heat loss from the substrate. Therefore, similar to single-layered materials, the thermal diffusivity result is more accurate for low conductivity (lower than 51.9 W/m-K, the conductivity of low carbon steel) substrate.

5.6 YSZ on low carbon steel substrate

The YSZ on low carbon steel substrate was fabricated by air plasma spraying technique. The thickness of YSZ is 0.28 mm, and the total thickness of the two-layered sample is 6.67 mm. The parameters used in the mathematical model are listed in Table 5-6, where α_1 is the parameter to be decided. This experiment features low thermal diffusivity coating on relatively high thermal diffusivity substrate. The experiment was conducted on the two-layered sample at the experiment temperature 50˚C, 60˚C, 70˚C, 80˚C 90˚C and 100˚C, and the test results are shown in Table 5-7.

The results table-Table 5-7 shows that in this group of experiments on YSZ on low carbon steel, the 50˚C and 60˚C experiments were able to provide thermal diffusivity result of YSZ as 1×10^{-8} m^2/s. A good agreement exists in the two sets of experiment with different temperature boundary condition. However no reference for the thermal diffusivity of YSZ was found. For the 70˚C, 80˚C, 90˚C, 100˚C experiments, none of the predicted temperature was able to make a match with the experiment. A typical experimental figure in high experiment temperature is shown in Fig. 5-11. Setting the boundary

condition as the comparison standard, experiment temperature data was compared with the predicted temperature data. It could be seen that the experiment data shows a sharp slope, while the slope of predicted temperature profile is relatively mild. In the first half of the experiment, temperature data, which were taken by thermocouple 0 at the surface of the coating material, were relatively far from the temperature boundary condition; the experiment temperature data was relatively far away from the boundary temperature. In the later part, the experiment temperature tended to go closer toward the boundary condition. Unlike the experimental temperature data, the temperature predicted at the surface of the coating had a relatively constant distance with the boundary condition.

Parameters for YSZ on low carbon steel				
a (mm)	b (mm)	k_1 (W/m-K)	k_2 (W/m-K)	α_2 (m^2/s)
0.28	5.67	1.2	51.9	1.65×10^{-5}

Table 5- 6 Parameters used in two-layered model for YSZ on low carbon steel substrate

Temperature set on the hot plate (˚C)	Thermal diffusivity results of YSZ (m^2/s)
50	1×10^{-8}
60	1×10^{-8}
70	Not decided($2 \times 10^{-8} \sim 5 \times 10^{-7}$)
80	Not decided($2 \times 10^{-8} \sim 5 \times 10^{-7}$)
90	Not decided($2 \times 10^{-8} \sim 5 \times 10^{-7}$)
100	Not decided($2 \times 10^{-8} \sim 5 \times 10^{-7}$)
Average	Not decided($2 \times 10^{-8} \sim 5 \times 10^{-7}$)

Table 5- 7 Thermal diffusivity table of YSZ
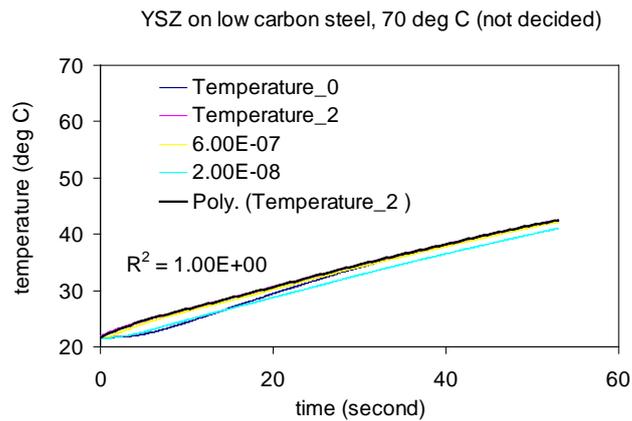
Figure 5 - 11 Tests on YSZ on low carbon steel, hot plate was set at 70˚C

This phenomenon is probably because the great difference between the thermal properties of the coating and substrate materials. As shown in Table5-4, the substrate is low carbon steel, and has a thermal conductivity value as 51.9 W/m-K, and thermal diffusivity as 1.65×10^{-5} m^2/s. For the coating material YSZ, from the literature, its thermal conductivity value was set as 1.2W/m-K in the mathematical model. The results for 50˚C and 60˚C experiments show that the thermal diffusivity result is as low as 1×10^{-8} m^2/s. The substrate is low carbon steel and the coating is YSZ. The two materials have great difference in thermal diffusivity values. When the temperature difference between the initial temperature and experiment temperature is low (experimental temperature as 50˚C and 60˚C), the different thermal properties of the two layers did not make a large impact on the experimental figure match. The match between the experiment temperature curve and the predicted temperature curve is good enough to provide a diffusivity value. Therefore, the experimental figures are similar to the ones of other samples such as PMMA and metal plates. When the temperature difference is high (with experimental temperature above 70˚C), the impact from different thermal diffusivity value between substrate and coating shows changes in form of temperature profile with sharp trend. This is further explained in Section 5.8.

5.7 Single-layered Pyrex and Nano-structured TiO₂ on Pyrex substrate

5.7.1 Test on single-layered Pyrex samples

In this group of tests, sets of experiments were conducted. Two single-layered Pyrex were tested by the single-layered model to obtain its thermal diffusivity value. Then the single-layered sample serves as substrate, TiO_2 coatings were fabricated on it. The TiO_2 coating was fabricated on the two Pyrex substrates at the same time. Therefore, the spraying parameter and spraying environment were the same, and the properties are the same. The two-layered sample is then studied by two-layered model to test the thermal diffusivity of the coating. The results are shown in Fig. 5-12.
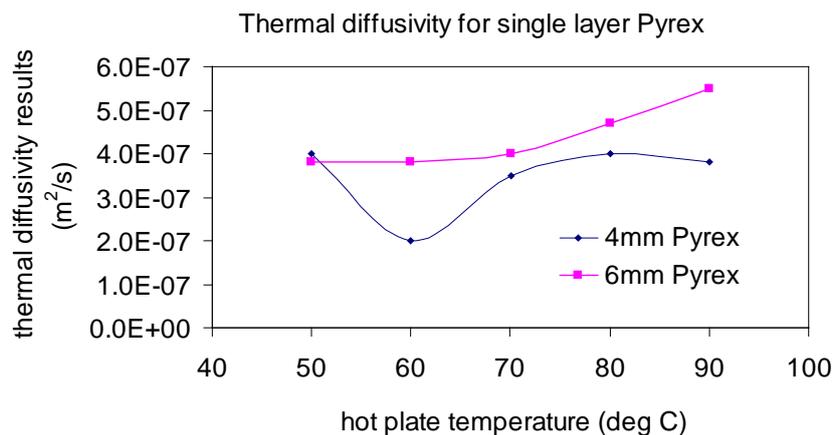
Figure 5 - 12 Thermal diffusivity for single-layered Pyrex

The test graphs of single-layered Pyrex slabs at each experiment temperature were checked. Thicker single Pyrex slab (6mm thick) provided good match for all experiment temperatures in thermal diffusivity results, which means the predicted temperature profiles agrees with the experiment temperature profile during the experiment period. By checking the test graphs of the 4 mm thick Pyrex closely, poor measurements, which meant predicted temperature profile showed deviation from the experimental temperature profile, happened at 60°C and 80°C experiment temperature. This deviation might be because of the experiment procedure, such like the Styrofoam was

not wrapped tight enough or the thermocouple attachment was loose. It should be noted that the deviation caused by these possible reasons did not happen in the tests for 6mm Pyrex. This proves that relatively thicker sample (6mm) works better for the thermal diffusivity measurement method. From Fig. 5-12, it could be seen that the thermal diffusivity range for both 4 mm and 6 mm Pyrex in all experiments (hot plate set at 50˚C to 90˚C) was between $2x10^{-7}$ m^2/s and $6x10^{-7} m^2$/s. 6 mm Pyrex shows a steady increasing trend, which ranges from $3.8x10^{-7}$ m^2/s to $5.5x10^{-7}$ m^2/s. For 4mm Pyrex, no distinct trend was shown. This is probably because of the poor match at temperature 60˚C and 80˚C. This phenomenon means that the thermal diffusivity result of Pyrex is sensitive to experiment temperature variation. Unlike the material PMMA, which showed great repeatability multiple tests, the small variation of experiment temperature would induce noticeable change in the thermal diffusivity values for Pyrex samples. The sensitivity of Pyrex was proved further by the experiments on two-layered sample TiO_2 on Pyrex.

Despite the differences between the thermal diffusivity results from the two Pyrex slabs, the thermal diffusivity results of Pyrex showed some unique features comparing with other samples. The experiment results of Pyrex were compared with the former experiments on PMMA, since in term of thermal diffusivity values; PMMA and Pyrex both have low thermal diffusivity values. In Table 5-8, we could see that PMMA had good repeatability for different experiment temperatures set on the hot plate. For Pyrex, however, Fig. 5-12 shows less agreement between thermal diffusivity results at different temperature boundary condition for this material. Each experiment resulted different thermal diffusivity results.

5.7.2 Nano TiO2 on Pyrex

The single-layered Pyrex samples tested in Section 5.7.1 were used as substrates for nano TiO_2 coatings, and the tested Pyrex thermal diffusivity

results were used in the process of thermal diffusivity determination for nano TiO$_2$ coatings. Table 5-8 shows all the thermal diffusivity results of Pyrex substrate by single-layered model and that of Nano TiO$_2$ coatings by two-layered model.

Thermal Diffusivity of Pyrex and Nano TiO$_2$ coating (m^2/s)				
Temperature (˚C)	4mm Pyrex	Nano TiO$_2$ on 4mm Pyrex	6mm Pyrex	Nano TiO$_2$ on 6mm Pyrex
50	4.00×10^{-7}	1.00×10^{-5}	3.80×10^{-7}	1.00×10^{-5}
60	2.00×10^{-7}*	not decided	3.80×10^{-7}	1.00×10^{-5}
70	3.50×10^{-7}	not decided	4.00×10^{-7}	not decided
80	4.00×10^{-7}*	5.00×10^{-6}	4.70×10^{-7}	not decided
90	3.80×10^{-7}	not decided	5.50×10^{-7}	not decided
Average	3.46×10^{-7}	N/A	4.36×10^{-7}	N/A

Table 5- 8 Thermal diffusivity of Pyrex and Nano TiO$_2$ coating (* *the thermal diffusivity results with * did not provide a good match between experiment and mathematical prediction*.)

From these test result, it could be seen that in the different tests temperatures, only 50˚C and 80˚C for 4 mm Pyrex could give thermal diffusivity results for nano-TiO$_2$ (1×10^{-5} m^2/s and 5×10^{-6} m^2/s). The two very different values indicate that the thermal diffusivity results might not be dependable. For thicker sample, nano-TiO$_2$ on 6mm Pyrex sample, for both 50˚C and 60˚C, the thermal diffusivity results for nano-TiO$_2$ were both 1×10^{-5} m^2/s. Few literature was found on the thermal diffusivity of nano-TiO$_2$ coating. The thermal diffusivity of bulk TiO$_2$ is 1.83×10^{-5} m^2/s. The means the test result had good agreement for the low temperature.

However, for high experiment temperature, no value could result a temperature profile to match the experiment temperature, with the thermal diffusivity of Pyrex set according to single-layered experiments. This indicates the property assumption of the other layer (Pyrex) might be incorrect.

The incorrect thermal diffusivity assumption of Pyrex is probably because of the mechanical and thermal treatment which was added on the material during the thermal spray process.

To prove the point, the following analysis was made. The coating thickness of Nano TiO$_2$ is 0.38 mm, while the thickness for substrate was either 4 mm or 6 mm. Since the thickness of the coating is very small compared to the substrate, the two-layered sample was assumed as a single-layered sample of Pyrex to observe the influence of the TiO$_2$ coatings on the thermal diffusivity value.

Therefore, single-layered model was applied to calculate the thermal diffusivity of the after sprayed Pyrex sample. The results achieved by these tests are called the estimated thermal diffusivity.

Figures 5-13 and 5-14 show the comparison between the single-layered results and estimated results on 4 mm sample and 6mm sample. Both figures show a clear trend that the estimated thermal diffusivity values of Pyrex are much higher than the thermal diffusivity value calculated by single-layered experiments. It is unlikely that the big thermal diffusivity change of Pyrex is due to the thermal property of the thin nano TiO$_2$ coating. This is a proof that that the thermal property of Pyrex experienced a big change after the flame spraying process. The thermal shock temperature of Pyrex is 160˚C, while the flame temperature of flame spray could reach 3000˚C. During the spraying the Pyrex had experienced a temperature that is much higher than its thermal shock temperature. Therefore, it is reasonable for the Pyrex thermal diffusivity to experience a big change. Because the change of Pyrex thermal properties were not able to be calculated, the two-layered model does not have access to correct properties of the substrate material , which are essential to the program, to calculate the thermal diffusivity of the Nano TiO$_2$ coating.

For the thicker sample, the estimated thermal diffusivity of Pyrex shows the same increasing trend as the calculated thermal diffusivity of single Pyrex. Similarly, this trend proves that Pyrex is very sensitive to temperature change for thicker samples.

thermal diffusivity of 4mm Pyrex
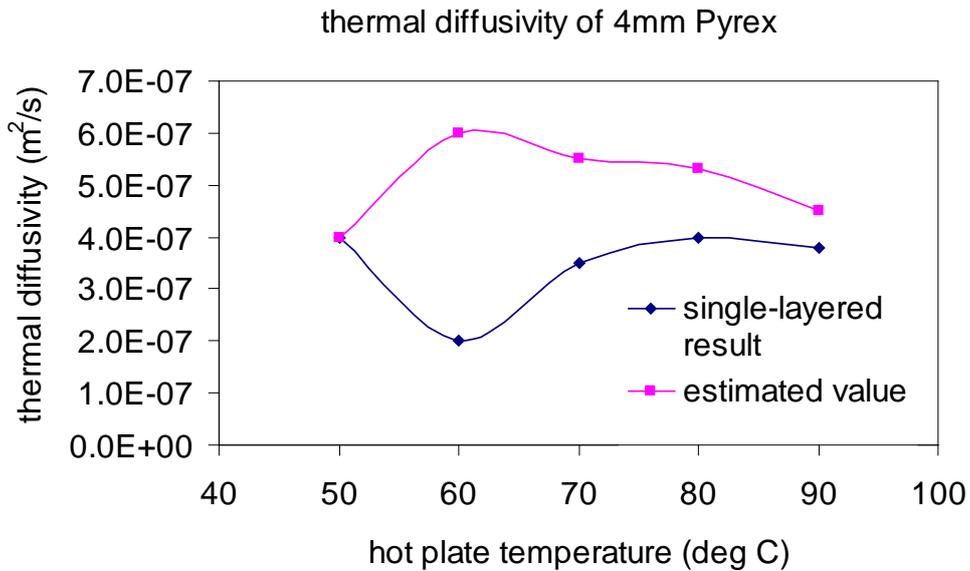
Figure 5 - 13 Thermal diffusivity of single-layered 4mm Pyrex based on single-layered experiment and estimated thermal diffusivity of Pyrex based on 4mm two-layered experiment

thermal diffusivity of 6 mm Pyrex
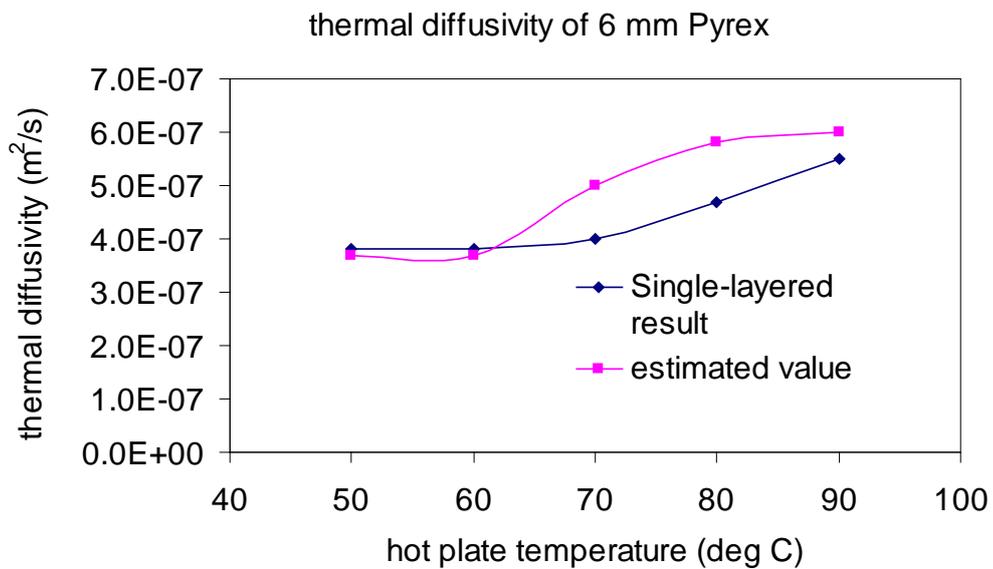
Figure 5 - 14 Thermal diffusivity of single-layered 6mm Pyrex based on single-layered experiment and estimated thermal diffusivity of Pyrex based on 6mm two-layered experiment

5.8 Heat loss analysis

By observing the temperature profiles for multiple experiments for different samples, it was found that the agreement between the experiment temperature and the predicted temperature showed an interesting trend. It is believed that heat loss plays an important part during the experiment; therefore the heat loss analysis was used to interpret the trend.

As for the heat loss analysis, Fig. 5-15 is a schematic diagram to explain the heat loss occurs in the sample during the experiment. In the experiment, insulating material Styrofoam was wrapped around the sample (except the heated surface) to simulate a perfect adiabatic boundary condition. However, even though the Styrofoam has low thermal diffusivity and low thermal conductivity value, heat loss occurs around the sample. The heat loss was categorized into two groups, namely heat loss from the top surface and heat loss from the side surfaces. Ideally, heat flux on all the side surfaces was assumed to be the same. The heat flux on the surface was assumed to be uniform.

For the two-layered sample, heat loss from the side surfaces was further separated into two categories, which were heat loss from the side of the substrate and heat loss from the side of coating.

Heat loss was governed by the area of heat loss, the heat conductivity, and the temperature gradient across that surface. The area was constant. The heat conductivity varied little within the small temperature range and was assumed to be constant for each material. The temperature gradient changed with time and position. In the heat loss analysis, to make analysis easy, the temperature gradient was assumed to be uniform on each surface and just vary with time. The mathematical description was shown in Eqn. (5-1) and Eqn. (5-2). Considering the small thickness of the coating, the side heat loss from

the side of coating could be ignored. In the following, several samples, which exhibit representative temperature curves, were studied with the heat loss analysis. It should be noticed that in the mathematical model, the problem was assumed to be one-dimensional to keep the problem simple. However, in the heat loss analysis, the reality case was considered and the heat loss was studied with two dimensions.
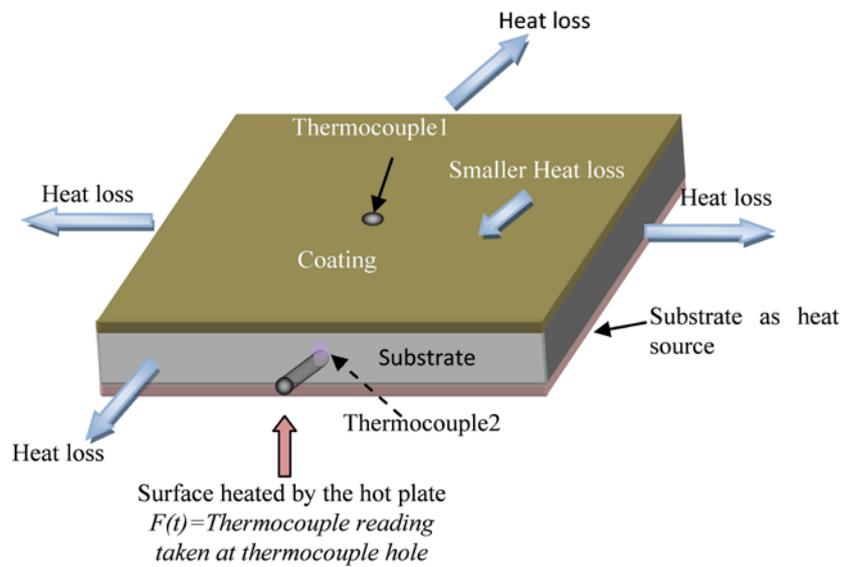
Figure 5 - 15 Heat flux on a two-layered sample

total heat loss

= side heat loss + top heat loss

=substrate side heat loss + coating side heat loss

+coating top heat loss

$$= \quad A_{2,s} \cdot k_2 \cdot \frac{\partial T(x, y)}{\partial y} + A_{1,s} \cdot k_1 \cdot \frac{\partial T(x, y)}{\partial y} + A_{1,t} \cdot k_1 \cdot \frac{\partial T(x, y)}{\partial x}$$

(5-1)

$q(t)$

$$= \int k_2 \cdot \frac{\partial T(x, y = edge, t)}{\partial y} dA_{2,s} + \int k_1 \cdot \frac{\partial T(x, y = edge, t)}{\partial y} dA_{1,s} + A_{1,t} \cdot k_1 \cdot \frac{\partial T(x, y = edge, t)}{\partial x}$$

$$= \int k_2 \cdot \frac{\partial T(y = edge, t)}{\partial y} dA_{2,s} + \int k_1 \cdot \frac{\partial T(y = edge, t)}{\partial y} dA_{1,s} + A_{1,t} \cdot k_1 \cdot \frac{\partial T(y = edge, t)}{\partial x}$$

$$= \int_a^b k_2 \cdot \frac{\partial T(y = edge, t)}{\partial y} \cdot C \cdot dx + \int_0^a k_1 \cdot \frac{\partial T(y = edge, t)}{\partial y} \cdot C dx + A_{1,t} \cdot k_1 \cdot \frac{\partial T(y = edge, t)}{\partial x}$$

$$(5\text{-}2)$$

5.8.1 Heat loss analysis for PMMA

Heart loss analysis for single-layered low thermal diffusivity materials PMMA was shown in Fig. 5-16. The magnitude of the heat loss from the top surface and that from the side surfaces are compared in this figure. Heat loss is represented by $A \cdot k \cdot \frac{\partial T(t)}{\partial r}$, where r represents x direction (vertical direction) for top surface heat loss, and represents y and z direction (horizontal direction) for side surface heat loss.
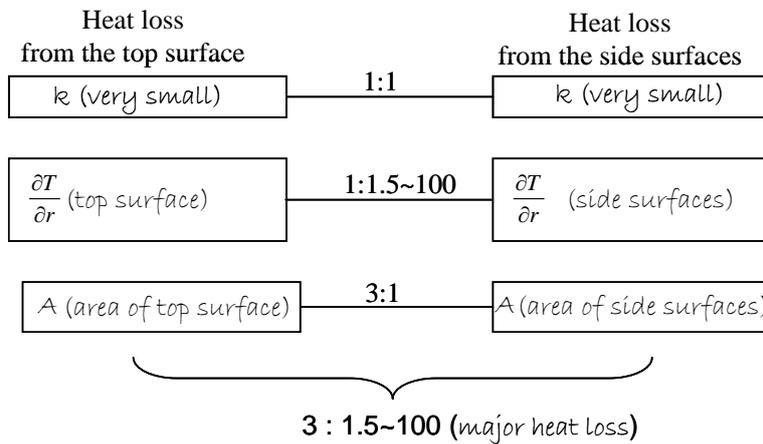
Figure 5 - 16 Heat loss analysis of PMMA

In this chart, the left part is the heat loss from top surface, and the right part is the heat loss from the side surfaces. For single-layered sample the conductivity for side surfaces heat loss and top surface heat loss was the same. The ratio of conductivity at top surface and side surfaces is 1:1. PMMA has a

very small heat conductivity value, which is between 9.5×10^{-8} m²/s and 1.5×10^{-8} m²/s.

The ratio of top surface area and side surface area is roughly calculated. Given the width and length of the sample is normally 40mm, and the thickness is proximately 3mm, the top surface area is 1600 mm² and the side surfaces area is 480mm². The ratio of top surface area and side surfaces area is about 3:1.

More concern should be taken on the temperature gradient. To simplify the analysis, the temperature gradient was assumed to be uniform throughout each surface and changed with time. The experiment data was used to give an estimate of the temperature gradient. The insulating material was assumed to be at the same temperature throughout the experiment, therefore the temperature gradient would be calculated by Eqn. (5-3). In this equation, insulating material temperature was assumed to be the environmental temperature which was the initial temperature T_i of the experiment. Temperature on top surface was measured by thermocouple 0, therefore represented by T_0. The temperature of the side surface was represented by the average of boundary temperature and top surface temperature $(T_2 + T_0)/2$, since the sample was assumed to be in uniform temperature to simplify the calculation.

$$
\frac{\partial T}{\partial r} \, on \, top \, surface : \frac{\partial T}{\partial r} \, on \, side \, surfaces
$$

$$
= \frac{\dfrac{temperature \, on \, top \, surface - insulating \, material \, temperature}{r}}{\dfrac{temperature \, on \, side \, surfaces - insulating \, material \, temperature}{r}}
$$

$$
= \frac{T_0 - T_i}{(T_1 + T_0)/2 - T_i}
\tag{5-3}
$$

The raw temperature data, collected by data acquisition system, were

used to calculate the temperature gradient ratio applying Eqn. (5-3). The raw data were transferred to EXCEL, and the data (around 1200 temperature data) for the whole time period, (60 second, with the frequency set as 10 Hz and two thermocouples readings) were used in this process. It was found out that the temperature gradient ratio of top surface to side surfaces is between 1:1.5 to 1: 100 for 6mm PMMA sample.

In this heat loss analysis graph, it could be seen that the ratio of heat loss from the top surface and the side surfaces is about 3:100, which means the heat loss from the side surfaces play dominant role in the heat loss analysis. The side surfaces area was very small as a consequence of small thickness and the heat conductivity value small as well. It could be concluded that heat loss from the side surfaces was small and further the overall heat loss for PMMA was in a very small amount. The sample could be assumed to be with a perfect insulation effect. This explains the good thermal diffusivity test result for the PMMA samples.

5.8.2 Heat loss analysis for copper
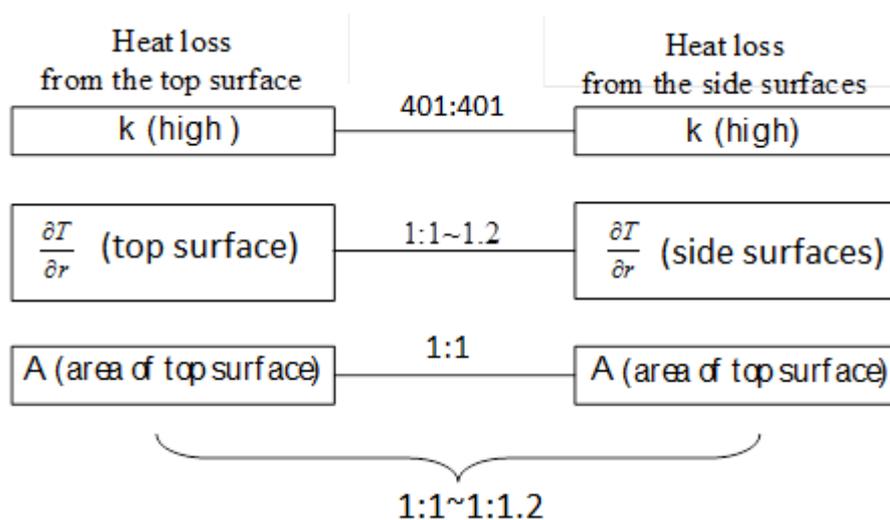
Figure 5 - 17 Heat loss analysis for single-layered 9 mm thick copper

Similar to the analysis of single-layered PMMA, the heat loss to 9 mm thick copper is analyzed in the same way. For single-layered sample, the

conductivity is the same and has the ratio as 1:1. Based on the experiments result, the temperature gradient ratio is 1:1 to 1:1.2 by Eqn. (5-3). The ratio of area of top surface to area of side surfaces is about 1:1. The heat loss ratio for the 9mm thick copper would be 1:1.2, which is very close to each other. Due to the high thermal conductivity value, the heat loss was great on both top surface and the side surfaces.

5.8.3 Heat loss analysis for YSZ on low carbon steel
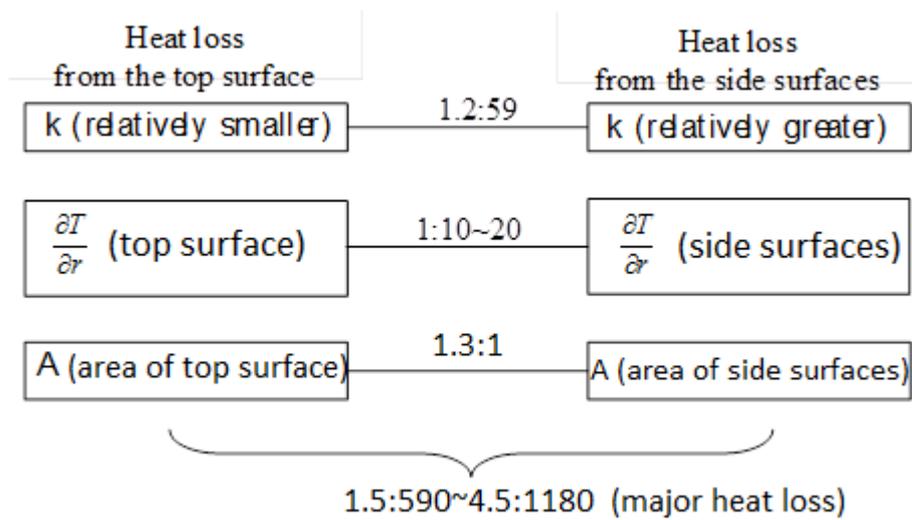
Figure 5 - 18 Heat loss analysis for YSZ coating on low carbon steel

As shown in Fig. 5-18, surface ratio for YSZ on low carbon steel would be 1.3:1. From this heat loss analysis for YSZ on low carbon steel, we could see that, compared with the heat loss from the side surfaces, the heat loss from the top surface is much lower. The ratio between the heat loss from the top surface and the heat loss from the side surfaces is about 1.5 to 590, which means the heat loss from the side surfaces plays a more important role in the heat loss analysis. Considering the high heat conductivity of the substrate low carbon steel, it can be known that the heat loss was as great as the single-layered high thermal diffusivity metal at the beginning of the heat transfer process. The heat transfer process was similar to that of the

single-layered sample in the beginning. However, in the later period, the special feature of YSZ on low carbon steel sample started to influence the shape of the experiment temperature profile. The top surface has very low heat conductivity value and therefore the temperature gradient ratio is very low. It was as if the top surface was well insulated, only the side surfaces were have heat loss. Therefore, the experiment temperature profile started to rise in the latter part of the experiment.

In this group of experiments on YSZ on low carbon steel, the 50°C and 60°C experiments were able to provide thermal diffusivity result of YSZ as $1x10^{-8}$ m^2/s. A good agreement was in the two sets of experiment with different temperature boundary condition. However, for the 70°C, 80°C, 90°C 100°C experiments (i.e. Fig. 5-13), it was shown in the experiment figures that none of the predicted temperature was able to make a match with the experiment. Comparing the experiment temperature data with predicted temperature data, it could be seen that the experiment data processed a sharp slope, while the slope of predicted temperature profile was mild. In the first half of the experiment, temperature data, which were taken by thermocouple 0 at the surface of the coating material, were relatively far from the temperature boundary condition.

This would probably be because the great difference between the thermal properties of the coating and substrate materials. As shown in Table 5-6, the substrate-low carbon steel had a heat conductivity value of 51.9 W/m-K, while the YSZ coating had a heat conductivity value 1.2W/m-K. The substrate-low carbon steel had a thermal diffusivity value of $1.65x10^{-5}$ m^2/s, while the YSZ coating had a tested value of thermal diffusivity $1x10^{-8}$ m^2/s for 50°C or 60°C tests. With this great differences in the thermal properties between the coating and substrate, heat process would be influenced by different temperatures during the heat conduction process. Even the heat conduction process was assumed to be adiabatic on the side surfaces and the surface of the YSZ

coating, heat loss occurred through these surfaces during the process.

On the YSZ coating top, less heat loss could occur as the consequences of low heat conductivity of the material YSZ. When the temperature was set to low experiment temperature on the hot plate as 50˚C or 60˚C, the heat flux enter through the bottom surface of the substrate would be small, therefore, the heat loss from the side and top surfaces of the sample was small. The small amount of heat loss resulted very little differences between the size surfaces heat loss and top surface heat loss. The temperature profile (Fig. 5-31 and Fig. 5-32) would develop as other two-layered samples which had similar thermal properties.

However, when the experiment temperature on the hot plate was set above 70˚C (Figs. 5-11), the heat loss went through the bottom surface would be greater. In the meantime the heat loss from the sample would increase with the heat flux input. Heat conductivity between two different materials, namely the substrate low carbon steel and the coating YSZ, would play an essential role in this process. Heat loss from the top surface would be much smaller than the heat loss from the side surfaces. It was like when the temperature on the hot plate was set higher, a better insulating material was placed on the top of the sample. Therefore temperature on the YSZ surface Temperature 0 would rise in a sharp slope.

5.8.4 Summary of heat loss analysis

In the analysis of heat loss, the heat loss from the top surface made an important influence on the shape of the experiment temperature profile. $A_{1,t}$ is the area of top surface of sample. In the description in Chapter 3, it is known that in the sample preparation, the top and bottom surface of the sample was much bigger than the side surfaces. $\dfrac{\partial T(x=b,t)}{\partial x}$ is the temperature gradient on the insulated surface of the sample.

The heat loss was proportional to the area, heat conductivity and temperature gradient. The temperature gradient increased with the time. The heat conductivity was decided by the material. The area was decided by the preparation of the sample. Heat loss includes two parts, namely the heat loss from the side of the sample and the heat loss from the top surface of the sample. Considering the area of top surface and side surface, apparently the top surface played a greater role in the heat loss analysis.

When the thermal diffusivity is of medium range, saying 1×10^{-5} m^2/s to 1×10^{-6} m^2/s, it was observed that, in the temperature profile figures, the predicted temperature profile with a proper assumption of thermal diffusivity value could match well with the temperature profile.

When the thermal diffusivity values of materials were of higher range, saying 1×10^{-4} m^2/s to 1×10^{-5} m^2/s, the heat loss function $A_{1,t} \cdot k_1 \cdot \dfrac{\partial T(x,t)}{\partial x}$ was analyzed. Thermal conductivity value was high; the area of the heat loss was big; thermal gradient $\dfrac{\partial T(x=b,t)}{\partial x}$ was small at the beginning, and became greater as time increased, according to Eqn. (5-3). In the beginning due to the small heat gradient, the third part had less influence on the overall heat loss. In the later part of the experiment, the heat gradient became greater, and the heat loss area was much bigger compared with the side surfaces. With a high thermal conductivity value, a big amount of heat loss existed from the top surface. Therefore, the tail part of the experiment temperature profile was generally lower than the predicted temperature.

A different situation happened in the sample of YSZ on low carbon steel. It was found that the tail of the experiment temperature rose higher than the predicted temperature profile (Fig. 5-36). It should be noted that when the substrate and coating having thermal diffusivities with great difference, the heat loss would be very different for the two layers. Therefore, at high

experiment temperature this method is not able to provide good test result.

Chapter 6: Conclusion

A new method of thermal diffusivity measurement was developed in this thesis. Single-layered sample, including low diffusivity (smaller than $10^{-6}\text{m}^2/\text{s}$) materials such as PMMA and Pyrex, metal materials such as copper and aluminum, and porous materials such as Al_2O_3 with 30% porosity were tested with single-layered model. For PMMA, 20 tests were conducted, with 5 different experiment temperatures. For each experiment temperature, the tests were repeated 4 times. In these tests, the thermal diffusivity results agreed with the referenced thermal diffusivity value and showed good repeatability. All the other materials are tested with several experiment temperatures, and each experiment temperature was conducted once.

The most important factor that undermines the accuracy of this measurement method is the heat loss that occurred during the experiment. The heat loss, which varied with time and position, was not assumed in the mathematical model. Therefore, when the heat loss in the experiment was low, the measurement results tended to be accurate, such as with the PMMA sample. When the heat loss was high, the measurement results tended to deviate from the referenced value, such as copper sample. When the heat loss was not in a relatively smooth variation, it was difficult for this method to determine the result, such as YSZ on low carbon steel substrate samples. This is because the dramatic variation of heat loss caused the experimental

temperature profiles to change into curves which did not imitate the predicted temperature profile.

For single-layered samples, it was found out that the thermal diffusivity of material Pyrex was sensitive to temperature change. For metal materials, the result of thermal diffusivity was lower than the referenced value. The thermal diffusivity result of copper was 7×10^{-5} m^2/s, and the thermal diffusivity result of alumina was 2×10^{-5} m^2/s. The lower test values were because that metal material had higher thermal conductivity value which would cause more heat loss in the experiment. Despite the inaccuracy of the thermal diffusivity results for metal materials, it could give a rough estimation of the thermal diffusivity range. The thermal diffusivity range could be improved when a material, whose thermal diffusivity is known beforehand, is also tested as a referenced material. For porous material Al_2O_3, the thermal diffusivity result was 7.4×10^{-7} m^2/s, which was much lower than the thermal diffusivity of the bulk material. It is because of the air pores within the material and other changes happened during the manufacturing process.

Among the two-layered materials, conventional material TiO_2 were tested on different substrate to study the influence of the substrate to the thermal diffusivity value of coatings. It was found out that the low carbon steel substrate would affect the thermal diffusivity result less compared with the copper substrate. It was because the material low carbon steel had lower thermal conductivity than copper, therefore, less heat loss from the substrate

during the experiment.

The YSZ thermal diffusivity result determined by studying YSZ on low carbon steel substrate sample shows that the thermal diffusivity result of YSZ was 1×10^{-8} m^2/s for both the 50˚C and 60˚C experimental temperatures. The thermal diffusivity results of YSZ could not be determined when the experiment temperature was above 70˚C. However, the experiment temperature figures showed an interesting trend. In the earlier stage of the experiment, the temperature profile possessed a mild slope and in the later stage the temperature profile showed a sharp slope and reached the temperature boundary condition profile. This profile was due to the occurrence of different heat loss on the side surfaces and top surfaces.

The effect of flame-sprayed TiO$_2$ coating on the material Pyrex was studied. Given that no agreement between the experimental and established diffusivity value of the TiO$_2$ coating could be obtained by using the thermal diffusivity result of Pyrex substrate (estimated before spraying process), it could be concluded that the thermal property of Pyrex substrate changed during the spraying process. Therefore, by testing the thermal diffusivity value, this method could be used to detect property changes.

The application field of the thermal diffusivity measurement method was studied. Based on the multiple tests of Pyrex, PMMA samples, it was found out that this method worked better for relatively thick coating, which ranged from 5mm to 9mm. This method worked well for low conductivity

materials. When dealing with the coatings on the substrate, it would be better that the thermal conductivity of the substrate and coating are not too different from each other. The great thermal conductivity difference would cause slope change in the temperature profile, and makes the temperature profile matching difficult.

This thermal diffusivity method was based on two-layered sample. It could measure thermal diffusivity of coatings without the need of coating detachment. Compared with other measurement methods, this method does not require expensive and complicated operation process. This test method could be improved by performing tests on more samples, to determine the thermal conductivity range of materials that is suitable for this test method.

As for the agreement between the predicted temperature curves and the experiment temperature curves, further work is recommended. Instead of comparing the curves by temperature data at different time point, least square fitting method could be used to provide more direct standard with quantization.

The accuracy of this test method would be greatly increased if the heat loss could be controlled. As for the convenient-simple-and-low-cost feature of this method, it would more reasonable to improve the mathematical model, instead of upgrading the experiment apparatus to achieve the goal. If the heat loss happened during the experiment could be estimated and put into the mathematical model as boundary condition or heat sink element, the deviation

from the real property value should increase a lot. Another solution might be using some empirical coefficient or function to modify the test result to get better accuracy.

More tests should be conducted on more samples with different thermal diffusivity, so that the application spectrum of this test method should be determined. It was noted that for materials with higher thermal diffusivity such as aluminum and copper plates (greater than 1.65×10^{-5} m^2/s), the test data results did not agree with the referenced data; for materials with low thermal diffusivity value, such as PMMA (lower than $1 \times 10^{-6} m^2/s$), the test result agreed with the referenced value. A more detailed "thermal diffusivity vs. error" chart is recommended for further work.

Reference

[1] A. Savarimuthu, H.Taber, I. Megat, I. Shadley, E, Rybicki, W. Cornell, W. Emery, D. Somerville, and J. Nuse, "Sliding wear behaviour of tungsten carbide thermal spray coatings for replacement of chromium electroplate in aircraft applications," J. Therm. Spray Technol., Vol.10, 2001, pp. 502-510

[2] X. Q. Cao, R. Vassen, and D. Stoever, "Ceramic materials for thermal barrier coatings," J. Eur. Ceram. Soc, Vol. 24, 2004, pp. 1-10

[3] J.Wu, X.Wei, N.P.Padture, P.G.Klemens, M.Gell, E.Garcia, P.Miranzo and M.I.Osendi, "Low-Thermal-Conductivity Rare-Earth Zirconates for Potential Thermal-Barrier-Coating Applications," J. Am. Ceram. Soc., Vol. 85, 2002, pp.3031-3035

[4] D Toma, W Brandl, and G Marginean, "Wear and corrosion behavior of thermally sprayed cermet coatings," Surf. Coat. Technol., Vol.138, 2001, pp. 149-158

[5] G. Barbezat, A.R. Nicol, and A. Sickinger, "Abrasion, erosion and scuffing resistance of carbide and oxide ceramic thermal sprayed coatings for different applications," Wear, Vol. 162-164, 1993, pp. 529-537

［6］ R.A. Miller, "thermal barrier coatings for air craft engines history and directions," J. Therm. Spray Technol., Vol.6 (1), 1997, pp. 35-42

[7] R.A.Miller, "Oxidation-Based Model for Thermal Barrier Coating Life," J. Am. Ceram. Soc., Vol.67, 1984, pp.517-521

[8] V.S. Stabican, "Phase Equilibria and Metastabilities in the Systems ZrO2-MgO, ZrO2-CaO, and ZrO2-Y2O3," A*dv. Ceram*, Vol. 24A, 1986, pp. 35-43

[9] J.E Palko, K.L Luthra, and D.W McKee, "Evaluation of performance of thermal barrier coatings under simulated industrial/utility gas turbine conditions," General Electric Co., Schenectady, NY (USA). Gas Turbine Div. 1978

[10] S.R. Levine and R.A. Miller, "Thermal Barrier Coatings for Utility Gas Turbines," NASA TM-85349, National Aeronautics and Space Administration, 1982

[11] R.C. Tucker, T.A. Taylor, and M.H. Weatherly, "Plasma Deposited Ni-CrAIY Airfoil and Zirconia/NiCrAIY Thermal Barrier Coatings," presented at the Third Conference on Gas Turbine Materials in a Marine Environment (Bath University, Bath, England), 20-23 Sept, 1976, session VII, and paper 2

[12] N.N. Ault, "Characteristics of Refractory Oxide Coatings Produced by Flame Spraying," J. Am. Ceram. Soc., vo1.40, 1957, pp. 69-74

[13] L. Lin, K. Han, "Optimization of surface properties by flame spray coating and boriding," Surf. Coat. Technol., Vol. 106, 1998, pp. 100-105

[14] K. Sang, Y. Li, "Cavitation erosion of flame spray weld coating of nickel-base alloy powder," Wear, Vol.189, 1995, pp.20-24

[15] M.L.Thorpe, "Thermal Spray: Industry in Transition," Avd. Mater. Process, Vol. 143(No. 5), 1993, pp.50-56

[16] "http://www.gordonengland.co.uk/cps.htm", Surface Engineering Forum, 2008

[17] J. Voyer, C. Peterlechner and U. Noster, "Flame Sprayed Al-12Si Coatings for the Improvement of the Adhesion of Composite Casting Profiles", J. Therm. Spray Technol., Vol. 17, 2008, pp.824-830.

[18] A.Segall, A. Papyrin, J.conway, D. Shapiro, "A cold-gas spray coating process for enhancing titanium", JOM, Vol. 50, 1998, pp. 52-54

[19] P.S. Phani, D.S.Rao, S.V.Joshi and G. Sundararajan, "Effect of Process Parameters and Heat Treatments on Properties of Cold Sprayed Copper Coatings," J. Therm. Spray Technol, Vol.16, 2007, pp. 425-434

[20] R.Dykhuizen and M. Smith, "Gas dynamic principles of cold spray", J. Therm. Spray Technol, Vol. 7, 1998, pp. 205-212

[21] S.Kuroda, J.Kawakita, M.Watanabe and H.Katanoda, "Warm spraying - a novel coating process based on high-velocity impact of solid particles," Sci. Technol. Adv. Mater, Vol. 9, 2008, pp.17-34

[22] C. H. Lee, H. K. Kim, H. S. Choi and H. S. Ahn, "Phase transformation and bond coat oxidation behavior of plasma-sprayed zirconia thermal barrier coating," Surf. Coat. Technol, Vol.124, 2000, pp.1-12

[23] S.J. Grisaffe, "Simplified Guide to Thermal-Spray Coatings," Mach Des., Vol.39, 1967, pp.174-181

[24] M. Movchan, Y. Rudoy, "Composition, structure and properties of gradient thermal barrier coatings (TBCs) produced by electron beam physical vapor deposition (EB-PVD)," Mater.Des., Vol. 19, 1998, pp.253-258

[25] A.N. Curren, S.G. Grisaffe, and K.C. Wycoff, "Hydrogen Plasma Tests of Some Insulating Coating Systems for the Nuclear Rocket Thrust Chamber," NASA TM X-2461, National Aeronautics and Space Administration, 1972

[26] J. Wigren, L. Pejryd, and H. Karlsson, "The Effect of Tungsten Contamination from the Spray Gun on the Performance of a Thermal Barrier Coating", Thermal Spray: A United Forum for Scientific and Technological

Advances, C.C. Berndt, ed., ASM International, Materials Park,OH, 1997, pp. 243-250

[27] "Thermal spraying", Sulzer Metco, 2008. [Online] Available: www.sulzermetco.com

[28] A. Salazar, A. Sanchez-Lavega, and J. Fernandez, "Thermal diffusivity measurements in solids by the 'mirage' technique: Experimental results," J. Appl. Phys, Vol.69, no.3, 1991, pp.1216-1223

[29] M.J.Adams and G.F. Kirkbright, "Thermal diffusivity and thickness measurements for solid samples utilizing the optoacoustic effect", Analyst, Vol.102, 1977, pp. 678–682

[30] M.J.Adams, G.F. Kirkbright, and K.R. Menon, "Effect of sample thickness on the magnitude of optoacoustic signals," Anal. Chem., Vol. 51, 1979, pp.508–511

[31] A.Bendada, N.Baddour, N.A.Mandelis, and C. Moreau, "Experimental Investigation on the Reliability of Thermal Wave Interferometry in the Thermophysical Characterization of Plasma Sprayed Coatings", Int. J. Thermophys., Vol. 26, 2005, pp.881-892

[32] S. Brahim, J.L. Bodnar, and P. Grossel, "Thermal diffusivity measurement by photothermal radiometry under random excitation and parametric analysis", J. Phys, Conference Series 214, 2010, 012065

[33] S. Patle, R.K. Sahoo (Guide), "Analysis and Measurement of Thermophysical Properties by Temperature Oscilation," Thesis (Doctor of Philosophy)

[34] K.B. Larson and K. Koyama, "Correction for Finite‑Pulse‑Time Effects in Very Thin Samples using the Flash Method of Measuring Thermal Diffusivity," J. Appl Phys, Vol.38, no.2, 1967, pp.465-474

[35] W. N. Santos, P.Mummery, and A. Wallwork, "Thermal diffusivity of polymers by the laser flash technique", Polym. Test., Vol. 24, Issue 5, 2005, pp. 628-634

[36]R. Taylor, "Construction of apparatus for heat pulse thermal diffusivity measurements from 300-3000K," J. Phys E: Sci. Instrum., Vol. 13, 1980, pp. 1193-1199

[37] L.M.Clark III; R.E. Taylor, "Radiation loss in the flash method for thermal diffusivity," J. Appl. Phys., Vol.46, no.2, 1975, pp.714-719

[38] B. Hay, J. Filtz, J. Hameury and L. Rongione, "Uncertainty of Thermal Diffusivity Measurements by Laser Flash Method," Int. J. Thermophys., Vol.26, 2005, pp. 1883-1898

[39] T. Baba and A. Ono, "Improvement of the laser flash method to reduce uncertainty in thermal diffusivity measurements," Meas. Sci. Technol., Vol.12, 2010, pp. 2046-2057

[40] C. A. Castro, B. Taxis, H.M. Roder, and W.A.Wakeham, "Thermal diffusivity measurement by the transient hot-wire technique: A reappraisal," Int. J. Thermophys., Vol. 9, 1988, pp. 293-316

[41] M. Gustavsson, E. Karawacki, and S.E. Gustafsson, "Thermal conductivity, thermal diffusivity, and specific heat of thin samples from transient measurements with hot disk sensors," Rev. Sci. Instrum., Vol.65, no.12,1994, pp.3856-3859

 [42] S.M.S. Mushed, K.C.Leong, and C. Yang, "Determination of the effective thermal diffusivity of nanofluids by the double hot-wire technique," J. Phys. D: Appl. Phys., Vol. 39, 2006, pp.5316-5322

[43] H. Xie, H. G, M. Fujii, and X.Zhang, "Short hot wire technique for measuring thermal conductivity and thermal diffusivity of various materials," Meas. Sci. Technol., Vol.17, 2006, pp.208-214

[44] Bendada, N. Baddour, A. Mandelis, and C.Moreau, "Experimental Investigation on the Reliability of Thermal Wave Interferometry in the Thermophysical Characterization of Plasma Sprayed Coatings," Int. J. Thermophys., Vol.26, 2005, pp. 881 – 892.

[45] A. Houlbert, P. Cielo, C. Moreau, and M. Lamontagne, "Measurement of thermal diffusivity and anisotropy of plasma-sprayed coatings," Int. J. Thermophys., Vol. 15, 1994, pp. 525 – 546.

[46] F.Cernuschi, P. Bianchi, M. Leoni, P.Scardi, "Thermal diffusivity/microstructure relationship in Y-PSZ thermal barrier coatings," J. Therm. Spray Technol., Vol.8, 1999, pp. 102-109

[47] W.J. Parker, R.J. Jenkins, C.P. Butler, and G.L. Abbott, "Flash Method of Determining Thermal Diffusivity, Heat Capacity, and Thermal Conductivity," J. Appl. Phys., Vol.32, no.9, 1961, pp.1679-1684

[48] Latiff M. Jiji, "Heat conduction" (2nd ed), Begell house, 2003

[49] M. Necati Ozisik, "Heat conduction" (2nd ed), New York, USA, 2003

[50] André McDonald, Christian Moreau and Sanjeev Chandra, "Thermal contact resistance between plasma-sprayed particles and a flat surface," Int. J. Heat Mass Transfer, Vol. 50, 2007, pp. 1737 – 1749

[51] Yunus A. Cengel, " Heat and mass transfer" (3rd ed), Mc Graw Hill, 2005

[52] A.Laachachi, M. Cochez, M.Ferriol, J.M.Lopez-Cuesta and E.Leroy, "Influence of TiO_2 and Fe_2O_3 fillers on the thermal properties of poly (methyl methacrylate) (PMMA)", Mater. Lett., Vol.59, 2005, pp. 36-39

[53] T. Stoltenhoff, C. Borchers, F. Gartner, and H. Kreye, "Microstructures and key properties of cold-sprayed and thermally sprayed copper coatings," Surf. Coat. Technol., Vol.200, 2006, pp. 4947-4960

[54] K. A. Khor and Y. W. Gu, "Thermal properties of plasma-sprayed functionally graded thermal barrier coatings," Thin Solid Films, Vol. 372, 2000, pp.104-113

[55]"http://www.efunda.com/materials/alloys/alloy_home/steels_properties.cf m", Engineering Fundamentals, 2011

[56] Ronald G. Munro, "Material Properties of Titanium Diboride," J. Res. Natl. Inst. Stand. Technol., Vol.105, 2000, pp. 709-720

Appendix

Solving the Auxiliary problem of Duhamel's method

This auxiliary problem could be solved by the method of separation of variables.

$$\overline{\eta}(x,t) = \psi(x,t) + \phi(x)$$

Introduce it to the governing equation of the auxiliary problem:

$$\frac{\partial^2 \psi}{\partial x_2} + \frac{d^2 \phi(x)}{dx^2} = \frac{1}{\alpha}\frac{\partial \psi}{\partial t} \qquad 0 \le x \le L, \quad t \ge 0$$

Therefore:

$$\frac{d^2 \phi(x)}{dx^2} = 0$$

$$\frac{\partial^2 \psi}{\partial x_2} = \frac{1}{\alpha}\frac{\partial \psi}{\partial t} \qquad 0 \le x \le L, \quad t \ge 0$$

With condition a and condition b

$$\psi(L,t) + \phi(L) = 1$$

$$\frac{\partial \psi(0,t)}{\partial x} + \frac{d\phi}{dx} = 0$$

Therefore,

$$\phi(L) = 1$$

$$\psi(L,t) = 0$$

$$\frac{\partial \psi(0,t)}{\partial x} = 0$$

$$\frac{d\phi}{dx} = 0$$

$$\psi(x,0) + \phi(x) = 0$$

Assuming that $\phi(x) = Ex + F$, it is calculated that $E = 0$ and $F = 1$, therefore,

$$\phi(x) = 1.$$

Assume that

$$\psi(x,t) = X(x)\tau(t)$$

$$\frac{d^2 X_n}{dx^2} + \lambda_n^2 X = 0 \qquad n = 1,2,3\ldots\ldots$$

$$\frac{d^2 X_0}{dx^2} = 0$$

$$\frac{d\tau_n}{dt} + \lambda_n^2 \alpha\tau = 0 \qquad\qquad n = 1,2,3\ldots\ldots$$

$$\frac{d\tau_0}{dt} = 0$$

For $n = 0$

$$X_0 = A_0 x + B_0$$

$$\tau_0 = c_0 t$$

For $n \neq 0$

$$X_n = A_n \sin(\lambda_n x) + B_n \cos(\lambda_n x)$$

$$\tau_n = c_n \exp(-\alpha\lambda_n^2 t)$$

It is calculated that $A_n = 0$ for $n = 0,1,2\ldots\ldots$

$$\lambda_n = \frac{(2n-1)}{2a}\pi$$

$$B_{0=}0$$

Therefore, the solution is

$$\theta(x,t) = \sum_{n=1}^{\infty} B_n \cos[\frac{(2n-1)\pi}{2a} x] \cdot C_n \exp(-\alpha \frac{(2n-1)^2 \pi^2}{4a^2} t) + 1$$

Use the initial condition,

$$\theta(x,0) = \sum_{n=1}^{\infty} a_n \cos[\frac{(2n-1)\pi}{2a} x] + 1$$

Apply orthogonally and integrate:

$$\int_0^a a_n \cos^2(\lambda_n x) dx = \int_0^a (-1) \cos^2(\lambda_n x) dx$$

$$\therefore a_n = \frac{(-1)^n}{\lambda_n} \frac{2}{a}$$

$$\therefore \overline{\theta} = \sum_{n=1}^{\infty} \frac{4 \cdot (-1)^n}{(2n-1)\pi} \cos[\frac{(2n-1)\pi}{2a} x] \cdot \exp(-\alpha \frac{(2n-1)^2 \pi^2}{4a^2} t) + 1$$